Université du Québec

INRS Institut national de la recherche scientifique

Énergie Matériaux Télécommunications

Electrochemical Fabrication and Characterization of Conical Tungsten Ultramicroelectrodes

Par

Uriel Bruno-Mota

Mémoire présenté(e) pour l'obtention du grade de

Maître ès Sciences (M.Sc.)

en sciences de l'Énergie et des Matériaux

Jury d'évaluation

Président du jury et examinateur interne	Prof. Mohamed Mohamedi INRS-EMT
Examinateur externe	Prof. Sasha Omanovic Department of Chemical Engineering Mc-Gill University
Directeur de recherche	Prof. Ana Tavares INRS-EMT
Codirecteur de recherche	Prof. Aycan Yurtsever INRS-EMT

© Droits réservés de Uriel Bruno Mota, le 02 Juillet 2020

ACKNOWLEDGEMENTS

I would like to acknowledge to the Institut National de la Recherche Scientifique for the financial support received through the exemption of the tuition fees for foreign students, for facilitating the use of state of the art infrastructure for the development of the experimental part of the present project and for giving me the opportunity to get involved in scientific research in a multicultural environment.

The financial contribution of Consejo Nacional de Ciencia y Tecnología (CONACYT, Mexican National Council for Science and Technology) is truly appreciated for granting the scholarship for the development of graduate studies abroad.

I wish to express my appreciation to my supervisors Prof. Ana C. Tavares and Prof. Aycan Yurtsever for their guidance, dedication and effort for the development of the present project.

I wish to express my appreciation to my tutor in Mexico, Prof. Miguel Angel Gonzalez Fuentes for his help and time for the elaboration of the academic reports for my scholarship.

I wish to thank all the members of the group whose assistance was a milestone in the completion of this project, with a special mention to Cybelle, who was always there willing to support me, to teach me and to remind me of how beautiful electrochemistry can be. Also, to Angel, Rasool and Fabiola for their contribution for the SEM imaging, interferometric measurements and the revision of the first drafts of the present work, respectively.

I wish to acknowledge the support and great love of my family, my parents, Marina and Mauro, and my brothers Ricardo and Mauricio. They kept me going on and this work would not have been possible without their input.

I also want to thank my friends, Elena, Aura and Yoandris who made my stay at INRS an outstanding experience, full of adventures in the lab, collaborations, fights, complains but also because it is with them that I had the chance to explore Canada and its beautiful landmarks.

I want to thank Pascale too for her contribution to the revision of the parts of the present work written in French.

And finally, to Vero, because she has always been a great intellectual motivation for me. She always reminds me of why I decided to start doing science. I will always owe to her the ability to get amazed after learning something new.

I would like to recognize the invaluable assistance that you all provided during my study.

RÉSUMÉ

L'étude de l'électrochimie à entité unique a été d'un grand intérêt dans plusieurs domaines dus à diverses raisons qui vont de l'étude des réactions sans limitation cinétique, au besoin d'une meilleure compréhension des réactions électrochimiques se produisant dans des cellules vivantes uniques ou dans des structures subcellulaires.

Grâce aux avancées récentes de la nano fabrication, des simulations assistées par ordinateur, ainsi que des potentiostats modernes, un progrès rapide est devenu possible dans le domaine de l'électrochimie à l'échelle nanométrique permettant la réalisation de mesures électrochimiques à partir d'entités submicroniques. Dans ce travail, nous présenterons notre approche concernant l'étude des réactions électrochimiques à l'échelle nanométrique, qui consiste en la fabrication d'embouts pointus de tungstène par gravure électrochimique et par gravure à faisceau ionique focalisé, caractérisés de façon microscopique et électrochimique.

Les premières preuves électrochimiques d'une concentration de champs électriques au sommet des embouts en raison de la forme et de la taille de ces électrodes ont été obtenues expérimentalement. Cette concentration du champ électrique s'est avérée utile pour développer de manière sélective des amas monocristallins de particules d'or au sommet de l'embout, rendant les électrodes développées potentiellement applicables pour l'étude de réactions électrochimiques au niveau d'entités uniques.

Mots-clés : Électrochimie à l'échelle nanométrique; Électrochimie à entité unique; Ultra-microélectrodes; Des UME; Électrochimie du tungstène; embout pointu de tungstène; Ultra-microélectrodes coniques; réponse voltampérométrique des UME.

ABSTRACT

The use of nano-electrochemistry and single-entity electrochemistry has been of great interest in different fields due to a diverse number of reasons, that go from the study of reactions of interest at the single particle level without kinetical limitations to the need of a better understanding of the electrochemical reactions happening at single living cells or subcellular structures.

With modern developments in nanofabrication, simulations and computer aided design, as well as in state of the art potentiostats, the rapid development of electrochemistry at the nanoscale was allowed making it possible to achieve electrochemical measurements from submicron entities. In this work we will present our contribution to the study of electrochemical reactions at the nanoscale, which consisted in the fabrication of sharp tungsten tips by electrochemical etching and focused ion beam etching techniques and their microscopic and electrochemical characterizations.

The first direct electrochemical evidence of the concentration of electric fields at the apex of the tips due to the shape and size of the electrodes was obtained experimentally. This concentration of the electric field demonstrated to be useful in order to selectively grow clusters of gold particles at the tip apex, making the developed electrodes potentially applicable for the eventual study of electrochemical reactions at single entities.

Keywords : Nanoscale electrochemistry; Single-entity electrochemistry; Ultra-microelectrodes; UME’s; tungsten electrochemistry; tungsten sharp tips; conic ultra-microelectrodes; voltammetric response of UME’s.

SOMMAIRE RÉCAPITULATIF

Introduction

De nombreux processus physiques et biologiques dans la nature impliquent des réactions qui créent ou utilisent des charges et des courants électriques. Ces processus ne se produisent qu'à des énergies spécifiques déterminées par le potentiel des réactions et des molécules impliquées. Il est possible d'étudier ces processus fondamentaux en mesurant expérimentalement leur potentiel caractéristique. Ce principe constitue la base de l'électrochimie, une branche des sciences physiques qui existe depuis 1800 [1].

Compte tenu de la fréquence des réactions électrochimiques dans la nature et dans les procédés industriels, plusieurs applications ont été trouvées dans divers domaines. De nombreuses technologies traditionnelles telles que la production d'aluminium à partir de minerai brut, la galvanoplastie, l'électrolyse de saumure pour la production de Cl_2 et de NaOH, le stockage d'énergie et les dispositifs de conversion d'énergie sont basées sur des réactions électrochimiques. Les nouvelles technologies émergentes, notamment la capture du CO_2 de la fumée industrielle et la purification efficace de l'eau, sont également basées sur l'électrochimie. De même, dans les organismes biologiques, l'électrochimie régit de nombreux processus vitaux tels que la communication entre les cellules et des réactions métaboliques dans la matrice cellulaire et dans le système membranaire [2]–[8].

Traditionnellement, les mesures électrochimiques sont effectuées avec des électrodes macroscopiques. À cet égard, les matériaux à l'étude sont généralement déposés sur des électrodes de taille millimétrique et centimétrique et le courant provenant de grandes zones macroscopiques est mesuré. Bien que cette approche traditionnelle produise des signaux forts qui sont idéals pour des analyses quantitatives [9]–[11], elle n'est pas appropriée lors de l'utilisation d'entités uniques ou des structures submicroniques hétérogènes. En effet, celles-ci contribuent au signal électrochimique et, par conséquent, il devient impossible d'effectuer des études approfondies des réactions chimiques se produisant sur ces sites.

Avec les récents développements de la nano fabrication, des simulations par ordinateur, ainsi que des potentiostats modernes, il est désormais possible de réaliser des mesures électrochimiques à partir d'entités submicroniques [12]–[14]. La richesse du monde microscopique et les perspectives scientifiques qui découleraient d'une telle réalisation constituent la base de l'intérêt de ces travaux, axés sur le développement et l'étude de systèmes électrochimiques submicroniques.

En étudiant l'électrochimie à une seule entité, des effets non conventionnels sont attendus. En électrochimie, nous nous intéressons aux processus de transfert d'électrons entre une électrode et des espèces chimiques en solution. Ce transfert d'électrons se produit à l'interface électrique formée entre l'électrode et l'électrolyte. Cette interface, communément appelée double couche électrique, est bien définie et se caractérise par une forte transition du potentiel électrique. Elle a des propriétés complètement différentes de celles de la solution. Cette différence de potentiel, typiquement comprise entre 0.1 et 1 V, s'étend sur la longueur de la double couche (dans l'ordre de grandeur des angströms) entraînant un champ électrique important (10^9-10^{10} V m^{-1}) responsable du transfert d'électrons entre l'électrode et l'espèce en solution.

L'un des principaux défis liés à l'étude de l'électrochimie à une seule entité (et de l'électrochimie à l'échelle nanométrique) repose sur le fait que des électrodes à l'échelle submicronique sont nécessaires pour minimiser la contribution de la surface de l'électrode au signal et pour atteindre une résolution spatiale élevée. De plus, un autre défi est que des intensités de courant très faibles (généralement de l'ordre de pA) sont produites dans ce type d'expériences nécessitant ainsi un équipement spécial ayant un rapport signal/bruit et une stabilité très élevée. [5]. Pour les tâches qui nécessitent une plage de mesure étendue non disponible avec des instruments conventionnels, comme pour détecter ou mesurer des courants inférieurs à 10 nA ou des résistances supérieures à 1 GΩ, des instruments avec des électromètres spéciaux sont nécessaires [13].

Des études expérimentales et informatiques récentes suggèrent que les électrodes formées par des nanoparticules ayant des structures coniques à l'échelle nanométrique (avec un embout d'un diamètre de < 30 nm) ont la capacité de concentrer les champs électriques (10 fois plus élevés par rapport à une électrode plane) par l'accumulation d'une grande concentration de cations à des embouts métalliques de taille nanométrique.[15]–[17]. Cette concentration de réactif induite par le champ a été utilisée pour expliquer l'augmentation de l'activité électrocatalytique des macroélectrodes formées par les nanoaiguilles d'or pour la réduction électrochimique du CO_2 par rapport aux autres nanoparticules d'or [18]. Cependant, ce type d'électrode se caractérise par une densité plus élevée des sites actifs, par de courtes voies de diffusion et donc, une concentration plus élevée d'espèces actives à proximité de l'électrode. Un transport amélioré des réactifs à la surface de l'électrode peut également augmenter la vitesse apparente de la réaction.

De nos jours, différentes approches sont utilisées pour étudier les processus électrochimiques à l'échelle microscopique et nanométrique, parmi lesquelles incluent des expériences d'impact de

nanoparticules, l'utilisation de nano et micropores et l'utilisation de la microscopie électrochimique à balayage [5].

La meilleure approche pour l'étude d'entités uniques est l'immobilisation de nanoparticules sur des ultra-microélectrodes (UME) afin d'enregistrer la réponse faradique directe. Il a été démontré que la réponse voltampérométrique dépend fortement de la taille de la nanoparticule. La faisabilité d'étudier des activités électrocatalytiques sur des nanoparticules simples a été prouvée [19], [20]. Cette approche est particulièrement utile afin d'avoir une meilleure compréhension de la relation structure-fonction lors d'électrocatalyse à base de nanoparticules.

Afin de réaliser l'immobilisation d'entités individuelles, il est nécessaire de développer des électrodes adaptées capables de les contenir et d'enregistrer leurs signaux électrochimiques. Les techniques les plus populaires consistent à encapsuler des métaux dans du verre afin de générer des électrodes de dimensions adaptées pour prendre en charge de telles petites entités.

La fabrication d'électrodes et d'embouts d'échelle nanométrique est en constante amélioration, mais toujours entravée par la nécessité d'étapes laborieuses (par exemple l'encapsulation, le pompage et le polissage des pipettes), par une instrumentation coûteuse (fraisage par faisceau d'ions focalisé de micropipettes remplies de carbone par dépôt chimique en phase vapeur) et par les taux de réussites qui sont parfois inférieurs à 10 % [5] [8]. Par conséquent, il est encore nécessaire de développer des techniques de fabrication simples d'électrodes submicroniques permettant d'étudier les processus électrochimiques à l'échelle nanométrique.

Les embouts métalliques pointus ont permis un grand nombre d'applications dans les techniques de microscopie à sonde à balayage telles que la microscopie à force atomique (AFM) ou la microscopie à effet tunnel (STM), pour les mesures de contact multipoint, la nanolithographie et la nanomanipulation [14]. En raison de leur stabilité chimique, les matériaux les plus couramment utilisés pour préparer ces embouts sont l'or, l'iridium, le nickel et le platine [15] [16] [20] [21]. Cependant, cette stabilité entraîne un processus d'aiguisage laborieux pour obtenir des pointes avec des formes et des diamètres contrôlables de l'ordre de quelques nanomètres.

Le tungstène a été utilisé comme matériau de pointe alternatif, car des embouts très pointus peuvent être préparés de manière simple et robuste en utilisant la gravure électrochimique [14] [17]–[19], [22]–[25]. Cependant, à notre connaissance, W n'a jamais été proposé comme matériau pour fabriquer des électrodes submicroniques pour l'électrochimie à une seule entité. Il existe deux principaux oxydes, le dioxyde de tungstène (WO_2) et le trioxyde de tungstène (WO_3) qui passivent la surface du tungstène. [26]–[29].Ces derniers ont empêché son application

comme matériau d'électrode. Cependant, lors de nos investigations préliminaires avec ce matériau, nous avons réalisé que nous pouvions utiliser la formation d'oxydes sur la surface du tungstène à notre avantage. Nous avons découvert que nous pouvions oxyder sélectivement la surface de l'électrode de W de manière contrôlée en WO_2, formant une surface très stable avec suffisamment de conductivité pour être utilisée comme électrode.

Objectif général

L'objectif du présent projet était le développement d'un montage expérimental pour la fabrication et la caractérisation microscopique et électrochimique de nanoélectrodes constituées d'embouts de tungstène pointus à des fins éventuelles d'utilisation comme support pour des entités uniques comme nanoparticules ou cellules vivantes.

Méthodologie

La méthodologie effectuée pour le développement du présent travail a été divisée en cinq sections principales : (i) la construction du montage expérimental, (ii) la fabrication des embouts pointus de tungstène, (iii) les études fondamentales sur le comportement électrochimique du tungstène réalisé au niveau des fils de tungstène, (iv) la caractérisation électrochimique et morphologique des embouts pointus de tungstène, et (v) le dépôt cathodique d'or sur les embouts de tungstène.

Pour le montage expérimental, l'une des extrémités du ET (0,5 cm) a été pliée dans un angle de 90 ° afin de pouvoir être maintenue dans un tube en cuivre (Sigma-Aldrich, diamètre extérieur: 3,0 mm, épaisseur de paroi: 0,9 mm, diamètre intérieur: 1,2 mm, longueur: 10 cm). Afin de contrôler la profondeur du fil à l'intérieur de la solution de travail, le tube de cuivre a été fixé à l'aide de boulons en acier inoxydable à un étage piézoélectrique de translation (Thorlabs, NFL5DP20 5,0 mm de course) fixé à un étage de translation micrométrique standard (Thorlabs , PT3 / M - 25 mm XYZ) comme le montre la figure 1.1 b. L'étage piézoélectrique a été utilisé pour effectuer des déplacements très fins (36 nm) à l'aide d'un contrôleur piézoélectrique, tandis que l'étage de traduction micrométrique standard a été utilisé pour effectuer des déplacements à l'échelle micrométrique. Toutes les expériences ont été surveillées in vivo avec un microscope USB optique (Adnostar, processeur Digital Image Monarch, capteur CMOS de haute qualité, résolution 640 * 480, couleurs vraies 24 bits RVB, USB 2.0, fréquence d'images de 30 images / s, grossissement 200x) qui a été placé à côté des cellules électrochimiques comme le montre la figure 4.1ab.

Pour les expériences électrochimiques, deux configurations différentes de cellules électrochimiques ont été utilisées. Pour la préparation d'embouts de tungstène pointus, une configuration à deux électrodes a été utilisée comme indiqué sur la figure 1.1a. Les électrodes de travail (ET) étaient des fils de tungstène attachés au tube de cuivre. Le CE était un anneau en fil de tungstène avec un diamètre similaire à la boîte de Petri et son extrémité était maintenue par un morceau de ruban de cuivre qui était utilisé pour établir un contact avec le potentiostat en utilisant une pince crocodile.

La deuxième configuration, pour la caractérisation électrochimique des fils de tungstène et des embouts de tungstène, consistait en une cellule électrochimique à trois électrodes comme indiqué dans l'encadré de la figure 1.1 b. Dans ce cas, soit des fils de tungstène de 2,5 cm de longueur et 100 µm de diamètre, soit les embouts qui en résultaient ont été utilisés comme ET, un fil de platine a été utilisé comme CE et Ag / AgCl (1 M KCl) était la RE. Pour toutes les expériences électrochimiques, la tension a été appliquée par un potentiostat / galvanostat (Autolab PGSTAT 101) illustré à la figure 1.1 b.

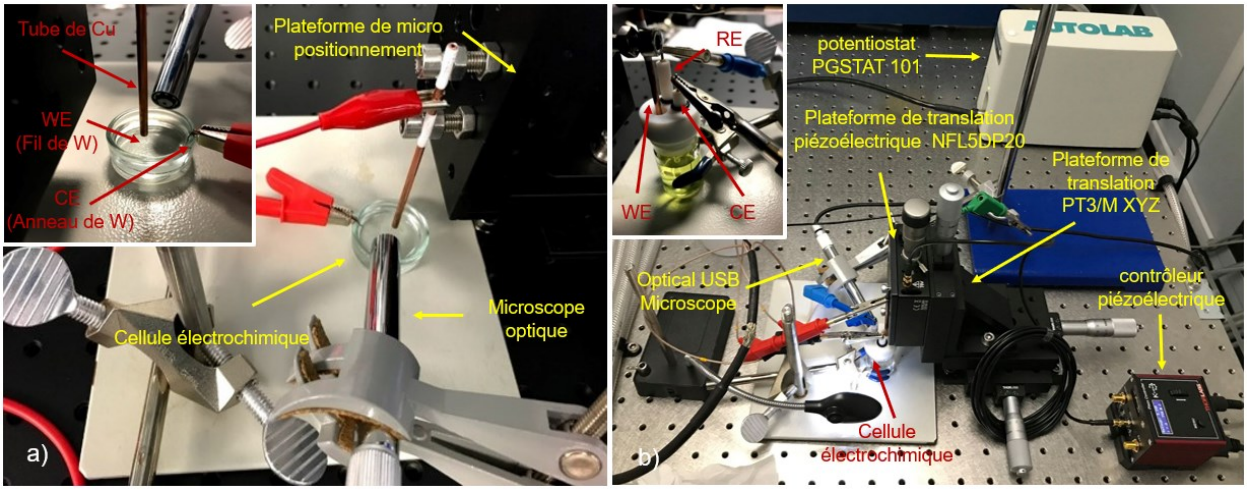

Figure 1.1 Montage expérimental

a) Montage pour la fabrication d'embouts de tungstène et b) Montage pour la caractérisation électrochimique des fils et des embouts de tungstène.

Comme nous avions pour objectif de travailler avec des électrodes ultras petites dont la réponse n'est que de quelques nanoampères, le montage expérimental s'est déroulé sur une table optique installée dans une pièce isolée des vibrations et du bruit, avec contrôle de température (22 °C) et

qui a servi comme cage de Faraday. Ceci, afin d'éviter toute interférence de perturbations mécaniques ou électromagnétiques sur les signaux électrochimiques.

Des embouts de tungstène pointus ont été préparés en utilisant une technique de gravure électrochimique connue sous le nom de méthode de « chute ». Cela consiste à plonger de petites portions de quelques millimètres de fil de tungstène dans une solution basique concentrée comme l'hydroxyde de potassium (KOH), puis à appliquer un potentiel électrique. Au fur et à mesure que la gravure progresse, un effet de rétrécissement est observé dans la partie du fil à l'interface air-solution en raison d'une vitesse de gravure non uniforme au long du fil. À un certain point, la résistance à la traction du col du fil gravé sera dépassée pour le poids de la partie inférieure du fil. Cela force la partie inférieure à tomber dans la solution, formant deux embouts pointus dans les parties inférieure et supérieure. Dans ce cas, une configuration à deux électrodes a été mise en œuvre, en utilisant une boîte de Petri comme cellule électrochimique (Figure 1.1 a).

Pour la caractérisation du comportement voltampérométrique des fils et des embouts de tungstène, une cellule électrochimique à trois électrodes a été utilisée comme le montre la Figure 1.1 b. Les solutions de travail pour lesquelles le comportement voltampérométrique du métal a été étudié étaient les suivantes: a) 0,5 M H_2SO_4 pour étudier l'électrochimie de la surface; et b) 5 mM $K_4Fe(CN)_6$ + 5 mM $K_3Fe(CN)_6$ + 0,5 M KCl comme sonde redox pour prouver la faisabilité de l'utilisation du tungstène comme électrode pour l'étude des transferts d'électrons hétérogènes. 5 mm des fils de tungstène ont été immergés en solution pour effectuer ces mesures électrochimiques.

La voltampérométrie cyclique a été réalisée dans deux fenêtres de potentiel différentes: (i) -0,01 à 0,55 V vs Ag / AgCl (1 M KCl); et (ii) de -0,01 à 1,5 V vs Ag / AgCl (1 M KCl). Ces deux fenêtres de potentiel ont été utilisées pour étudier la formation et le comportement de deux oxydes de tungstène différents (WO_2 et WO_3) sur la surface métallique pure. Les voltampérogrammes ont été enregistrés à 10 mVs^{-1} et 100 mVs^{-1} pour évaluer l'effet de la vitesse de balayage sur la formation et la dissolution des couches d'oxyde de tungstène.

Les pointes en tungstène ont été caractérisées par voltampérométrie cyclique en utilisant une solution de KCl 0,5 M contenant 5 mM de $Fe(CN)_6^{-4}$ et $Fe(CN)_6^{-3}$, un couple redox dont le comportement est déjà très bien connu [21].

Finalement, le dépôt d'or a été effectué sur les pointes de tungstène par dépôt cathodique électrochimique. Cette technique consiste en un dépôt d'un revêtement mince et fortement

adhérent d'un métal sur la surface d'un substrat conducteur par simple électrolyse d'une solution contenant l'ion métallique souhaité ou son complexe chimique.

L'électrodéposition de l'or a été effectuée en utilisant le dispositif expérimental illustré à la Figure 1.1 b. La profondeur des embouts dans la solution pendant la déposition était ce que nous appelons « la hauteur du ménisque », qui correspond à la profondeur minimale réalisable avec les étages de micropositionnement dans notre montage expérimental. La hauteur du revêtement d'or donne une bonne approximation de la contribution du ménisque à la superficie étudiée.

Le comportement électrochimique du revêtement d'or sur les embouts de tungstène a été étudié par voltampérométrie cyclique dans une solution de 0,5 M H_2SO_4 en utilisant le montage expérimental montré dans la Figure 1.1 b. Les voltampérogrammes ont été enregistrés dans une plage de potentiel de -0,01 à 1,5 V vs Ag/AgCl (1M KCl) afin de trouver les pics caractéristiques d'oxydations et de réductions d'une surface d'or polycristalline.

Résultats

1. **Caractérisation électrochimique du tungstène**

La réponse électrochimique des fils de tungstène a été étudiée par VC dans une solution de 0,5 M de H_2SO_4 afin de découvrir la fenêtre de potentiel ou le tungstène peut être utilisé comme matériel d'électrode. La Figure 1.2 montre les voltampérogrammes cycliques du fil à différentes vitesses de balayage. Lors du balayage à 100 mV s^{-1}, il y a deux pics principaux observables sur le voltampérogramme situés à 0,47 V et 0,70 V, indiquant que deux oxydes de tungstène différents se sont formés pendant le balayage.

Lors du balayage inverse du premier cycle, il y a une diminution remarquable du courant anodique qui pourrait indiquer que dans cette fenêtre de potentiel la polarisation anodique produit un film passif, ce qui est mis en évidence par le comportement observé dans les cycles suivants. Le comportement entre 1,2 et 1,55 V est intéressant, car après la chute évidente du courant, indiquant la passivation complète de la surface due à la formation d'une couche d'oxyde, dans cette région, le courant recommence à augmenter dans les cycles suivants. Cela pourrait être expliqué par une dissolution lente de la couche de WO_3 qui permet à la surface de récupérer lentement sa conductivité. La dissolution du trioxyde de tungstène dans des milieux acides a été étudiée auparavant et il a été confirmé que même si elle est très lente, elle se produit et dépend de la concentration de la solution utilisée [22].

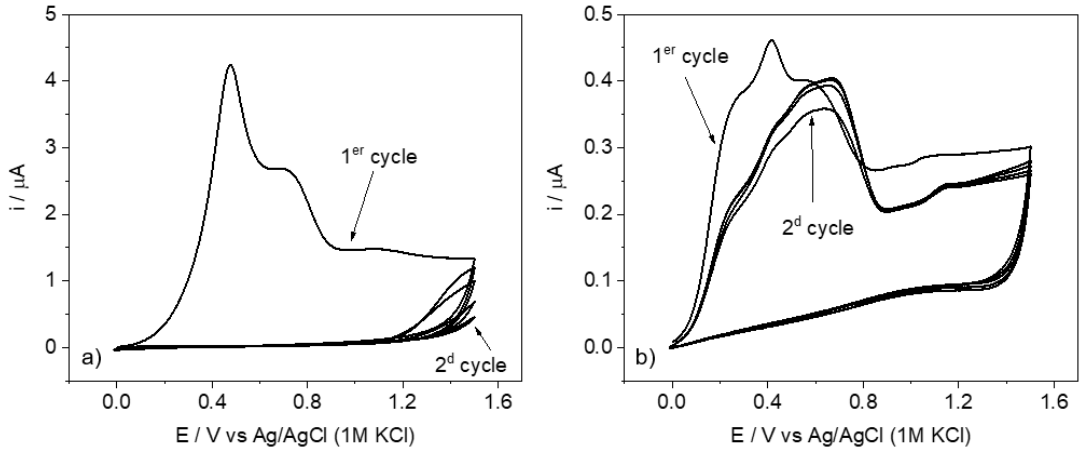

Figure 1.2. Voltampérogrammes cycliques de fils de tungstène en solution 0,5 M H_2SO_4 à différentes vitesses de balayage

Les voltampérogrammes cycliques ont été enregistrés dans une solution 0,5 M de H_2SO_4 à (a) 100 mVs^{-1} et (b) 10 mVs^{-1}.

La Figure 1.2 b montre les voltampérogrammes dans la même fenêtre de potentiel à 10 mV s^{-1}. Il est possible d'observer trois principaux signaux : à 0,27 V, à 0,46 V et à 0,55 V. Il a été suggéré que le premier signal correspond à la formation d'un sous-oxyde WO_{2-x} qui n'est pas thermodynamiquement stable [23]. Les signaux qui suivent correspondent aux mêmes processus électrochimiques que ceux observés à 100 mV s^{-1}. Dans le balayage inverse, une petite augmentation du courant peut être observée à 1,32 V qui peut être attribuée à une réactivation de la surface après la polarisation anodique.

Dans le balayage vers l'avant, même s'il y a une diminution notable des courants après le premier cycle, les signaux d'oxydation peuvent toujours être reconnus. Le fait que la récupération de la conductivité de surface devient plus importante à de faibles vitesses de balayage peut être dû à la dissolution chimique des espèces formées pendant le balayage vers l'avant de la même manière que pour les solutions alcalines [23].

De plus, la réponse électrochimique du tungstène a été enregistrée dans une plage de potentiel plus étroite pour évaluer le comportement de WO_2, dont la formation correspond au premier pic. La réponse, dans cette plage de potentiel, présente un comportement très similaire à celui obtenu en balayage complet, ce qui signifie que le premier oxyde est capable de former une couche de passivation à la surface de l'électrode, ou qu'après le premier cycle, la surface de l'électrode n'est plus réactive en raison d'une transformation complète du tungstène en WO_2. Cette dernière explication ne signifie pas que la surface n'est pas conductrice et pour le prouver, nous avons procédé à des expériences similaires, mais en présence du couple redox ferroferricyanure.

La Figure 1.3 montre la réponse typique du processus d'oxydation du tungstène dans une solution 5 mM ferroferricyanure à 100 mV s^{-1}. Dans le premier cycle, l'oxydation de la surface et des espèces de Fe est observée et dans les cycles suivants, il ne reste que l'oxydation des espèces de Fe, ce qui met en évidence l'aptitude du matériel à être utilisé comme électrode pour l'étude des réactions redox d'une sonde en solution. Le cyclage a été poursuivi jusqu'à l'obtention d'un voltampérogramme stable (généralement 10 cycles), puis les embouts obtenus ont été directement utilisés pour effectuer les mesures électrochimiques afin de les caractériser.

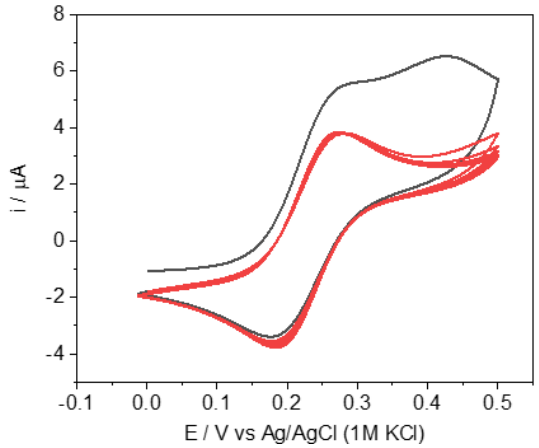

Figure 1.3. Réponse typique de l'oxydation des embouts de tungstène pour l'obtention d'embouts de WO_2

Les CV sont enregistrés dans une solution de 0,5 M KCl + 5 mM Fe $(CN)_6^{3-}$ + 5 mM Fe $(CN)_6^{4-}$ à 100 mVs^{-1}. La courbe noire correspond au premier balayage et les rouges sont les balayages suivants. Il peut être apprécié qu'une réponse stable a été obtenue.

2. Fabrication des embouts de tungstène

Deux approches de gravure électrochimique ont été menées afin d'obtenir des embouts en tungstène ayant les caractéristiques souhaitées, à savoir : un rapport de forme (*H*) élevé, une faible rugosité et un petit rayon de courbure. La forme, la rugosité, la taille et le diamètre des embouts obtenus dépendent sensiblement des conditions dans lesquelles la gravure électrochimique est effectuée. Par conséquent, la première étape a été de surveiller ce processus avec un microscope optique USB. La Figure 1.4a montre un schéma lié à l'effet de rétrécissement produit pendant le processus de gravure. La Figure 1.4 b montre l'embout de tungstène à différents moments. On peut voir que quelques minutes après avoir commencé à appliquer une tension, il y a un effet de rétrécissement dans le fil de tungstène à l'interface liquide-air.

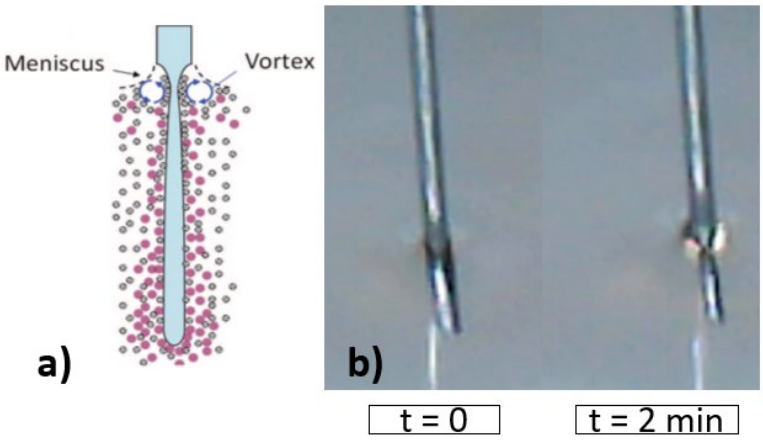

Figure 1.4. Suivi du processus de gravure électrochimique.

a) schéma montrant le mécanisme de l'effet de rétrécissement lors de la gravure électrochimique; et b) image optique montrant le processus de gravure du fil de tungstène à différents moments.

Parmi les facteurs qui affectent la forme et la taille finales des embouts, il y a la concentration de la solution électrolytique, la tension appliquée pendant le processus de gravure, la profondeur du fil de tungstène dans la solution pendant la gravure et les effets capillaires formant un ménisque à l'interface liquide-air.

L'une des principales préoccupations lors de la gravure des pointes de tungstène est le comportement du ménisque causé par la mouillabilité de la surface du tungstène par la solution de travail. En général, deux comportements différents en rapport au ménisque ont été observés. Dans le premier cas, le ménisque ne se déplace pas de sa position d'origine pendant le processus de gravure complet. Ce cas a entraîné la création d'embouts trop courts et concaves.

En raison de ces défis, il a été décidé d'adopter une méthode qui permettrait d'obtenir des embouts lisses et longs en même temps. Pour ce faire et en raison de l'importance de l'impact du ménisque sur la forme des embouts, comme évoqués précédemment, nous avons opté pour un régime de ménisque dynamique. Dans ce cas, le ménisque se déplace en une série d'étapes vers l'interface air-solution, ce qui a abouti en la création d'embouts longs et lisses qui peuvent être utilisés pour des expériences électrochimiques.

La Figure 1.5 montre la progression du processus de gravure illustrant le déplacement du ménisque au cours de la gravure, donnant lieu à la formation d'une pointe très longue, pointue et ayant une surface très lisse (voir Figure 1.5 e) comparativement à celles obtenues en régime ménisque statique.

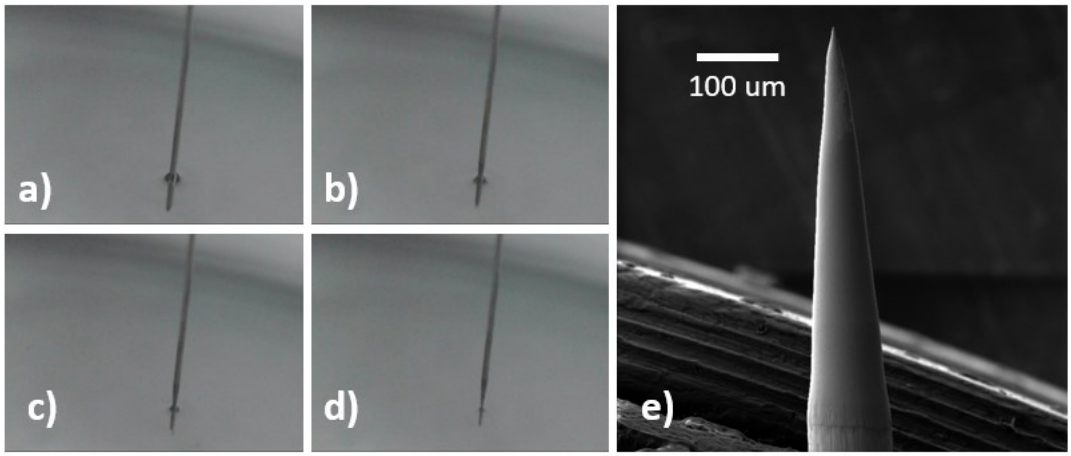

Figure 1.5 Régime de ménisque dynamique induit pour obtenir des pointes pointues et lisses

Photographies optiques montrant: a) la position du fil au début du processus de gravure, b) la position à 30 s, c) la position du fil à 1 min et) la position du fil après 1,5 min e) Image SEM de la pointe obtenue avec cette méthode.

Afin de réduire davantage la rugosité de la surface de l'embout, certaines des pointes produites avec la méthode du régime de ménisque dynamique ont été gravées par FIB. Dans ce cas, le faisceau d'ions a été focalisé parallèlement aux pointes de tungstène et la gravure a été réalisée suivant un régime radial partant de la partie externe du fil et se déplaçant vers l'axe de rotation de la pointe.

3. Caractérisation électrochimique des embouts

La voltampérométrie cyclique a été utilisée en employant un embout de tungstène, nommée pointe 1, possédant un *ROC* de 100 nm mise dans une solution de ferroferricyanure. Les voltampérogrammes ont été enregistrés à différentes profondeurs de la pointe en solution, tout en contrôlant sa position avec les micromètres de la plateforme de translation. Une image de la pointe 1 et de quelques voltampérogrammes cycliques enregistrés en fonction de la profondeur de l'embout est illustrée à la Figure 1.6.

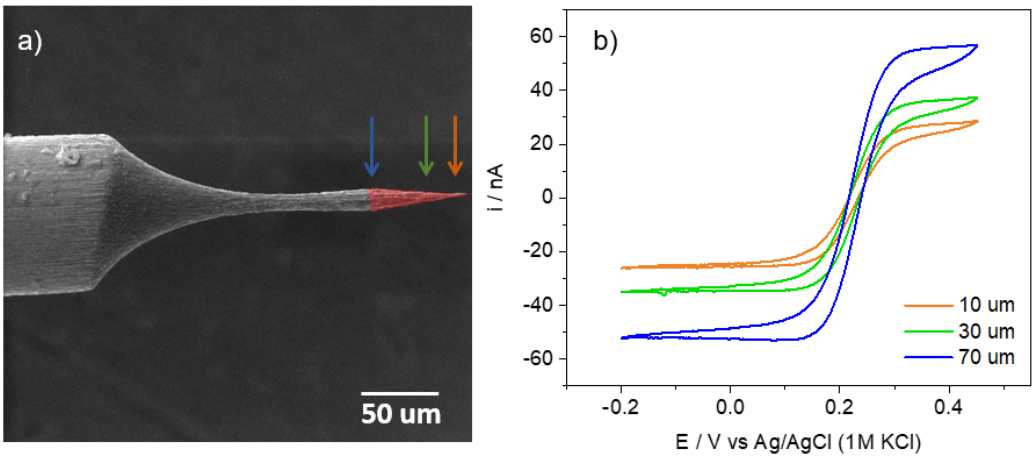

Figure 1.6 **a) Image SEM de la pointe 1 montrant les différentes profondeurs de la solution de travail auxquelles des voltampérogrammes cycliques (b) ont été enregistrés.**

Dans la Figure 1.6 b, les voltampérogrammes cycliques avec un comportement en régime stationnaire, c'est-à-dire ou le courant des électrodes est contrôlé par la diffusion, ont été obtenus. De plus, les voltampérogrammes cycliques enregistrés à différentes profondeurs montrent une augmentation du courant en régime stationnaire (i_{ss}) à mesure que la profondeur augmente, ce qui est attendu en raison d'une augmentation de la surface exposée à la solution.

La surface électroactive en contact avec la solution a été calculée à partir des voltampérogrammes cycliques selon l'équation suivante:

$$a = \frac{i_{cone}^{ss}}{4nFDc(1 + qH^p)}$$

Dans cette équation, *n* représente le nombre d'électrons transférés au cours du processus qui, dans notre cas spécifique, équivaut à un; *F* est la constante de Faraday égale à 96489 C mol^{-1}; *D* correspond au coefficient de diffusion de l'espèce réduite équivalente à 0,667 x 10^{-5} cm^2 s^{-1}; *c* est la concentration des espèces réduites en solution égale à 5 x 10^{-6} moles cm^{-3}; *a* représente le rayon de la base du cône formé par la pointe à la profondeur donnée en solution; *q* et *p* sont des constantes statistiques dont les valeurs sont respectivement de 0,30661 et de 1,14466 afin d'obtenir une précision à 1 % près [24]; et *H* représente le rapport d'aspect du cône formé par l'embout à la profondeur correspondante dans la solution. Le rapport d'aspect, *H*, a été calculé

en divisant la profondeur de l'embout en solution, *h* sur le rayon et, *a* a été mesuré à partir des images SEM. Pour la pointe 1, *H* est égal à 10.

La surface électroactive correspondant à la surface latérale du cône calculée électrochimiquement a été comparée à la surface géométrique théorique calculée directement à partir de l'image SEM représentée sur la Figure 1.6a traitée à l'aide du logiciel *Image J*.

La surface électroactive et la géométrique (GA) tracées en fonction de la profondeur de la pointe en solution sur la Figure 1.7a, montrent que les v les valeurs obtenues sont du même ordre de grandeur. Cependant, la surface électroactive est plus élevée en raison de la rugosité de la surface de la pointe. Les tendances suivies par les augmentations de surface avec la profondeur ne sont pas les mêmes. Pour cette raison, nous soupçonnons qu'il existe d'autres effets affectant notre calcul, qui, comme mentionnés précédemment, pourraient être la rugosité de surface et la contribution du ménisque.

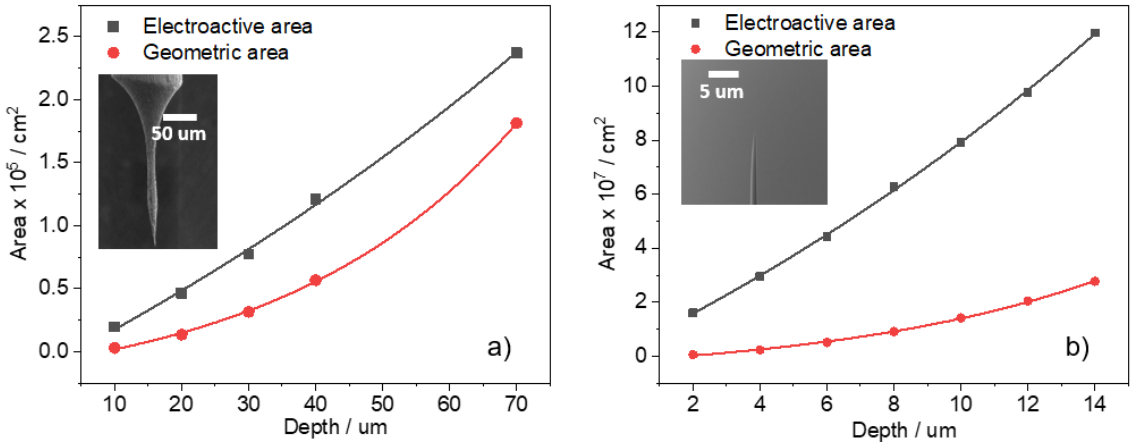

Figure 1.7 **Paramètres géométriques du cône liés à la surface latérale pour a) la pointe 1 et b) la pointe 2.**

Une deuxième électrode, nommée pointe 2, a été gravée par FIB après la fabrication électrochimique afin de la rendre plus nette et plus lisse. Pour cette électrode, la surface spécifique s'est avérée être considérablement plus petite par rapport à celle de la pointe 1. Comme le montre la figure 1.7 b, les valeurs de la surface électroactive sont comparables à celles géométriques calculées par SEM pour les deux pointes. Les expériences ont été confirmées avec trois pointes différentes.

La Figure 1.8 montre le rapport de la surface électroactive à celle géométrique ESA/GA en fonction de la profondeur de la pointe dans la solution pour trois embouts différents. Le graphique

montre un comportement intéressant dans lequel le rapport ESA / GA augmente rapidement lorsque la profondeur de la pointe en solution est inférieure à 20 µm, ce qui pourrait être indicatif qu'au sommet de la structure conique il y a une amélioration du transfert d'électrons en raison de la forme et des dimensions. Il est intéressant de noter que même si la forme de la pointe, le *ROC* et le rapport d'aspect *H* sont très différents pour les trois pointes présentées, le comportement du rapport *ESA / GA* est similaire pour chacun d'eux. Cependant, il n'y a pas de relation apparente entre le rapport *ESA / GA* et *ROC* ou *H*, ce qui est mis en évidence par le fait que le rapport semble diminuer plus rapidement avec la profondeur de la pointe pour la pointe 3 (courbe bleue), tandis que pour les pointes 1 et 2, les valeurs semblent plus proches.

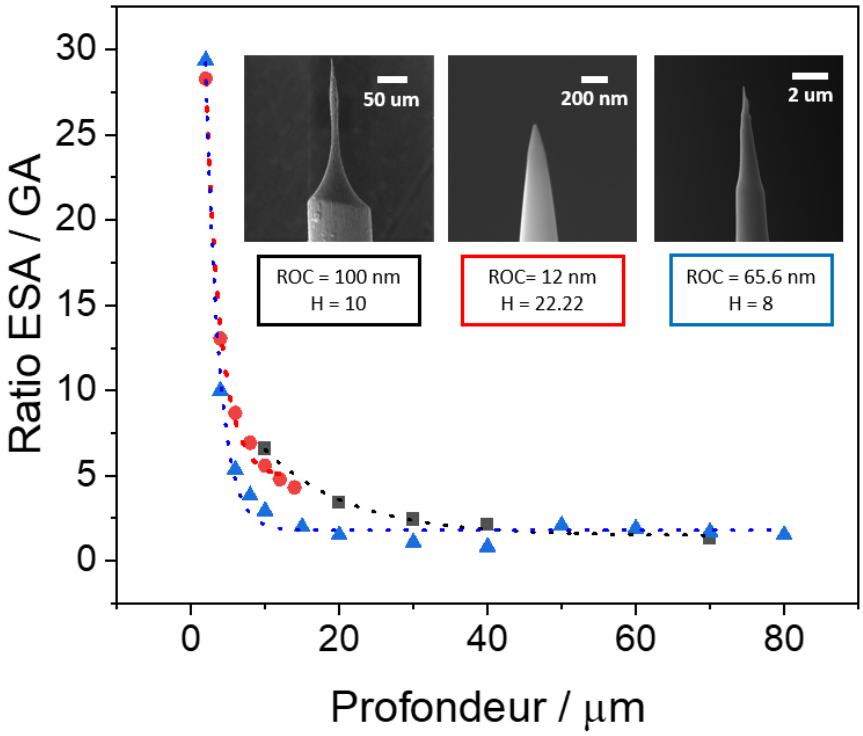

Figure 1.8 **Ratio ESA / GA en fonction de la profondeur de la pointe en solution, pour trois pointes différentes**

Également, il est à noter à la figure 1.8 que les valeurs du rapport ESA / GA sont similaires (entre 1 et 2) pour les pointes 1 et 3 (courbes noire et bleue) lorsque la profondeur de la pointe est de 40 à 70 µm. Étant donné que ces valeurs semblent devenir constantes, nous pourrions considérer cela comme la contribution de la rugosité. Par conséquent, l'augmentation soudaine des valeurs de rapport avec des profondeurs inférieures à 20 µm peut être attribuée à une amélioration du

transfert d'électrons dans le sommet de la pointe dû à un effet de concentration du champ électrique, ou à la contribution du ménisque.

Il a été précédemment rapporté [15], [17], [18] que les électrodes nanostructurées sont capables de produire à de faibles surtensions appliquées, des champs électriques locaux élevés qui concentrent les cations électrolytiques, conduisant à une augmentation de la réduction de CO_2 due à une concentration accrue . Selon des simulations effectuées par Liu et al. [17], cela pourrait être dû à une éventuelle amélioration du champ électrique, car il existe un champ électrique dix fois plus élevé associé aux pointes métalliques de taille nanométrique par rapport aux régions d'électrons quasi-planaires. Ce fait est intéressant, car il a été démontré que les performances d'une nano aiguille dépassent d'un ordre de grandeur les performances de pratiquement n'importe quel catalyseur à base de métaux nobles, de nanoparticules et d'oxydes [17].

D'autres études basées sur des simulations proposent la concentration des champs électriques au sommet de réseaux de nanocônes en Au [17], Cu @ Sn [18] et structures de Cu_1^0 – Cu_1^{x+0} [15]. On pense que cette concentration du champ électrique a augmenté la concentration de cations électrolytiques en raison d'une caractéristique conique nette qui à son tour a conduit à une concentration locale élevée de CO_2 améliorant sa réduction électrochimique.

4. Déposition d'or

L'un des facteurs qui affectent la forme des pointes de tungstène résultantes est le ménisque qui se forme à l'interface air-solution lors de la gravure des fils. Cependant, ce ménisque est également présent lors des mesures électrochimiques aux pointes de tungstène. Il est donc important de quantifier sa contribution au signal électrochimique enregistré dans les voltampérogrammes cycliques. Dans le présent travail, la hauteur du ménisque a été mesurée en fonction du diamètre du fil, pour quantifier la surface de l'électrode recouverte par le ménisque.

Le dépôt électrochimique d'or a été effectué sur des fils de tungstène de diamètres différents dans une solution à 1 % en poids d'acide chloroaurique ($HAuCl_4$) à la hauteur du ménisque. Pour ce faire, les fils de tungstène ont été approchés à la surface de la solution jusqu'à ce qu'il prenne contact. Une fois en contact avec la solution, un potentiel de -0,2 V vs AgAgCl (1M KCl) a été appliqué aux fils pendant 15 secondes pour poursuivre le dépôt cathodique d'or.

Les valeurs de la hauteur du ménisque ont été tracées en fonction du diamètre du fil de tungstène comme le montre la figure 1.9. Le comportement de la hauteur du ménisque (h) présente une variation linéaire avec le diamètre du fil (d). L'équation décrivant ce comportement indique que la

hauteur du ménisque double approximativement le diamètre du fil, et suivant cette tendance, la hauteur du ménisque pour les pointes de tungstène fabriquées passerait d'environ 25 à 635 nm en prenant les diamètres au sommet comme *d*. Cependant, la variation du diamètre due à la structure conique des pointes n'est pas prise en compte dans ces résultats et il a été nécessaire d'effectuer des études similaires en utilisant des pointes coniques plutôt que des fils.

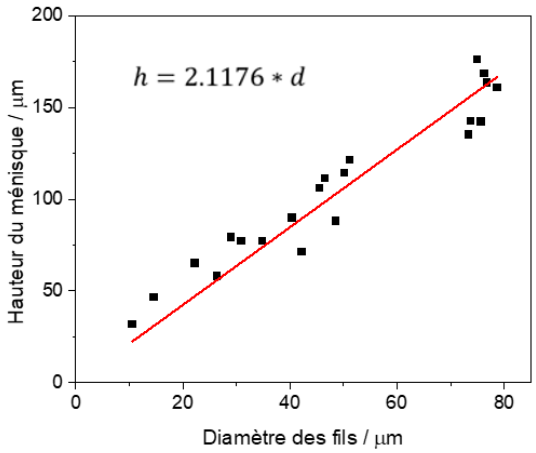

Figure 1.9 **Hauteur du ménisque vs diamètre des fils de tungstène**

Le dépôt d'or a donc été effectué sur la surface des pointes de tungstène. La Figure 1.10 montre les images SEM obtenues à partir de quatre embouts différents après l'électrodéposition de l'or. Pour les Figures 1.10 a et b, il a été possible de déposer de petites grappes de nanoparticules et d'agglomérats de type chou-fleur d'or d'environ 200 à 500 nm, montrant une concentration accrue à l'extrémité de la pointe ou à proximité. La caractérisation électrochimique de ces embouts a été tentée, mais seul le signal du tungstène a été obtenu. Cela pourrait être dû à la plus grande quantité de tungstène par rapport à celle d'or.

Pour cette raison, des temps de dépôt plus longs ont été tentés. Les Figures 1.10 c et d montrent que la croissance de l'or sur les embouts ne forme plus des particules ressemblant à du chou-fleur, mais plutôt à des dendrites, dont la longueur est plus élevée en se rapprochant au sommet de la pointe.

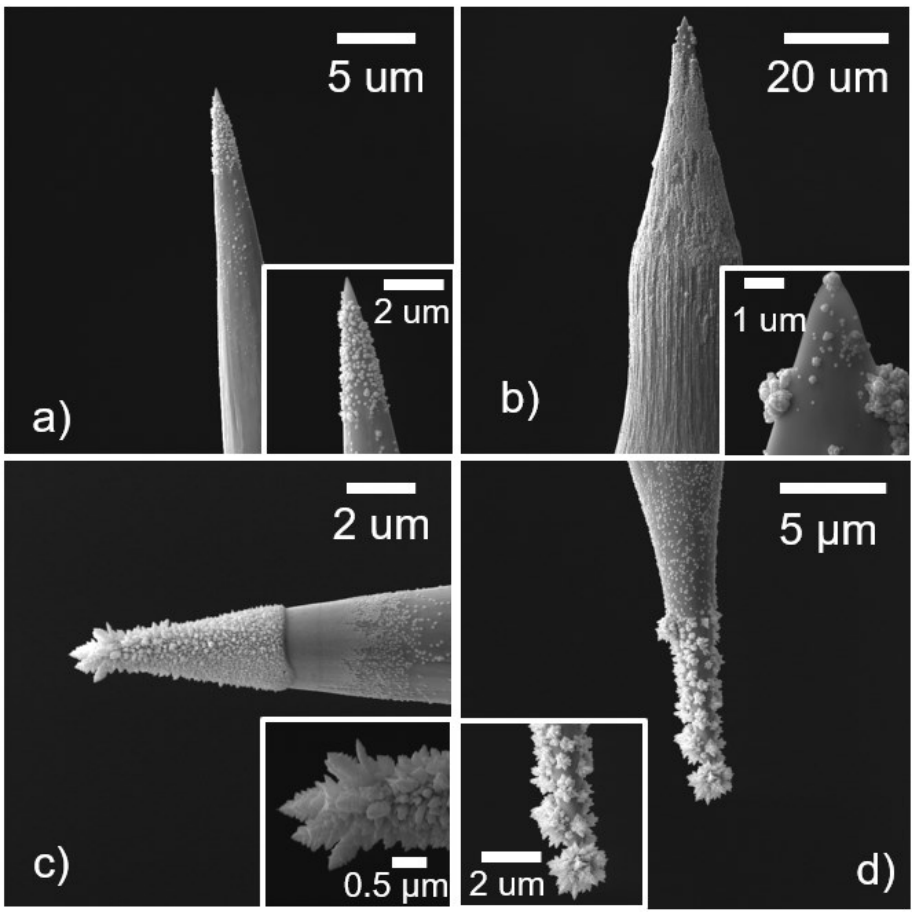

Figure 1.10 Différentes pointes après le dépôt d'or

Le dépôt d'or a été effectué dans une solution aqueuse de 0,1 % en poids de $HAuCl_4$ à -0,2 V vs Ag / AgCl (1 M KCl), pendant a-b) 5 s; c) 10 s; et d) 15 s.

Les différentes morphologies obtenues pourraient être une indication des changements dans la direction de croissance des faces de cristal d'or sur les pointes de tungstène. Cela a déjà été étudié par El-Deab et ses collègues, qui ont utilisé l'électrolyse par étapes potentielles pour faire croître des nanoparticules d'or sur une électrode de carbone vitreuse à partir d'un bain électrolytique comprenant $NaAuCl_4$ et H_2SO_4. La caractérisation a révélé que les particules déposées présentaient le plan Au (111) comme orientation cristalline prédominante avec une taille de particule supérieure à 100 nm [25], [26].

Le comportement électrochimique des différentes structures qui se forment à la surface des pointes de tungstène a été testé sur des embouts obtenus avec différents paramètres. La Figure 1.11 montre les voltampérogrammes cycliques correspondants effectués sur ces pointes déposées avec de l'or. Pour chacun d'eux, le pic caractéristique indiquant l'oxydation de la surface

de l'or apparaît, et même si la plage de potentiel de travail est la même auquel le tungstène s'oxyde, aucun signal correspondant à la formation de l'un des oxydes de tungstène n'est observé. Pour chacune des pointes étudiées, il a été observé qu'avec un cyclage continu, le courant de pic pour l'oxydation et la réduction diminuent, ce qui indique une dissolution de l'or. Ce comportement est également couramment observé avec les macroélectrodes [19].

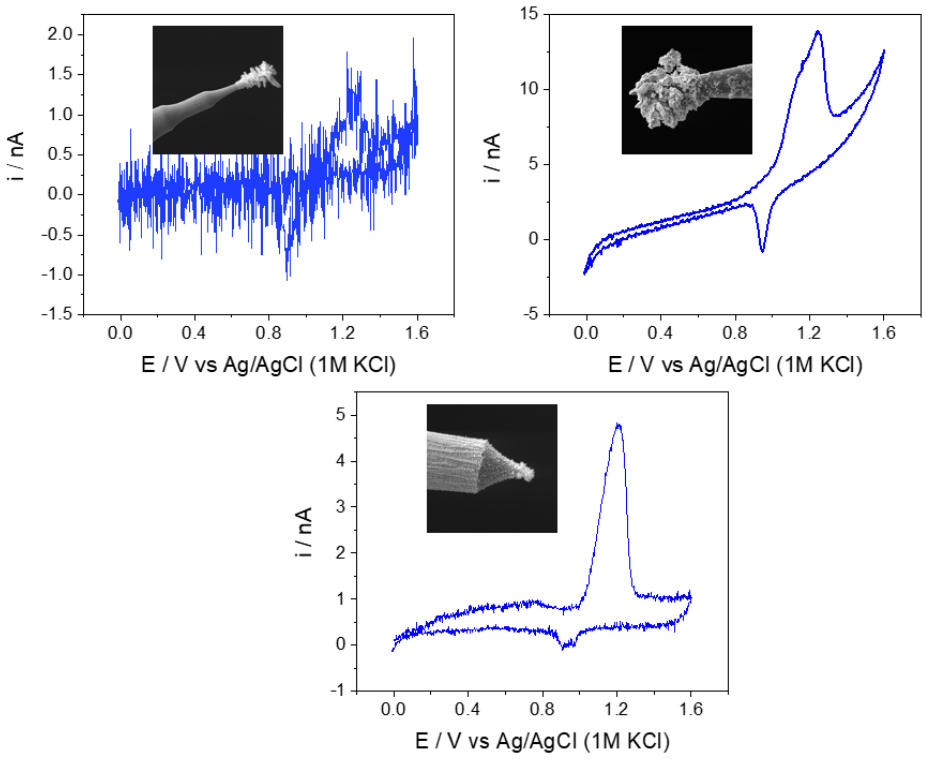

Figure 1.11 **Voltampérogrammes cycliques de pointes déposées avec de l'or dans de l'acide sulfurique 0,5 M.**

Dans la Figure 1.11, les valeurs de potentiel de pic pour l'oxydation de l'or sont : 0,993, 0,932 et 0,988 V vs SHE respectivement. Si on compare ces valeurs avec ceux rapportés dans la bibliographie, on peut dire que les plans prédominants dans chacune des pointes sont (110) pour a, (100) pour b et (110) pour c. Cette découverte indique qu'il serait possible d'obtenir sélectivement certains plans cristallins qui sont prédominants. Cependant, ces expériences nécessitent une validation supplémentaire, car les vitesses de balayage de la littérature et ceux expérimentaux sont différents. En outre, il est prévu que l'Au (111) domine, car c'est le plan le plus stable thermodynamiquement [27]. Cependant, à partir des voltampérogrammes de la figure 1.11, on peut conclure qu'il existe différents plans poussant sur nos pointes en fonction de la

position différente des pics d'oxydation, même si les voltampérogrammes ont été enregistrés dans les mêmes conditions expérimentales.

La sélectivité des plans cristallins obtenue lors de la croissance électrochimique de l'or sur les pointes de tungstène est très importante, car il est bien connu que ce matériel est un bon électrocatalyseur pour l'oxydation de différentes molécules comme les alcools, le CO et la réaction de réduction de l'oxygène. Ces molécules s'adsorbent directement sur la surface métallique subissant des réactions de transfert d'électrons. Donc, la cinétique de réaction dépend directement des propriétés des électrodes telles que les plans cristallins exposés et les défauts.

Ainsi, la caractérisation électrochimique de quelques nanoparticules d'or bien définies permettrait de corréler l'activité et la stabilité avec la structure. Il permettra de surmonter une limitation des approches traditionnelles où le courant provient de grandes zones macroscopiques.

Conclusions

Une méthode basée sur l'induction intentionnelle de perturbations du système en rétractant lentement les fils tungstène de la solution pendant le processus de gravure a été développée, résultant en des pointes longues et pointues.

Les principales limites de l'utilisation d'ultra-microélectrodes de forme conique ont été identifiées comme étant le diamètre de la pointe, la rugosité de la surface et la possible contribution non homogène du ménisque au signal électrochimique à l'interface air-solution. Le diamètre de la pointe peut être partiellement contrôlé pendant la gravure électrochimique et encore être modifié par la gravure concentrée des grains ioniques. Cette dernière technique a été utilisée avec succès pour résoudre le problème de la rugosité de surface. Cependant, la contribution non homogène du ménisque au signal électrochimique reste à étudier. Des simulations numériques d'expériences similaires seront effectuées afin de découvrir la conformité avec les résultats expérimentaux pour écarter la contribution du ménisque au signal électrochimique.

Nous avons trouvé des preuves expérimentales directes suggérant une concentration du champ électrique à l'apex de la pointe en raison de sa forme et de sa taille. La preuve la plus importante a été trouvée par l'électrochimie, où il a été observé que le rapport de ESA / GA présente une énorme augmentation exponentielle lors de l'exécution des mesures dans des zones proches de l'apex et devenant presque constante lorsque la pointe est plus profonde en solution. Enfin, les dernières preuves ont été observées lors du dépôt d'or sur les pointes, où une croissance

dendritique a été observée, où plus on s’approche du sommet de la pointe, plus les dendrites sont longues.

Tous les résultats obtenus montrent que l'approche que nous avons utilisée a un grand potentiel pour étudier l'électrochimie à entité unique, ce qui contribuerait à la compréhension globale des principes physiques sous-jacents, des mécanismes de réaction et de la dynamique des processus électrochimiques. En outre, grâce à la taille et à la forme des électrodes obtenues, elles ont également des applications biologiques potentielles pour l'étude des réactions redox métaboliques se produisant à l'intérieur des cellules vivantes individuelles ou même des organites simples tels que la mitochondrie. Ces réactions ont été largement étudiées par les biochimistes et ils sont d’une grande importance pour la fonction générale des organismes vivants, mais jouent également un rôle très important dans le développement de certaines maladies chroniques telles que le cancer.

TABLE OF CONTENTS

LIST OF FIGURES

LIST OF TABLES

1 INTRODUCTION

Many physical and biological processes in nature involve reactions that entail electrons, creating or using electronic charges and currents. These processes occur only at specific energies determined by the potential of the reactions involved and it is possible to study them by experimentally measuring their fingerprint potential. This principle forms the basis of electrochemistry, a branch of physical sciences that exists since 1800 [1].

Given the widespread occurrence of electrochemical reactions in nature and industrial processes, several applications of electrochemistry have been found in different fields. Many traditional technologies such as the production of aluminum from raw ore, electroplating, brine electrolysis for Cl_2 and NaOH production, energy storage and energy conversion devices are based on electrochemical reactions. New emerging technologies including the reduction of CO_2 from industrial smoke and efficient water cleaning, are as well based in electrochemistry. Similarly, in biological organisms, electrochemistry governs many vital processes such as communication between cells and metabolic reactions in the cellular matrix and in the membrane system [2]–[8].

Traditionally, electrochemical measurements are made with macroscopic, bulk electrodes. In this regard, the materials of interest are usually shaped on millimetre to centimeter sized electrodes and the current originating from large macroscopic areas is measured. Although, this traditional approach produces strong signals that are perfect for quantitative analysis [9]–[11], it lacks the capability to resolve single entities, or submicron structural heterogeneities, that contribute to the electrochemical signal. It averages out different structures and hence, it becomes impossible to perform in depth studies of chemical reactions occurring at different sites.

With modern developments in nanofabrication, simulations and computer-aided design, as well as in state of the art potentiostats, it is now possible to achieve electrochemical measurements from submicron-entities [12]–[14]. The richness of the microscopic world and the scientific prospects that would follow from such an achievement, form the basis of the interest of this work, focused on developing and studying sub-micron electrochemical systems.

As we go from bulk to single-entity electrochemistry, unconventional effects are expected to appear. In electrochemistry, we are interested in the electron transfer processes between an electrode and chemical species in a solution. This electron transfer occurs at the electrical interface formed between the electrode and the electrolyte. This interface commonly referred as electrical double layer, is well defined and is characterized by a sharp transition of the electrical

potential and it has properties that are completely different from those of the bulk solution. This potential difference, typically between 0.1 and 1 V, extends over the length of the double layer (in the order of angstroms) resulting in a large electric field (10^9 – 10^{10} Vm^{-1}) which is responsible for the electron transfer between the electrode and the species in solution.

One of the main challenges related to the study of single entity electrochemistry (and electrochemistry at the nanoscale) lays on the fact that submicron scale electrodes are needed to minimize the contribution of the electrode's surface to the signal and to achieve high spatial resolution. Another is that very low current intensities (usually of the order of pA) are produced by the entities of interest in this kind of experiments which requires special equipment with a very high signal/noise ratio and stability [5]. For tasks that require an extended measurement range unavailable with conventional instruments, such as for detecting or measuring currents less than 10 nA or resistances greater than 1 GΩ, instruments with special electrometers are needed [13].

There are many approaches to study single nanoparticle electrochemistry, being the main one the study of particle collisions on an UME, where the intrinsic electron transfer properties of the nanoparticles and the interaction between the nanoparticle and the electrode surface are studied [28]. The second approach is the use of SECM where an UME is used to probe a single nanoparticle. From these experiments it was possible to obtain quantitative physicochemical information from the nano-electrochemical data. The advantage of this approach is that one nanoparticle can be electrochemically characterized in situ and afterwards be used again to perform kinetic experiments. And one of the main characteristics of SECM in one of its operational modes is that by using the tunneling effect between the electrode and the nanoparticle, it is possible to perform the imaging of the entity to obtain topographical information [29]. With this approach it is possible to characterize the shape and differentiate between, for example cubic and spherical nanoparticles. These results have been confirmed by transmission electron microscopy (TEM) [30].

The most convenient approach for the study of single entities is the immobilization of nanoparticles on ultra-microelectrodes (UME's) in order to record the direct faradic response. It has been demonstrated that the voltammetric response strongly depends on the size of the nanoparticle and the feasibility of studying electrocatalytic activities on single nanoparticles has been proved [19], [20]. This approach is especially useful to better understand the structure-function relationship in nanoparticle-based electrocatalysis.

In order to carry out the immobilization of single entities it is necessary at first to develop suitable electrodes capable of holding and recording their electrochemical signals. The most popular techniques consist on the encapsulation of metals into glass or the micropipette pulling technique in order to generate electrodes with suitable dimensions to support such small entities [31], [32].

The fabrication of nanoscale electrodes and tips is in constant improvement, but still hindered by the need of laborious steps (eg. encapsulation, pipette puling and polishing), expensive instrumentation (focused ion beam milling of chemical vapor deposition carbon filled micropipettes) and the success rates are sometimes less than 10 % [5] [8]. Therefore, it is still necessary to develop simple fabrication techniques of submicron electrodes that allow us to study electrochemical processes at the nanoscale.

The evaluation of nanometer size electrodes has been done before by Mirkin et al. [33] by using scanning electrochemical microscopy SECM and they found that the steady-state current-distance (i_T-d) characteristic curves for microelectrodes are highly dependant on the electrode geometry. Due to this dependence they came to the conclusion that the shape of an ultramicroelectrode can be determined from its scanning electrochemical microscopy response [33].

Recent experimental and computational studies suggested that electrodes formed by nanoparticles with conical (tips) structures at the nanoscale (with a tip diameter of < 30 nm) have the ability to concentrate electric fields (10 times higher compared to a planar electrode) via the accumulation of a large concentration of electrolyte cations at metallic nanometer-sized tips [15]–[17]. This field-induced reagent concentration was used to explain increased electrocatalytic activity of macro electrodes formed by gold nanoneedles for the electrochemical reduction of CO_2 to formate compared to other gold nanoparticles [18]. However, this kind of electrodes are characterized by a higher density of active sites, short diffusion pathways and thus a higher concentration of active species near the electrode. An enhanced transport of reactants to the surface of the electrode can also increase the apparent rate of the reaction.

Metallic sharp tips have found a wide number of applications in scanning probe microscopy techniques such as atomic force microscopy (AFM) or scanning tunneling microscopy (STM), for multipoint contact measurements, nanolithography and nano-manipulation [14]. Due to their chemical stability, the most common materials used to prepare these tips are gold, iridium, nickel and platinum [15], [16], [20], [21]. However, this stability implies a laborious sharpening process to obtain tips with controllable shapes and diameters down to some nanometers.

Tungsten has been used as an alternative tip material because very sharp tips can be prepared in a simple and robust way by using electrochemical etching [14], [17]–[19], [22]–[25]. However, to the best of our knowledge, W has never been proposed as a material to fabricate submicron electrodes for single entity electrochemistry. There are two main oxides that passivate the surface of tungsten, tungsten dioxide (WO_2) and tungsten trioxide (WO_3) [26]–[29], which have prevented its wide application as electrode material. However, during our investigations with this material, we realized that we can use the formation of oxides on the tungsten surface in our favor, as it will be explained in section 5. We found out that we can selectively oxidize the surface of the W electrode in a controlled fashion to WO_2, forming a very stable and conductive surface whose potential to be used as an electrode is shown in section 5.

Many authors have immobilized single metallic nanoparticles on platinum and gold nanoelectrode and studied their fundamental electrochemical properties and their size-dependant electrocatalytic activities [13], [19], [29], [34]. This is important because the challenge of only being able to get averaged responses from ensembles using the traditional methods has been overcome. Also, the sensitive character of the nanoparticle ensembles to spacing has been solved this way, because when immobilizing a single nanoparticle on an electrode surface, the overlapping of diffusion layers is avoided.

In this work we successfully fabricated and characterized micro and nanoscale electrodes using simple electrochemical techniques. This represents one of the first building blocks for electrochemistry at the nanoscale and eventually at single entities.

2 Objectives

2.1 General objective

The objective of the present project is the fabrication, microscopical and electrochemical characterization of nanoelectrodes consisting of sharp tungsten tips, that could eventually be used as a support for single entities, i. e. gold nanoparticles, or clusters of them.

The specific objectives of the present project are the following:

2.2 Specific objectives

- Construction of the experimental setup to be used for the preparation of sharp tungsten tips and in the electrochemical measurements at the nanoscale.
- Characterization of the voltammetric response of tungsten to demonstrate its feasibility to be used as an electrode material.
- Standardization of a methodology to fabricate very sharp tungsten tips to be used as electrodes.
- Morphological and electrochemical characterization of the tip-electrodes.
- Deposit or growth of single gold particles or clusters of them at the tip-electrode apex.
- Voltammetric characterization of the entities attached to the tip apex.

3 BIBLIOGRAPHIC REVIEW

Much of the contemporary chemistry focuses on small scale structures, and in fact, all molecular sciences are intrinsically at the nanometer scale. For that reason, all the scientific disciplines from biology to physics have developed a great interest in nanotechnology and nanoscience. According to a statement of the US National Science and Technology council [35], "*the essence of nanotechnology is the ability to work at the molecular level, atom by atom to create large structures with fundamentally new molecular organization. The aim is to exploit these properties by gaining control of structures and devices at atomic, molecular and supramolecular levels and to learn to efficiently manufacture and use these devices"*. Nanoscience is the study of properties and behaviours of structures and materials at the scale of nanometers, including the study of natural phenomena such as the fascinating field of bio-systems whose fundamental reactions occur at the micro and nanoscale.

For centuries, electrochemistry has played a key role in important areas for various technologies including as electroplating, corrosion and energy conversion and storage. However, in the last two decades, electrochemistry has become very active in research at the nanoscale. There is a continuous emergence of new experiments, methods, tools and applications that take advantage of the complementarity of both nanoscience and nanotechnology, focusing on the development of single nanoelectrodes, nanopores and nanoparticles with dimensions of only a few nanometers.

The developments in the modern society and the improvement of quality of life has benefitted strongly by the advances in electrochemistry and therefore it is important to understand the fundamentals of this discipline. In the following sections an introduction to electrochemistry will be given starting from a general point of view to finally get to the study of electrochemical reactions at the nanoscale.

3.1 Electrochemistry

Electrochemistry is defined in most of the literature as the branch of chemistry that studies the transformation between electric and chemical energy [36]. However, a more accurate statement would be that electrochemistry is the study of phenomena at electrified interfaces, taking a special focus on the interactions between phases containing electrons, and phases containing ions.

Our world is full of interfaces that are electrically charged and their understanding at different levels is of the interests of different disciplines. For example, the understanding of how these charges move and interact at the interfaces is a direct goal of physics, while putting them together into a cell for their study brings in the materials science of the electrodes and the chemistry of the species in solution. Not to mention that a great amount of these processes is of interest for biology, since most of the metabolic reactions happen at interfaces in the living cells. In this way, electrochemistry spans a swathe of science that involves a multidisciplinary approach.

The phenomena studied by electrochemistry are denominated electrochemical processes and they consist on redox (reduction-oxidation) reactions where the energy that is released by a spontaneous reaction becomes electricity, or where the electricity is used to induce a non-spontaneous chemical reaction [37].

These electrochemical processes are studied for a variety of reasons. In some investigations, electrochemical methods can be used as a tool for the study of chemical systems such as when trying to obtain thermodynamic information from a chemical reaction; to generate unstable radicals to study its rate of decay or when analyzing a solution for traces of metallic ions or organic molecules. In some cases, the electrical and conversion efficiencies of the systems are a priority like when designing new power sources or when carrying out the electrosynthesis of chemical products respectively [38].

Even though the idea of studying processes at single interfaces sounds natural, it is not possible to do it due to the lack of experimental tools that allow us to deal with isolated boundaries. Therefore, it is necessary to study the properties of a collection of interfaces called electrochemical cell [38]. Usually these systems are defined as two conductors called electrodes immersed in, and separated by at least one electrolytic phase [37]. A difference in electric potential can be measured between the two electrodes, which is a measure of the energy available to drive charge externally between the two electrodes. These two conductors are called anode and cathode. The anode is the one at which an oxidation reaction occurs, and the cathode is where reduction takes place.

There are two different kinds of electrochemical cells. Galvanic cells are those at which the reactions at the electrodes happen spontaneously and produce a movement of electrons from the anode to the cathode through an external conductor. The main function of these cells is to store electrical energy such as in batteries, which are usually made from several galvanic cells connected in series to produce higher voltages than a single cell can produce. On the other hand, at electrolytic cells, the reactions at the electrodes do not happen spontaneously and therefore an external source of electrical energy is needed for operation [37]. For the purposes of the present project, electrolytic cells as the one shown in Figure 3.1 were used.

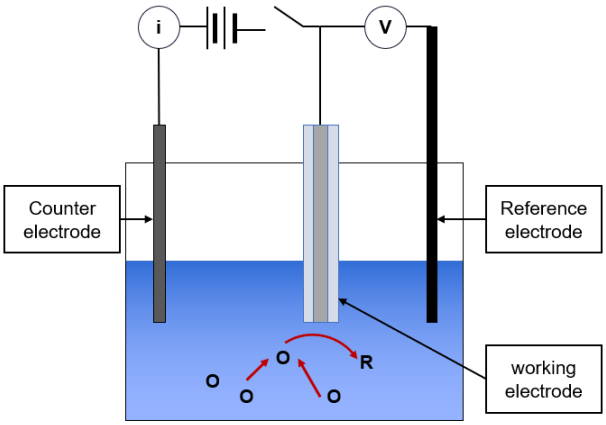

Figure 3.1 Example of electrolytic cell

(V) represents the externally applied voltage between the working and the reference electrodes, that are connected by a high impedance circuit to avoid the electrons to flow towards or from the reference electrode. As a result of this voltage, the generated current (*i*) flows from or towards the counter electrode. The red arrows in the Figure represent the oxidized species (O) in the electrolyte solution moving towards the working electrode (anode) and the resulting reduced species (R).

In electrolytic cells, it is common that only the electrochemical process occurring at one of these electrodes is the one of interest and therefore this electrode is called the working electrode (WE). The electrode at which the opposite reaction occurs takes the name of counter electrode (CE). Since there is an electric current flowing between WE and CE to make the corresponding reactions happen, it is necessary to have a third electrode that allows us to measure and/or control the voltage of the WE without having the interference of the reactions happening at the CE. This third electrode is called the reference electrode (RE) and is made up of phases with a constant composition and therefore a constant potential that allows us to say that any changes in the electrochemical cell are ascribable to the WE.

The internationally accepted reference electrode is called the normal hydrogen electrode (NHE) or standard hydrogen electrode (SHE) because all its components are at unit activity [38]. The potentials are commonly reported with respect to different references such as the silver-silver chloride electrode (Ag/AgCl (1M KCl)) whose potential is 0.58 V vs SHE.

In an electrochemical cell, the reactions of interest happen at the electrode-electrolyte interface. This zone is known as the electrical double layer. The side of the solution in this region is thought to be made up of several layers [38] (Figure 3.2). The inner layer contains solvent molecules and sometimes ions that are specifically adsorbed. The locus of this layer is known as the inner Helmholtz plane (*IHP*) that is at a distance x_1 and has a total charge density σ^i due to the specific adsorbed ions. The solvated ions in solution can approach the electrode surface only to a distance X_2. The locus of the center of the nearest solvated ions is called the outer Helmholtz plane (*OHP*). The ions in this layer are non-specifically adsorbed.

The non-specifically adsorbed ions are distributed in a three-dimensional region called the diffusion layer that extends from the *OHP* to the bulk of the electrolytic solution. In this diffusion layer, the ions move freely due to thermal agitation. The excess charge density in the diffusion layer is σ^d. The thickness of the diffusion layer depends on the concentration of the electrolyte. For concentrations greater than 10^{-2} M, the thickness is less than 100 Å [38].

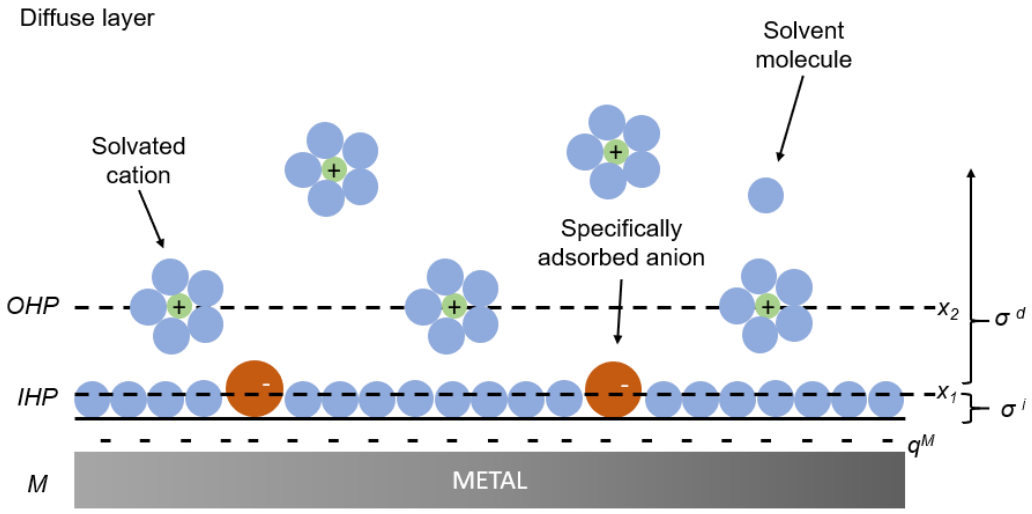

Figure 3.2 **The electrical double layer** [38]

The structure of the double layer affects the rates of electrode processes. This is because the electroactive species approach the electrode surface only until the *OHP* and the total potential it experiences is less than the one between the electrode and the solution due to the potential drop across the diffusion layer [38].

An important characteristic of the electrical double layer is the double layer capacitance (C_{dl}), which appears at the interface between the conductive electrode and the adjacent liquid electrolyte. At this boundary two layers of opposite charges are formed, one at the surface of the electrode, and one in the electrolyte. These two layers, electrons on the electrode and ions in the electrolyte, are typically separated by a single layer of solvent molecules that adhere to the surface of the electrode and act like a dielectric does in a conventional capacitor. The amount of electric charge stored in the double layer is called the double layer capacitance (C_{dl}).

In electrochemistry it is common to say that we either measure or control the potential with respect to the reference electrode and this is equivalent to say that we can measure or control the energy of the electrons on the working electrode. Thus, by polarizing the electrode to negative potentials, the electrons energy is raised and if the polarization is high enough, they can reach a level at which they can be transferred to vacant electronic states of the electrolyte, generating what is known as a reduction current. In a similar way, a flow of electrons from the solution to the electrode can be generated by imposing a more positive potential, giving place to an oxidation current [38].

As mentioned before, in a typical electrochemical experiment we focus our attention on the reactions happening at the working electrode. If we take the reduction of Fe^{3+} to Fe^{2+} at the cathode, we know that every ion reduced needs one electron that must be transported to the electrode from the external circuit. The source of such electron is another chemical species in the solution that is oxidized at the anode. This electron flow from the anode to the cathode by way of the external circuit is what is called *current* and since the electrons are supplied in an integral stoichiometric basis in the electrode reactions, the flow is directly proportional to the rate of reaction [39], [40].

Depending on the way that the variations of potential are applied to the electrodes, different electrochemical techniques have been developed and from all of them, different information about the reaction happening at the interface electrode/solution is obtained.

3.1.1 Electrochemical methods

Even though only potential, current and time are the three basic parameters in electrochemistry, there are many different possible experimental designs. In general, the electrochemical methods can be divided in bulk techniques where a property of the solution in the cell is measured (i. e., the solution's conductivity), and interfacial techniques in which the current, charge and potential depend on the species that are present at the interface between the electrode and the solution [39]. For the purposes of the present work, only the interfacial techniques are of interest.

In order to understand the interfacial electrochemical techniques there are some important things to be taken into account: (i) electrochemical systems are not homogeneous; (ii) the electrode potential determines the analyte's form (oxidized or reduced) at the electrode surface; (iii) the concentration of the chemical species might not be the same at the electrode surface compared to the bulk solution; (iv) other chemical reactions besides the reduction-oxidation ones might take place; (v) the current is a measure of the rate of oxidation or reduction of the analyte; (vi) potential is an expression of electron energy; and (vii) it is not possible to simultaneously control the current and the potential [39]. As explained in the following chapters, species containing iron were used for the experimental part of this work and therefore the Fe^{3+}/Fe^{2+} redox couple will be used to explain these concepts.

The fact that the electrode potential determines the form of the chemical species in solution can be illustrated by Figure 3.3. If an electrode is placed in a solution containing Fe^{3+} and Sn^{4+} and its potential is adjusted to 0.5 V vs SHE, the Fe^{3+} would be reduced to Fe^{2+} but the Sn^{4+} species would remain in the same oxidation state. This is due to the standard reduction potential (E^0) of the two different redox couples. Thus, the oxidized species of Sn are stable at potential values higher than 0.154 V while the oxidized species of Fe is stable only at potential values higher than 0.771 V.

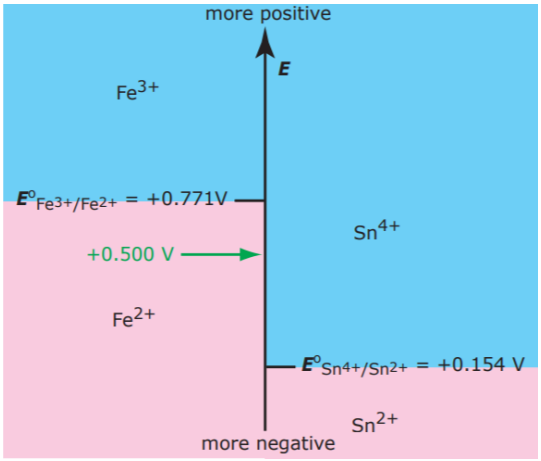

Figure 3.3 Ladder diagram for Fe^{3+}/Fe^{2+} and Sn^{4+}/Sn^{2+} couples

Blue areas represent the potential ranges at which the oxidized species are stable. The reduced species dominate in the pink areas. Reprinted with permission from [39].

Since the electrode potential determines the oxidation state of the analytes in solution, we can then say that the concentration of chemical species is not the same in the vicinity of the electrode surface and in bulk solution. For example, if we put an electrode into a solution of Fe^{3+} and fix the potential to 1 V, the concentration of the oxidized species will remain the same at all distances from the electrode because it is stable at those potentials as it is shown in Figure 3.3. However, when moving the potential to 0.5 V, the concentration of Fe^{3+} ions will decrease to almost zero in the area nearby the electrode because they will be reduced to Fe^{2+}. The concentration of Fe^{3+} will increase as we move away from the electrode surface until it equals the concentration in the bulk. This concentration gradient will result in the movement of more Fe^{3+} ions moving towards the electrode surface, due to the normal Brownian motion that tends to homogenize the solution, giving place to what we know as diffusion of chemical species [40].

The previous concepts have already shown that electrochemical systems are heterogenous due to different factors. However, one of the concepts that make the electrochemical systems more complex is the fact that many processes happen simultaneously. This means that not only heterogeneous electron transfers occur. There are other heterogeneous processes such as adsorption or desorption of precursors, migration of atoms across a surface during the electro crystallization of metals, or the recombination of atoms or radicals [40]. For the specific case of the Fe^{3+}/Fe^{2+} system, the reduction of Fe^{3+} to Fe^{2+} might not be the only reaction that affects the concentration of Fe^{3+} in the bulk solution. Instead, the adsorption of Fe^{3+} at the electrode surface,

or the formation of a metal ligand complex such as $Fe(OH)^{2+}$ can be carried out in solution and therefore affect the concentration of Fe^{3+} [39].

One important concept to be understood is the standard potential (E^0), which is the critical energy at which both the oxidized and reduced species are at equilibrium, meaning that typically in a zone of about 100 mV wide centered on E^0, a statistical equilibrium of electrons on the electrode and on species in solution permits the mixture of both species in considerable amounts.

If a system is in equilibrium, for example a solution of Fe^{3+} and Fe^{2+}, the current in the external system is zero and a potential value governed by Nernst Equation will be read:

$$E = E^0 - \frac{RT}{nF} log \frac{[Fe^{2+}]}{[Fe^{3+}]} = E^0 - \frac{0.05916}{1} log \frac{[Fe^{2+}]}{[Fe^{3+}]} \quad (1)$$

Where E is the electrode's potential and E^0 is the standard-state reduction potential for the reaction $Fe^{3+} \leftrightarrow Fe^{2+} + e^-$. R is the universal gas constant (8.31446 J K^{-1} mol^{-1}), T is the temperature in Kelvin, F is the Faraday constant (96485.3321 C mol^{-1}) and n is the number of electrons transferred in the reaction.

If the potential is changed from the equilibrium position, a current will flow as the system moves to a new equilibrium position until it reaches zero again. Alternatively, if we pass a fixed current through the system, the reduction of Fe^{3+} to Fe^{2+} will be forced and therefore a concentration gradient will be produced, giving place to a change of the potential over time. Therefore, we can conclude that if we decide to control the potential, we cannot control the resulting current and vice versa [39], [40].

Since current and potential cannot be controlled at the same time, there are three main experimental designs used in electrochemistry: (i) the potential can be measured when the current is zero; (ii) the potential can be measured when the current is controlled; or (iii) the current can be measured while the potential is controlled.

For the different experimental designs, there are different instruments that can be used such as: a potentiometer that measures the potential of an electrochemical cell under a zero-current condition; a galvanostat that allows to control the current flowing through an electrochemical cell; or a potentiostat that allows to control the potential of the working electrode [38].

3.1.2 Voltammetric techniques

As mentioned before, in electrochemistry the interfacial techniques are of greater interest than the bulk techniques. Interfacial electrochemical techniques can be divided at the first level in static, where no current can pass through the solution; and dynamic, where current flows through the solution. Most of the interfacial techniques are in the dynamic group [39]. Figure 3.4 shows a general classification of the interfacial electrochemical techniques.

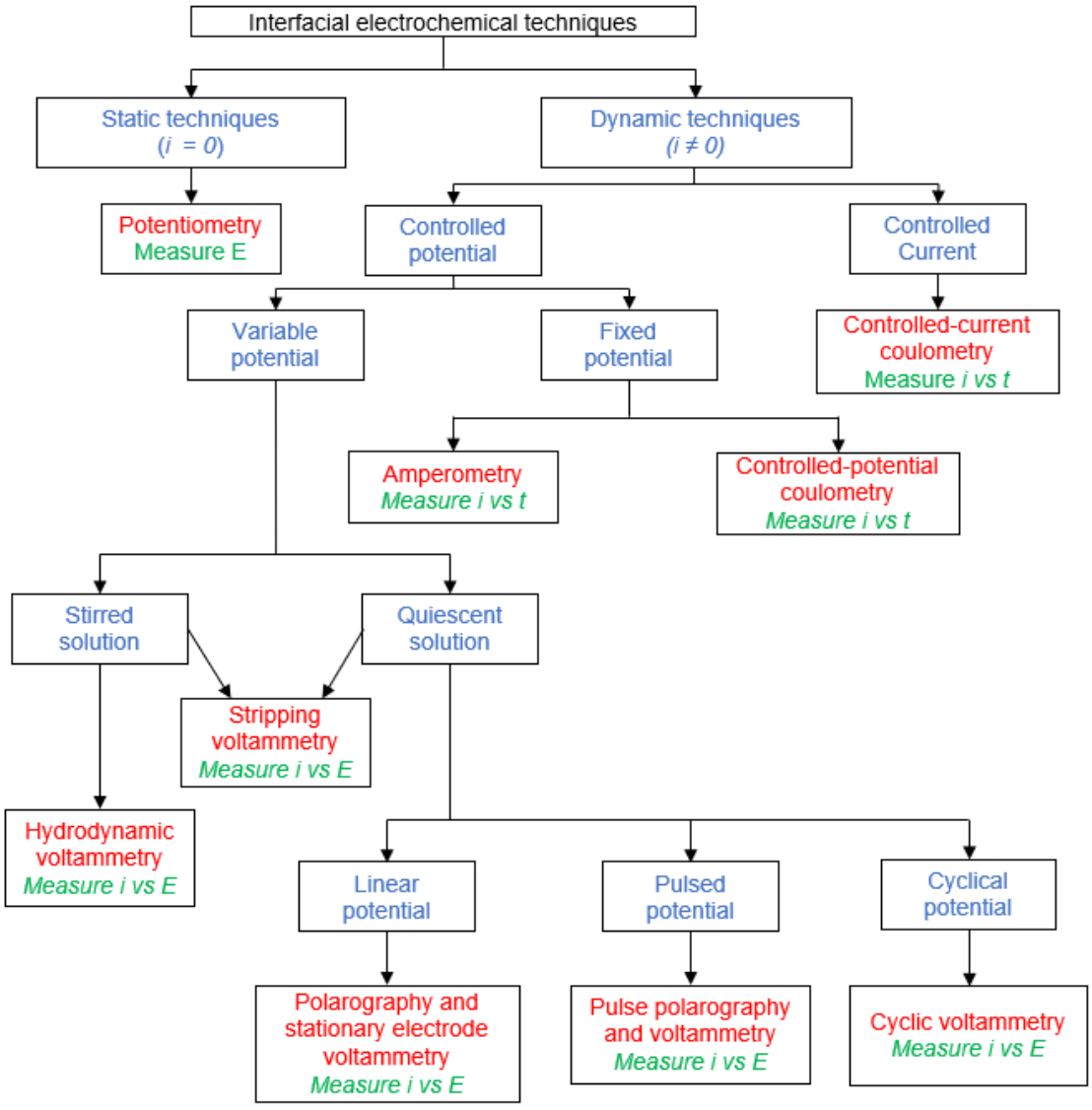

Figure 3.4 **Classification of the interfacial electrochemical techniques. Adapted with permission from [39.]**

All these interfacial electrochemical techniques are well described in literature, and there is very detailed information regarding the theory behind, and the applications for all of them. However, for the purpose of the present project, only voltammetric methods will be discussed, since the principal electrochemical technique used for the experimental part was cyclic voltammetry (CV).

Voltammetric techniques are considered as the fundamental electrochemical experiments which consist in applying a time-dependant potential to an electrochemical cell and the resulting current is measured as a function of the applied potential. The resulting plots are called voltammograms and provide qualitative and quantitative information about the species involved in the oxidation and reduction reactions. Additionally, from a physical-chemical point of view, thermodynamic and kinetic information of the electrochemical system can be extracted from them [41].

It is necessary to understand all the factors that influence the shape of a voltammogram in order to be able to extract information from them. The redox couple $Fe(CN)_6^{3-}/Fe(CN)_6^{4-}$ will be used in order to explain the main principles behind voltammetric measurements.

As explained before, when an analyte is oxidized at the working electrode, the electrons will pass through the potentiostat and they will arrive to the counter electrode where the reduction of either the solvent or other chemical species in solution will occur. Likewise, if we reduce an analyte at the working electrode, the current will flow from the counter electrode. In both cases, the current is due to the redox reactions taking place. These currents are known as faradaic currents.

If we assume a solution with an initial concentration of $Fe(CN)_6^{3-}$ of 1 mM, with no $Fe(CN)_6^{4-}$ species present and a potential more positive to that of the standard reduction potential is applied to the working electrode, the concentrations of both species will remain unchanged because no redox reaction will take place. However if we apply a potential equal to the standard reduction potential of the redox couple, some of the $Fe(CN)_6^{3-}$ species will be reduced until an equimolar concentration of 0.5 mM is reached at the electrode surface.

It is important to remember that the concentration of the species at the working electrode-electrolyte interface and in bulk solution are different. While the concentration of $Fe(CN)_6^{3-}$ decreases and $Fe(CN)_6^{4-}$ increases at the interface, the concentration of $Fe(CN)_6^{3-}$ remains unchanged at the bulk solution and the one for $Fe(CN)_6^{4-}$ continues to be zero. This concentration gradient creates a driving force that transports $Fe(CN)_6^{4-}$ away from the electrode surface and that brings $Fe(CN)_6^{3-}$ to the working electrode surface as illustrated in Figure 3.5. As the reduction reaction occurs, a faradic current will continue to flow until the concentrations of both species are the same at the working electrode surface and at the bulk solution [39].

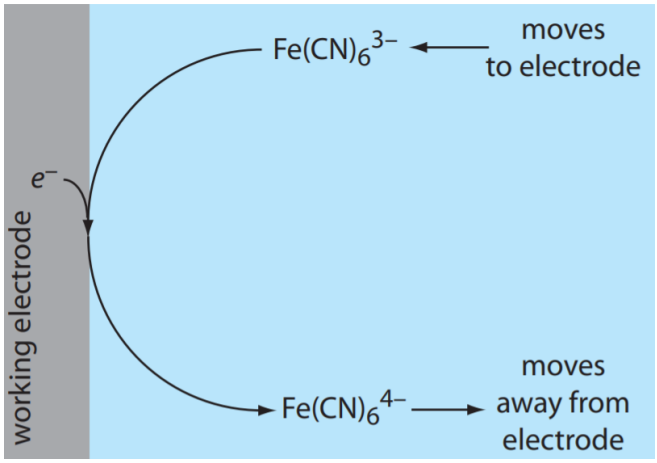

Figure 3.5 **Illustration of the transport of $Fe(CN)_6^{3-}$ towards the working electrode surface and the movement of $Fe(CN)_6^{4-}$ to the bulk solution due to the concentration gradient. Reprinted with permission from** [39].

It is clear that the potential of the working electrode determines whether a faradic current flows or not but the magnitude of this current is determined by the reaction rate, that is influenced mainly by three different factors: mass transport from the bulk to the electrode surface, the charge transfer at the electrode-electrolyte interface and electrolyte concentration [41].

Mass transport is the rate at which the reactants are transported to and from the electrode and it happens in three different ways: Diffusion, migration and convection.

Diffusion is the spontaneous movement of chemicals that happens when the concentration of a molecule at the surface of the working electrode and the one at the bulk solution is different. Thus, if a potential is applied to reduce $Fe(CN)_6^{3-}$ molecules, the result will be a concentration gradient as the one illustrated in Figure 3.6. The region nearby the electrode where diffusion occurs is known as the diffusion layer, and its width (δ) increases over time as the $Fe(CN)_6^{3-}$ has to diffuse from increasingly greater distances. This phenomenon occurs only when no other mass transport mechanisms exist in the electrochemical system under study [39].

Convection is the movement of materials contained within a volume of a stirred solution carrying reactants towards the electrode surface and removing products from the electrode. This mass transport mechanism can be minimized by keeping the solution quiescent.

Migration involves the movement of charged particles in an electric field. Since only charged particles are affected by this mass transfer mechanism, by adding a supporting electrolyte in 100-fold excess to the solution containing the ionic material of interest, the electric field of the electrode is dissipated over all the ions of the solution and not only the electroactive material of interest.[39], [41].

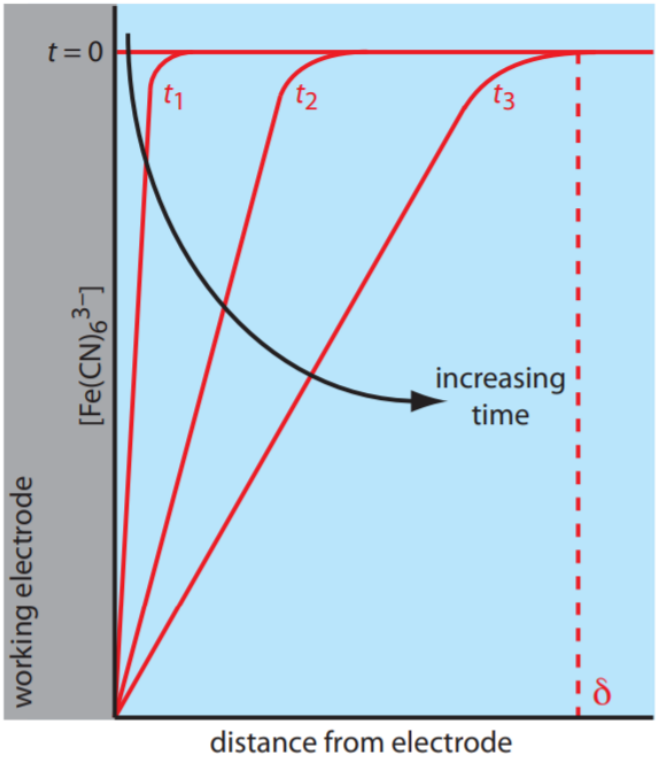

Figure 3.6 **Concentration gradients for $Fe(CN)_6^{3-}$ following the application of a potential that completely reduces it to $Fe(CN)_6^{4-}$.Reprinted with permission from** [39].

Another factor influencing the current in voltammetric experiments is the ease at which electrons are transferred between the electrode and the species in solution. When the kinetics is fast, the redox reaction is at equilibrium and the electrochemical reaction is reversible or Nernstian. Similarly, when the kinetics is slow, the system is considered electrochemically irreversible [38], [41].

Additional to the faradaic currents, there are other current sources that contribute to the magnitude of the current in a voltammogram. The main one is named *charging current*, and it happens when changing the electrode potential, due to a re-arrangement of the ions in the area nearby the surface (the electrical double layer) to equilibrate the charge between the electrode and the solution [39].

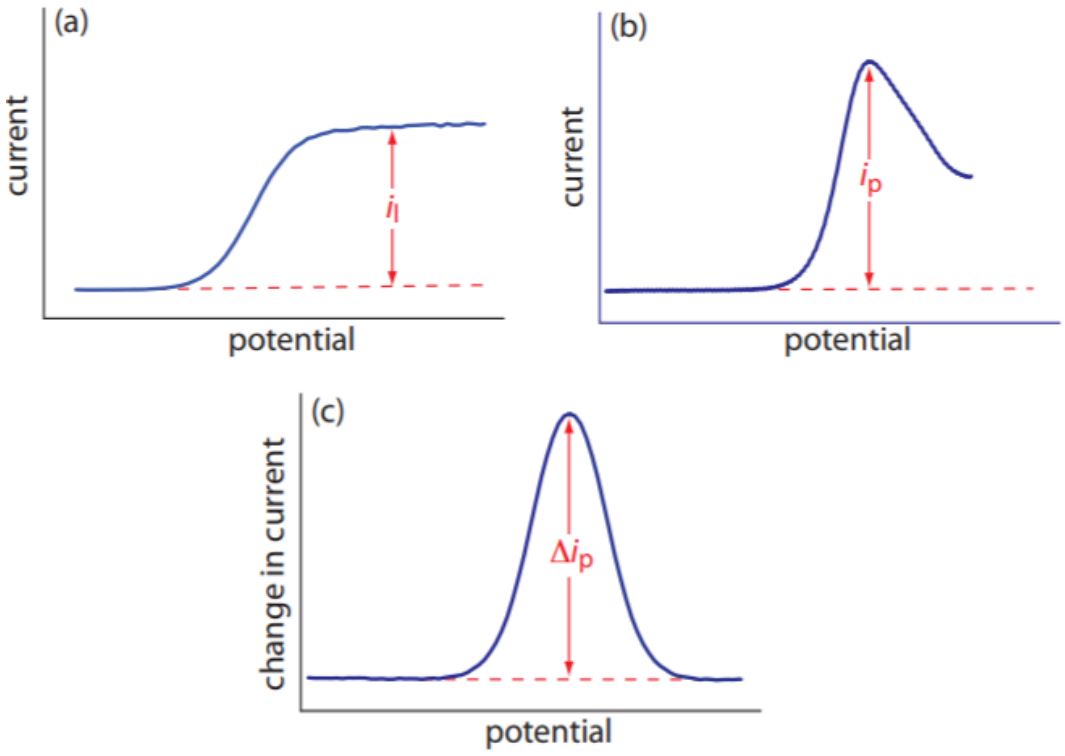

Figure 3.7 **Common shapes of voltammograms. Reprinted with permission from** [39].

As it was previously mentioned, in voltammetric experiments there are mainly four different parameters that can be controlled: (i) the way the potential of the working electrode is changed; (ii) the scan rate; (iii) the time at which the current is sampled and (iv) whether the solution is kept stirred or not. Depending on the desired parameters to control, there are many different voltammetric techniques. However, there are only three common shapes of voltammograms.

The current can increase from a background current to a value known as *limiting current* as illustrated in Figure 3.7a. This limiting current can be reached only if the width of the diffusion layer is kept constant while stirring the solution, because as explained before, the faradaic current is inversely proportional to the diffusion layer width (δ). Without stirring, the width of the diffusion layer increases with time (see Figure 3.6) and the voltammogram ends up with a *peak current* instead of a limiting current as shown in Figure 3.7b due to an increasing decay of the concentration near to the electrode surface. Finally, not only the current can be monitored as a function of the potential applied but also a change in current that follows a change in potential, which will end up having a peak shape too as shown in Figure 3.7c.

As one can imagine at this point, voltammetric experiments are of great utility to get information from electrochemical systems, from a qualitative and quantitative point of view. The information

that we can get depends on the voltammetric technique that we use. Currently there are plenty of them such as polarography, hydrodynamic voltammetry, stripping voltammetry and cyclic voltammetry. For the purposes of the present work, only the last one is going to be explained from a general point of view and in the next sections, the effect of the electrode size on the electrochemical response will be discussed.

3.1.3 Cyclic voltammetry

Cyclic voltammetry (CV) is a technique where a complete potential scan is performed in two different directions. This means that the potential can be scanned to more positive values in a first step, resulting in the oxidation of a reduced species *R*. When the potential reaches a predetermined value, the direction of the scan is reversed towards more negative potential values giving place to the reduction of the oxidized species in solution *O*.

Since cyclic voltammetry is performed in an unstirred solution, the resulting current (*i)* vs potential (*E)* curve will be peak shaped instead of with a limiting current, like the ones showed in Figure 3.8. In the same Figure the two commonly used conventions to report CV data are shown. In the US convention the reduction currents are considered as positive and the oxidation ones as negative. On the other hand, for the IUPAC convention the oxidation currents are considered as positive and the reduction ones as negative. Visually, the data in the two conventions appear to be rotated 180^{O} [42]. The results of the present work are all reported according to the IUPAC convention.

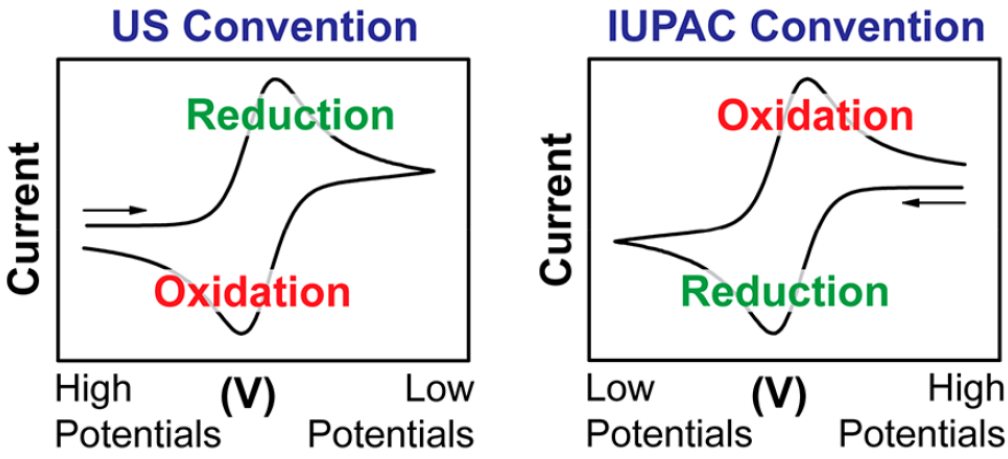

Figure 3.8 **Different conventions for reporting cyclic voltammetry data Reprinted with permission from** [42] **https://pubs.acs.org/doi/10.1021/acs.jchemed.7b00361. Further permission related to the excerpted content should be directed to the ACS.**

A very important parameter in CV is the scan rate which controls how fast the applied potential is scanned. When increasing the scan rate, the diffusion layer reduces its width and consequently, higher currents are observed in the voltammograms. For electrochemically reversible processes with freely diffusing redox species, Equation 2, known as Randles-Sevcik equation describes how the peak current i_p (A) varies linearly with the square root of the scan rate v (V s^{-1}). In the equation, n is the number of electrons transferred in the redox event, A (cm^2) is the electrode surface area, D_0 (cm^2 s^{-1}) is the diffusion coefficient of the oxidized analyte, and C^0 (mol cm^{-3}) is the bulk concentration of the analyte [38].

$$i_p = 0.446nFAC^0 \left(\frac{nFvD_0}{RT}\right)^{1/2} \quad (2)$$

One can obtain from voltammograms either the electrode surface area or the diffusion coefficient using the Randles-Sevcik equation, if the rest of the parameters are known. Also, it can be used to determine if an analyte is freely diffusing in solution [42].

As mentioned in the previous section, there are many other factors that can affect the shape of voltammograms, since electrochemical systems are not homogeneous and there are multiple processes besides the ones of interest that occur simultaneously. For instance, most of the electrochemical systems would give a response much more complex than the duck-shaped showed in Figure 3.8. The simplest variations of the voltammograms can be due to slow electron transfer, electrochemical irreversibility or multiple electron transfers. But much more complex systems where coupled chemical reactions take place can be found. Fortunately, CV represents a tool to be used in order to characterize those systems that for the purpose of the present work lack of interest and will not be further explained [38], [39], [41], [42].

Increasingly, many researchers are interested in using electrochemistry because it is a powerful tool for exploring electron transfer reactions of interest for many different disciplines such as renewable energies, or fundamental mechanistic chemistry. In the last two decades, electrochemistry and specially, voltammetric experiments have been taken importance in the field of nano sciences due too the very particular properties that the systems have at this scale. And as it will be explained in the next section, many of the concepts that are valid for CV at the macroscale, are not useful anymore when working at the ultra-microscale or at the nanoscale.

The main fundamental concepts explained in this and last section are useful for the understanding of ultra small electrochemical systems.

3.2 Electrochemistry at the micro and nanoscale

In the last decades, electrochemistry at the micro and nanoscale has become a very active area of research with a continuous development of experiments, methods and applications in different fields of science from physics to biology. This is due to the unique information that nanoscale electrochemistry provides, which is unattainable with traditional macroscale methods. For instance, the use of nanoelectrodes allows to measure ultra fast electron transfer reactions that are usually too fast to be investigated with conventional electrodes [43], [44].

During many years, the main questions that have been raised surrounding the study of electrochemistry at the micro and nanoscale are: what can one learn about the ensemble of properties by studying systems at very small scales? Is this knowledge useful to get a better understanding and a better macroscopic performance if structuring materials in a micro or nanoscale? And, is there any additional value when studying individual molecules and particles? The answers to these questions depend on the context where they are answered and it results difficult to make a connection [45]. However, a lot of progress has been made in the last few years and now it is well known, for example that the behaviour of nanoparticles is different from the bulk, and it affects the catalytic properties of the material.

The behavior of an ensemble of particles has been rationalized based on the single particle reactivity information, and some information at the single-molecule level has been achieved, where the ensemble properties are no longer of interest [43]–[46]. For instance, Zhang and co-workers [47] showed that particle size is an important factor needed in the description of kinetics of phase transformations in nanoparticles. They explored the quantitative relationship between the kinetic rate constant and particle size, for phase transformation in nanocrystalline anatase via interface nucleation at particle-particle contacts. Their Arrhenius analyses of the rate constant revealed that the preexponential factor increases dramatically as the particle size decreases.

The main tool to perform electrochemistry at the micro and nanoscale is a nanoelectrode. In the next sections, the main properties of these electrodes will be discussed along with the most popular fabrication methods and materials used for their preparation.

3.2.1 Unique properties of ultra-microelectrodes

Single entity electrochemistry is usually defined as a discipline that describes a recent trend in state-of-the-art electrochemistry applied to the study of individual things [13]. This discipline results interesting for contemporary research due to the unification of different branches of electrochemistry and to the different approaches and techniques being developed toward similar goals.

The glamour of single entity electrochemistry lays on the fact that the single things or entities under study, could be virtually anything depending on the field of study. Thus, a single entity could be a nanoparticle, a living cell or a molecule. This multi-faceted character brings together cellular biology, catalysis, organic chemistry, physics, among other disciplines [13].

The main questions regarding electrochemistry at single entities are why should we measure single entities? And once we make it clear that those measurements are important, why do we use electrochemistry to do so? Among the main answers that have been demonstrated so far in the different fields, the main one is that we want to separate the individual responses from the bulk which is important because if we are able to understand how a single entity contributes to the ensemble, a better understanding of the underlying chemistry can be determined. Thus, for example if we understand how a single molecule is transformed at a catalyst, the chemical transformation can be optimized. This is the case for the study of many single particle electrochemistry measurements [19], [20], [29], [30].

Naturally, the primary tool to perform electrochemistry at single entities of such size, is a suitable electrode of comparable dimensions. By definition, a nanoelectrode is an electrode that has at least one critical dimension smaller or equal to 100 nm [44], [46]. However, it has been found that most of the molecular chemistry happens in the 1-1000 nm range, where the properties of the electrochemical signals does not change considerably [43].

An ultra microelectrode (UME) is defined as an electrode that has at least one critical dimension smaller or equal to 25 μm. UME's possess a great number of extraordinary properties that attract the attention of researchers because they allow the study of new areas from the fundamental and the applied point of view of electrochemistry.

The most obvious benefit of the use of UME's is that they allow us to work in increasingly small spaces, which is the first reason why they were developed when trying to monitor the kinetics of the release of electroactive neurotransmitters in the brain [48]. And these small spaces include not only small portions of tissues but also single living cells, and even single molecules, which is

the ultimate goal of miniaturizing the working electrode to such small dimensions. This produced openings to voltammetry to be recorded close or even within living cells, and giving place to the development of a different form of microscopy called scanning electrochemical microscopy (SECM) [43].

The double layer capacitance along with the resistance of the working solution (R_s) places many limitations on electrochemical experiments at the macroscale [43]. This represents other reasons that motivated the use of UME's. The small dimensions of an UME significantly decrease the C_{dl}, which results in a small $C_{dl}R_s$ product, which represents the time constant on which the working electrode potential can be controlled. Small $C_{dl}R_s$ enable experiments at the nanosecond time scale and the study of ultrafast electron transfer reactions on the electrode and the detection of short-lived intermediate species [43], [44].

Another notable feature of UME's is that scaling down the size of the electrode allows radial diffusion to be the dominant form of mass transport to its surface. This enables steady state currents to be easily monitored, simplifying and facilitating the use of UME's under conditions where potential variations are disadvantageous [48]. The faster mass transport at UME's in comparison to that for macroscale electrodes contributes as well as to the study of fast electron transfer kinetics by using steady-state experiments.

The final advantage of UME's and nanoelectrodes is that due to their dimensions they could enable the study of interesting fundamental processes and phenomena such as of the double layer structure, mass transport within a diffusion layer with dimensions comparable to those of the double layer, reactions of molecules on surfaces of comparable size and even quantum size effects of small nanoelectrodes [43], [44], [46], [48].

3.2.2 Voltammetric response of UME's

As mentioned in past sections, in a typical electrochemical system with an unstirred solution and an excess of electrolyte to mitigate both migration and convection, diffusion is the dominant mass transport mechanism that due to its planar profile gives place to peak-shaped voltammograms like the one showed in Figure 3.9a. This is because with this type of experiments, both diffusion and concentration information are convoluted in the voltammograms.

At microelectrodes, when performing cyclic voltammetry, the obtained voltammogram looks like the one showed in Figure 3.9b, in which instead of obtaining a peak-shaped curve, a steady-state current can be observed [43], [44], [48]. This behaviour arises because the rate of the reaction is

controlled by the analytes' mass transfer towards the surface of the working electrode. Contrary to what happens at macroelectrodes, the diffusion profile at UME's is radial, as shown in the inset of Figure 3.9b. Under this radial profile, the diffusion towards the edges of disk-shaped electrodes becomes as important as the perpendicular to the electrode surface. This effect is difficult to be observed at larger electrodes because the scan rate should be very slow for the radial diffusion to considerably contribute to the current. Similarly, if an experiment is carried out in a UME using extremely high scan rates, a peak-shaped voltammogram can be obtained due to the modification of the diffusion profile to a planar one because of the higher rate of the reaction in comparison to the diffusion rate [48].

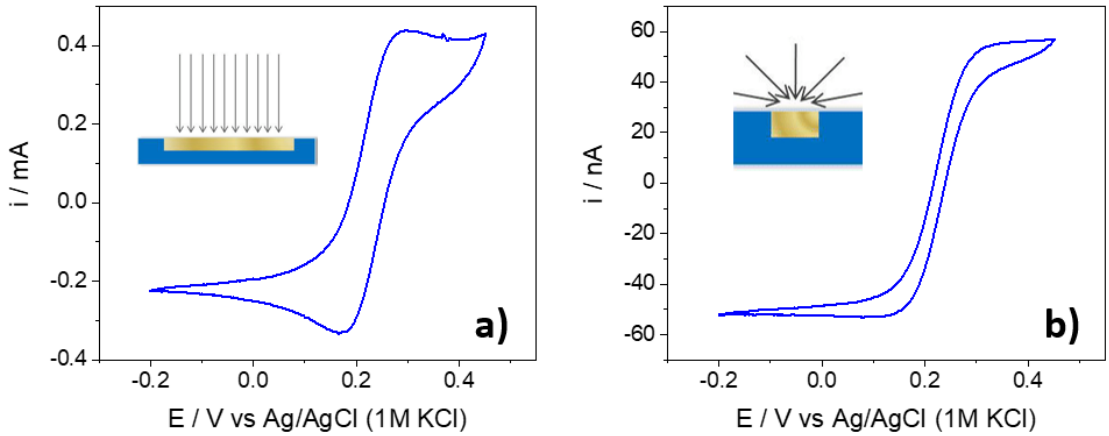

Figure 3.9 **Cyclic voltammograms of a 5 mM solution of $Fe(CN)_6^{3+}$ and $Fe(CN)_6^{4+}$ at a) a macroelectrode and b) an UME. The insets show the corresponding diffusion profiles.**

Other factors that can affect the voltammetric response at UME's are the rates of chemical reactions occurring in solution, called coupled chemical reactions, and the rate of electron transfer at the electrode surface. It has been reported before that the rate of electron transfer reactions is similar at micro electrodes and at macro electrodes. However, it is due to the effect of diffusion that reactions with faster heterogeneous rate constants can be studied at microelectrodes, which is interesting from a fundamental point of view but that in practical terms only means that the rate of electron transfer may distort the voltammograms more at microelectrodes in comparison than to macroelectrodes [48].

The predicted behavior of the voltammograms at microelectrodes can also be distorted due to the presence of coupled chemical reactions that precede or follow the electron transfer reaction. However, these effect will not be discussed in detail because the electrochemical system used in

this project has been already well characterized and no homogeneous coupled chemical reactions have been detected [48].

In general, many different types of UME's have been prepared depending on the method of fabrication. Geometries like cylinders, spheres, rods, disks and virtually any other shape is attainable and if they have a small enough size, their voltammetric behavior will be similar to what has been described in the last paragraphs [44], [46], [48], [49]. However, there are some aspects that must be considered when analyzing and extracting data from the voltammograms, depending on the electrode geometry. In the following sections, the most used methods for the fabrication of UME's will be described along with the consequences of the geometry on the voltammetric response.

3.2.3 Fabrication and characterization of UME's

Several fabrication methods for UME's have been proposed. The simplest ones are: (i) the electrochemical or chemical etching of thin metallic wires to a conical shape followed by the insulation of all but the apex of the tips; and (ii) the micropipette pulling method [43], [44], [46], [50]. The second is perhaps the most used and it consists on encapsulating or sealing the electrode material into an insulator and then expose the electrode by mechanically polishing or chemically etching the insulator. This approach was used by Wightman to create the first useful nanoelectrode [48].

The problem with the Wightman approach, and its variations, such as the micropipette pulling technique, is that the polishing of the electrode surface requires specialized equipment and the rate of success to get electrodes with diameters of nanometric sized is of only 10 % [19]. This method is more suitable to obtain electrodes with diameters from 10 to 25 μm, and it is very popular for scanning electrochemical microscopy because with this technique, the entities subject to study are in the micrometric rather than the nanometric scale [33], [49], [51]–[53].

The relatively simplest method is the etching of metallic wires that produces cone electrodes that are approximated by a hemisphere in their electrochemical characterization as it will be discussed in the next paragraphs [24], [50]. This method consists in submerging a metallic wire of some micrometers of diameter into an etching solution and apply a voltage in order to generate the dissolution of the metal until a cone-shaped electrode is obtained [54]–[56]. The advantage of this method over the others is that after obtaining the sharp tips it is possible to insulate the metal using special polymers and a post-insulating electrochemical etching step can be implemented to produce disk-nanoelectrodes, giving to this method great versatility depending on the application

[50]. It is for these reasons that in this work, the electrochemical etching approach was used to produce submicron-sized electrodes.

The ideal shape of a microelectrode from the point of view of a uniform flux of mass transport of the analytes to the electrode surface, and uniform current density across the metal/solution interface, is a perfect hemisphere surrounded by flat shroud at the level of the hemisphere's rim as the one shown in Figure 3.10a [43]. It has been demonstrated that even though the diffusion is three dimensional and fast for all UME's, the electrode geometry affects drastically the diffusion profile of the analyte towards the electrode surface and therefore the steady state current value is described by different equations depending on the electrode geometry. In Figure 3.10 the perfect hemisphere (a), an inlaid disk (b) and a recessed disk (c) are shown along with the equations that describe the value of the steady state current (I_{ss})as a function of the electrode geometry [24], [33], [50], [54], [56].

At the times when scanning electron microscopy (SEM) characterization did not have enough resolution in order to visualize the nanoelectrodes, the researchers were totally dependant on the electrochemical signal coming from the electrodes in order to get an idea of their dimensions [50]. To do that, well known electrochemical probes with a very well characterized behaviour were used. Among the most used we find ferrocene, $Ru(NH_3)_6^{3+}$, dopamine, and the ferro-ferricyanide system $Fe(CN)_6^{4-}/Fe(CN)_6^{3-}$ that is the one to be used in the present work to perform the electrochemical characterization of our electrodes [57]–[60]

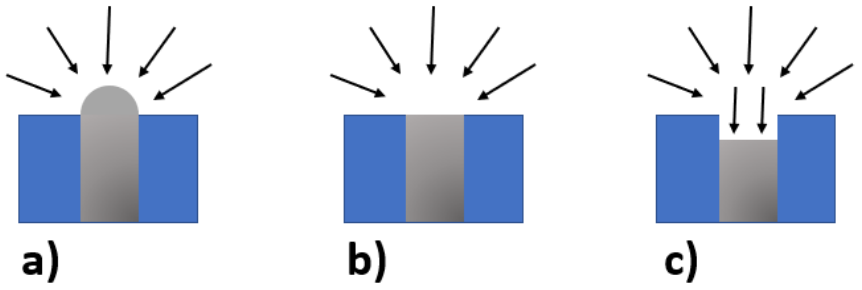

Figure 3.10 Different UME's geometries

a) perfect hemisphere; b) inlaid disk; and c) a recessed disk. In the equations *F* is the Faraday constant, *D* is the diffusion coefficient of the analyte under study, *C* is the concentration of the analyte, *r* the radius of the UME.

In this work we decided to opt for the electrochemical etching of wires that gives place to conical UME's. This geometry has as the main advantage that it enables the use of the electrodes in very small spaces to record electrochemical signals (i.e. living cells and gold nanoparticles). Due to the geometry, the way we analyze data to obtain the right information out of the voltammograms is very important. Equation in Figure 3.10a has been used to describe the steady-state current behavior of conic nanoelectrodes using the radius of a disk with the same surface area than that of the cone, due to the similar diffusion profile that these structures present in comparison with perfect hemispheres [43], [50]. However, Hermans and Wightman showed that the steady state current of a cone surrounded by an insulator material is related to the one of a disk with the same radius than the base of the cone according to Equation 3, where i_{cone}^{ss} is the steady-state current of the conical electrode, i_{disk}^{ss} is the steady-state current of a disk electrode, *RG* is the ratio of the radius of the base of the insulating sheath over the radius of the cone, and *A*, *B*, *C* and *D* are numerical constants that depend on the aspect ratio *H* of the cone.

$$i_{cone}^{ss} = i_{disk}^{ss}[A + B(RG - C)^{D}] \quad (3)$$

From Equation 3 the electroactive surface area can be obtained if we have the steady-state current from the corresponding voltammogram. However, in our work we did not use an insulating sheath for our electrodes. For this kind of electrodes, Zoski [24] proposed Equation 4, which can be used to predict the steady-state current from conical micro electrodes as a function of the aspect ratio, *H*, of the cone.

$$i_{cone}^{ss} = 4nFDCr(1 + qH^{p}) \quad (4)$$

In Equation 4, *n* is the number of electrodes transferred, *F* is the Faraday constant, *D* is the diffusion coefficient, *C* is the concentration of the analyte and *r* is the radius of the base of the cone; *H* is the aspect ratio calculated as the cone height over the cone radius; and *q* and *p* are numerical constants with values 0.30661 and 1.14466 respectively.

In the study realized by Zoski [24] it was demonstrated that even though the steady state behaviour of conical electrodes is very similar to that of perfect hemispheres, it is necessary to study the behaviour following Equation 4 in order to get precise results that fit theoretical

approaches within 1%. For this reason, in the present work, Equation 4 was used to obtain the radius of the conical electrodes that was further used to calculate the electroactive surface area.

So far, all the theory behind the fundamental technique used for the characterization of our electrodes and its particularities at the micro and nanoscale have been discussed. However, another important matter to discuss before getting into the results is the electrode material, which plays a primordial role on the electrochemical measurements, and that will be explained in the following section.

3.2.4 Working electrode materials

The choice of the working electrode's material must be based on the specific purposes for which it will be used. Thus, if our objective is to study a probe in solution whose oxidation or reduction occurs at very positive or negative potentials respectively, we need to choose a material with high overpotentials. However, materials with low overpotential can be used to study the oxidation-reduction of their surface itself.

In the specific field of electrochemistry at the micro and nanoscale, the main materials used to fabricate electrodes are platinum, gold, silver and carbon due to their versatility and for the ease of preparation of electrodes by micropipette pulling technique, in the case of the metals [19], [20], [29]. However, they all present the problem of being "soft" materials that break very easily, making its manipulation very complicated. Additionally, the preparation of conical tips from gold or platinum is quite complicated due to the special conditions needed, like very fast potential pulses that cannot be performed without specific function generators [61].

The chosen material for our experiments was tungsten due to its unique characteristics. The study of the electrochemical behavior of tungsten has been subject of a great number of publications due to the technological importance of the material in many different disciplines and industries like the optoelectronic, solar energy, semiconductors, etc. In Table 3.1 [62] some applications with an electrochemical basis of this material are shown.

General studies regarding the voltammetric behaviour of tungsten have been carried out along with its dependence on the pH of the solution, the solvent and the dissolution kinetics of the tungsten oxide layers that are formed on the metal surface due to is relatively high reactivity with the environment [62]–[67].

The etching process of tungsten wires to get sharp tips is relatively easy, it does not need special equipment and many of the factors defining the length and sharpness of the obtained tips have

been discussed before [31]–[33], [54], [55], [68]–[72]. This material is used to prepare such small tips mainly due to its robustness and extremely high melting point which allow to get very stiff electrodes at the end and facilitates the resistive annealing of the surface to remove the corresponding oxides [61]. Tungsten tips are typically used as samples for atomic probe microscopes such STM, AFM and SEM [31], [68], [69], [71].

Tungsten tips were proposed in 2006 as substrates for the preparation of UME's [56]. Because of the reactivity of the W, in that study, the resulting tip electrodes were subject to an oxide removal process after which either platinum or gold were electroplated. Other tips were deposited with carbon by photoresist followed by pyrolysis. These subsequent steps render the tip preparation more laborious.

In the present work, the electrochemistry of tungsten was revisited in order to find the conditions under which the metal itself or one of its oxides can be used directly as an electrode with no need of extra deposition of metals or carbon, which simplifies the UME's preparation process.

Table 3.1 Electrochemical processes in the industrial application of tungsten

Form of W	Industry	Application/process	Purpose
WO_3	Optoelectronic	Electrochromism	The insertion of ions (H^+, Li^+) in the crystalline structure of WO_3 to modify its physicochemical properties
WO_3	Solar energy	Photoelectrolysis of water	Use of semiconductor WO_3 electrode to decompose water photoelectrochemically to produce H_2 (as a fuel)
W/WO_3	Chemical industry nuclear energy	Corrosion/protection	Formation of a stable/protective oxide
W	Machining and shaping	Electromachining and etching	High-rate dissolution as well as formation of a stable oxide on the surface to protect unmachined parts
W	Metal and alloy wastes	Recycling	Selective dissolution in base solutions
W/WO_3	Semiconductor	CMP	Kinetics of oxide growth, dissolution, and solubility of metal and metal oxides

Table obtained from [62]**.**

3.3 Perspective

Even though in this work we only carried out the fabrication and characterization of sharp conical UME's, it is important to mention that our original motivation to develop this project is to eventually attempt single entity electrochemistry. This is very appealing in the field of biology because among all the different systems, these are the most heterogeneous. For example in an ensemble of living cells under the same conditions, the behavior of each cell can be completely different, and this is not taken into account with the traditional approaches where it is assumed that all the entities are identical [13], [34], [73]–[75]. With the approach used in the present work, we aim to study single biological entities in the future, from single living cells, single organelles and single biomolecules as an ultimate goal. In this regard, this can be possible thanks to the great advances that have been made in this field, to the point that even single atoms or clusters of up to nine atoms have been successfully deposited and electrochemically characterized, highlighting thus the scope of the single entity electrochemistry [76], [77].

4 METHODOLOGY

The present project consisted in solving two main technical and technological challenges. The first one consisted in the preparation and characterization of tungsten tips with very sharp and controllable profiles. Such features are desired for potential applications as support for single entities or small clusters of them. The second challenge was the electrochemical characterization of such electrodes aiming at their future application as potential electrodes for single entity electrochemistry. In order to achieve this, we developed a simple and versatile set-up for both types of experiments.

The methodology followed for the development of the present work was divided in five main sections: (i) The construction of the experimental set-up; (ii) the fabrication of sharp tungsten tips; (iii) fundamental studies on the electrochemical behavior of tungsten that were performed at tungsten wires; (IV) electrochemical and physical characterization of the sharp tungsten tips; and (V) Cathodic deposition of gold on tungsten wires and tips and their characterization.

4.1 Construction of the experimental set-up

The main objective of the experimental set-up is to be able to study the electrochemistry of tungsten thin wires, prepare electrodes with nanometric dimensions from them and to perform several electrochemical measurements by varying the surface area exposed to the working solution. To achieve the this, it was necessary to find a suitable support for the tungsten wires (to be used as working electrodes) that allows to move them in a vertical axis to control their length inside the corresponding working solution. Figure 4.1 shows the experimental set-up configuration.

One of the ends of the WE (0.5 cm) was folded in a 90° angle so that it could be held into a copper tube (Sigma-Aldrich, outside diameter: 3.0 mm, wall thickness: 0.9 mm, inside diameter: 1.2 mm, length: 10 cm). In order to control the depth of the wire inside the working solution, the copper tube was fixed with the help of stainless-steel bolts to a translation piezoelectric stage (Thorlabs, NFL5DP20 5.0 mm travel) which was fixed to standard micrometer translation stage (Thorlabs, PT3/M - 25 mm XYZ) as seen in Figure 4.1b. The piezoelectric stage was used to make very fine displacements (36 nm) with the help of a piezoelectric controller, while the standard micrometer translation stage was used to make displacements in the micrometer scale. The calibration of the piezoelectric stage is discussed in Appendix I.

All the experiments where monitored with an optical USB microcope (Adnostar, Digital Image Monarch processor, high-quality CMOS sensor, 640*480 resolution, true color 24bit RGB, USB 2.0, 30 frames/sec frame rate, 200x magnification) that was placed next to the electrochemical cells as shown in Figure 4.1a-b.

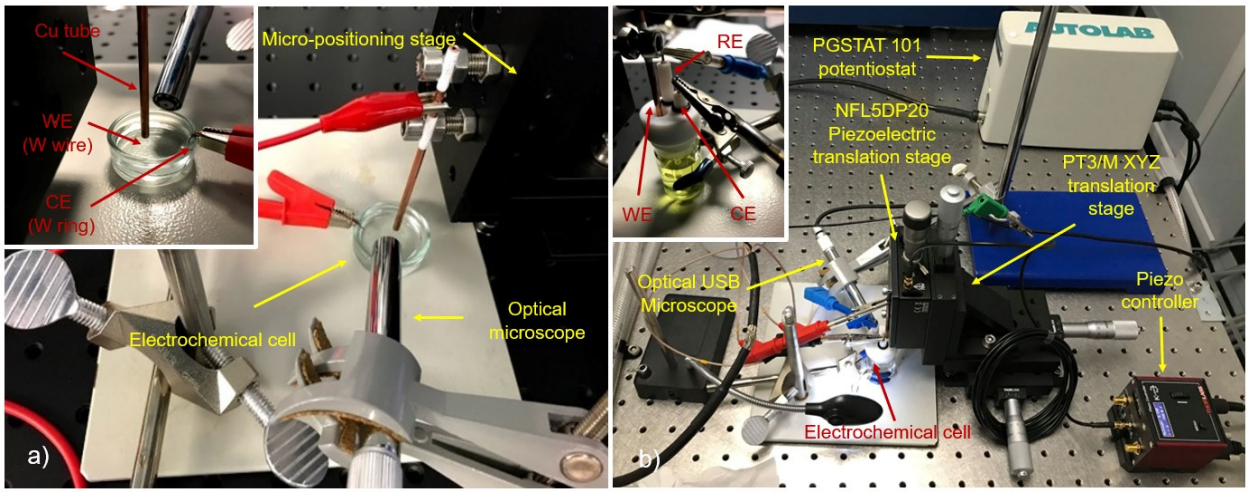

Figure 4.1 Experimental set up

a) represents the set-up for the tip preparation and b) the one for the electrochemical characterization.

For the electrochemical experiments, two different configurations of electrochemical cells were used. For the preparation of the sharp tungsten tips, a two-electrode configuration was used as shown in Figure 4.1a. The WEs were tungsten wires held to the copper tube. The CE was a tungsten wire ring with a similar diameter of the petri dish and its end was held by a piece of copper tape that was used to make contact between the wire and the lead with alligator clip.

The second configuration, for the electrochemical characterization of tungsten wires and the resulting tungsten tips, consisted in a three-electrode electrochemical cell as shown in the inset of Figure 4.1b. In this case, either tungsten wires of 2.5 cm in length and 100 μm in diameter, or the resulting sharp tips were used as WE's, a platinum wire was used as CE, and Ag/AgCl (1 M KCl) was the RE. For all the electrochemical experiments, the voltage was applied by a potentiostat/galvanostat (Autolab PGSTAT 101) shown in Figure 4.1b.

The CE and WEs were cleaned before and after performing the electrochemical measurements and any characterization experiment, to eliminate any traces of organic matter and tungsten oxides on the surface. The cleaning was performed with an advanced plasma system (Gatan, Solarus: Model 950) using a mixture of hydrogen and argon with a gas flow of 6.4 and 32 sccm, respectively, for 5 minutes.

Finally, it is important to mention that since we aimed to work with ultra small electrodes whose response is of only a few nanoamperes, the experimental set-up was settled on an optical table installed in an vibration and noise-isolated room, with temperature control (22 ^{o}C) and that served as a Faraday cage. This, in order to avoid any interference of mechanical or electromagnetic perturbations on the electrochemical signals.

4.2 Sharp tungsten tips fabrication

Sharp tungsten tips were prepared using an electrochemical etching technique known as the “drop-off” method. It consists on dipping typically few millimetres of a tungsten wire into a concentrated basic solution like potassium hydroxide (KOH), and then applying an electrical potential. As the etching progresses, a necking effect is observed in the portion of the wire at the air-solution interface due to the formation of a meniscus and a non-uniform etching rate along the wire. At some point, the tensile strength of the etched wire neck will be exceeded by the weight of the lower part of the wire. This forces the lower portion to drop in solution, forming two sharp tips in the bottom and upper portions. Figure 4.2 shows a general scheme of the etching progress during the drop-off method.

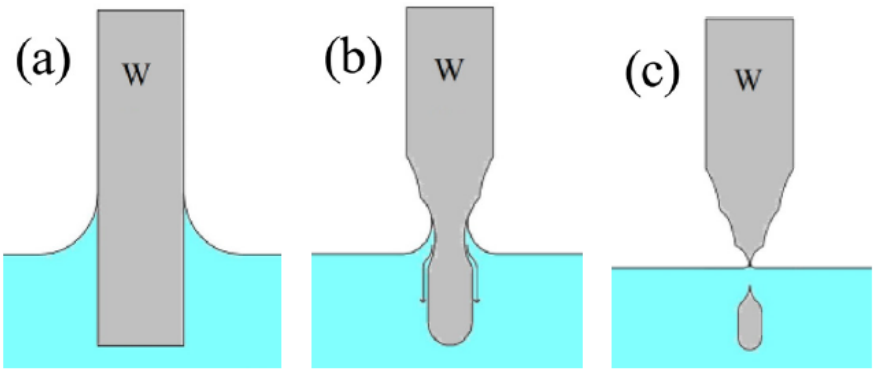

Figure 4.2 Etching progress during the drop-off method.

The different steps of the electrochemical etching can be appreciated. a) represents the initial state of the tungsten wire before applying a current. In b) it can be seen the necking effect at the air-solution interface and in c) the drop-off occurs due to the weight of the lower part of the wire giving place to the formation of two sharp tips, from which the lower one cannot be recovered due to it’s size [32].

The observed necking effect can be attributed to a non-homogeneous concentration of the OH^- ions along the surface of the tungsten wire. It has been proposed [32] that the concentration at the top of the meniscus is lower than in the bulk solution due to a slow mass transfer of the OH^- ions. During the etching process, soluble tungstate ions (WO_4^{-2}) are formed giving place to a viscous flow along the wire surface that accumulates at the bottom part of the wire. This viscous layer lowers the activity of OH^- ions making the reaction to be slower in this part in comparison to the top of the meniscus. Due to the concentration gradient of OH ions, a vortex is formed below the meniscus generating a flow splitting that removes the reaction products at the neck [54].

One of the main concerns when etching tungsten tips is the behavior of the meniscus caused by the wettability of the tungsten surface by the working solution. In general, there were two different meniscus behaviors observed: (i) Static meniscus regime and (ii) Dynamic meniscus regime. In the first case, the meniscus does not move from its original position during the complete etching process. This kind of behavior has been observed before [54] and it is illustrated in Figure 4.3.

This regime resulted in the creation of very short and concave tips. In Figure 4.3 it can be seen how the bottom part of the wire gets thinner with time until the drop-off occurs, but the meniscus remains always in the same place. The problem with the resulting tips is that they are too short and when trying to perform electrochemical measurements with them, instead of touching the solution with only the apex of the tip, the solution would cover the complete concave surface due to the attraction of the solution to the rest of the tungsten wire.

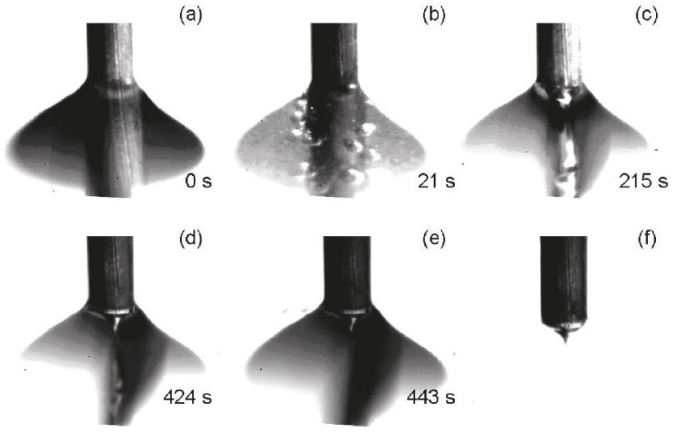

Figure 4.3 **Static meniscus during the etching process** [54]**. Reprinted with permission from M. Kulakov, I. Luzinov, and K. G. Kornev, "Capillary and surface effects in the formation of nanosharp tungsten tips by electropolishing," Langmuir, vol. 25, no. 8, pp. 4462–4468, 2009. Copyright 2020 American Chemical Society.**

The behaviour of the meniscus is important not only in terms of the fabrication of the tips but also for their electrochemical characterization. Every time a tungsten wire or tip touches the solution surface, a meniscus is formed. This meniscus covers a part of the surface that will thus contribute to the electrochemical signal obtained during the measurements. This is due to the hydrophilic character of tungsten and this effect is enhanced by the surface roughness due to capillarity.

Because of these challenges, we opted for a different approach that allowed to get smooth and long tips simultaneously, and that is called the dynamic meniscus regime [54]. In this regime, the meniscus moves in a series of steps towards the flat air-solution interface as shown in Figure 4.4. According to Kulakov et al. [54], this behavior of the meniscus is observed when the diameter of the tungsten wire is larger than 0.5 mm. However, our tungsten wires have diameters of 100 nm and therefore the dynamic meniscus regime needs to be induced.

Once in contact with the solution, the wires were immersed 1 mm and the etching process started. Different solutions of KOH (Fisher scientific, technical grade) were used in order to test the effect of the concentration (1-8 M) on the tip profile. Different voltages (1 – 8 V) were applied to test its effect on the tip profile. To generate a dynamic behavior of the meniscus during the etching process, the tips were withdrawn from the solution in small steps with help of the micrometers of the standard translation stage in our experimental set-up.

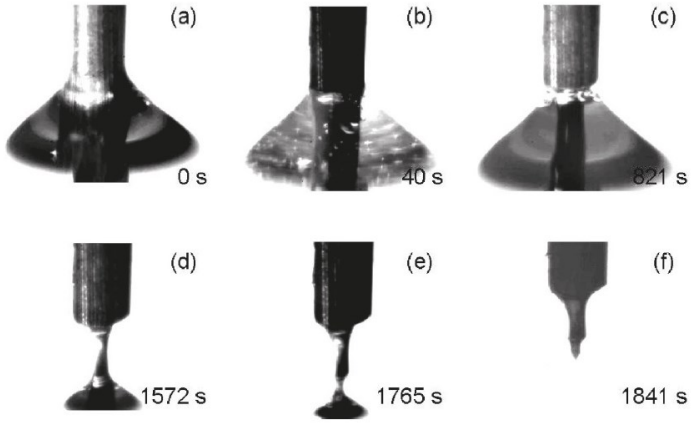

Figure 4.4 **Dynamic meniscus during the etching process** [54]**. Reprinted with permission from M. Kulakov, I. Luzinov, and K. G. Kornev, "Capillary and surface effects in the formation of nanosharp tungsten tips by electropolishing," Langmuir, vol. 25, no. 8, pp. 4462–4468, 2009. Copyright 2020 American Chemical Society.**

Some of the resulting tips were further etched using a focused ion beam etching (FIB) to make them sharper and with a much smoother surface than the ones obtained after the electrochemical etching process. An SEM microscope (Tescan LYRA 3 XMH FIB/SEM) was used for these purposes.

4.3 Characterization of wires and tips

4.3.1 Physical characterization

Scanning electron microscopy (SEM) was used to obtain high resolution images of the tungsten wires and tips. A scanning electron microscope (Tescan LYRA 3 XMH FIB/SEM) was used for this purpose.

The obtained images were processed with help of the software *Image j* to get important parameters. For the wires, only the diameter was measured. However, for the tips due to their conical geometry, other parameters such as the cone height (*h*), the cone base radius (*a*), the lateral height of the cone (*l*) and the radius of curvature (ROC) of the tip apex were measured (See Figure 4.5). From these parameters, the surface area of the tips was calculated along with their aspect ratio (*H*) that corresponds to *h*/*a*. All this information was used for further analysis.

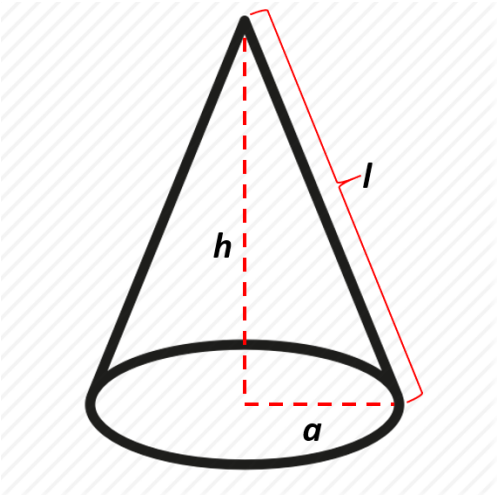

Figure 4.5 **Geometric parameters of the cone related to the lateral surface area**

4.3.2 Electrochemical characterization

For the characterization of the voltammetric behaviour of tungsten wires, a three-electrode electrochemical cell was used as shown in Figure 4.1b.

The working solutions at which the voltammetric behaviour of the metal was studied were a) 0.5 M H_2SO_4 to study the electrochemistry of the surface itself; and b) 5 mM $K_4Fe(CN)_6$ + 5 mM $K_3Fe(CN)_6$ + 0.5 M KCl as a redox pair whose behaviour is already very well known.[21] and that allowed to prove the feasibility of the use of tungsten as an electrode for the study of heterogeneous electron transfers. Only 5 mm of the tungsten wires were submerged in solution to perform these electrochemical measurements.

Cyclic voltammetry was performed in two different potential windows: (i) -0.01 to 0.55 V vs Ag/AgCl (1M KCl); and (ii) from -0.01 to 1.5 V vs Ag/AgCl (1M KCl). These two potential windows were used to study the formation and behaviour of two different tungsten oxides (WO_2 and WO_3) on the pure metallic surface. The voltammograms were recorded at 10 mVs^{-1} and 100 mVs^{-1} to evaluate the effect of the scan rate on the formation and dissolution of the tungsten oxide layers.

For the electrochemical characterization of the tungsten tips, the same three-electrode configuration of the electrochemical cell shown in Figure 4.1b was used. The tungsten tips were characterized by Cyclic Voltammetry using a 0.5 M KCl solution containing 5 mM $Fe(CN)_6^{-4}$ and $Fe(CN)_6^{-3}$.

The first step for the electrochemical characterization was to determine when the tips first touched the solution. This cannot be done with a USB optical microscope because the tip apex dimensions are too small. Therefore, we monitored the open circuit potential (OCP), which has a specific value for every electrochemical system, while approaching the WE to the electrolyte.

When the working electrode is in the air without touching the solution, the OCP value is very high (in the order of 10 V) because the distance between the WE and the CE is large. In contrast, as soon as the tip touches the solution, the OCP value drops to the characteristic value for our system (~0.1 V). In order to make sure that only the apex of the tip touches the solution at the beginning of the experiment, the next steps were followed: with the micrometer screws in the standard translation stage, the tip is approached to the solution while monitoring the OCP until the drop is observed. The position of the micrometer screw is recorded and then the tip is completely withdrawn from the solution. Then, the tip is approached once again to the solution, but the motion is stopped at two micrometers before the previously recorded position. Finally, the

piezoelectric controller is used to approach the WE in steps of 36 nanometers and without mechanical perturbations until the drop in OCP is observed again.

After corroborating that the apex of the tip was touching the solution, the electrode was immersed in solution in steps of 2 or 10 µm, and at each depth a total of 10 potential sweeps were recorded from -0.01 V to 1.45 V vs Ag/AgCl (1M KCl). The last potential sweep was used for the data analysis.

4.4 Electrochemical deposition of gold

In order to address the problem of the contribution of the meniscus to the electrochemical signals, the deposition of gold was performed on tungsten wires of different diameters at the meniscus height. This means that the tungsten wires were approached to the solution using the electrochemical approach based on the monitoring of the OCP described in section 4.3.2, making sure that the minimum possible depth of the wires was in the solution.

The technique consists of a deposition of an adherent coating of gold onto the surface of the conductor substrate by simple electrolysis of a solution containing the desired metal ion or its chemical complex. The height of the coating on the tungsten wires gives us a good approximation of the meniscus height and a relationship between the wire diameter and the meniscus height can be obtained.

For our purposes, the three-electrode configuration of the electrochemical cell was used. A 1 % w.t. chloroauric acid ($HAuCl_4$, Sigma Aldrich, analytical grade) solution was used as the working electrolyte. Dilutions 1:10 of the same solution were prepared in order to evaluate the effect of the concentration on the characteristics of the coating. The applied voltage during the electrolytic process was -0.2 V vs Ag/AgCl (1 M KCl). The duration of the applied potential was varied (5, 10 and 15 seconds) in order to see its effects on the coating characteristics.

Similar experiments were attempted on the tungsten tips. However, as explained in section 5, it was not possible to establish a relationship between the tip *ROC* and the meniscus height due to the variation of the tip geometries. Thus, we decided to evaluate the electrochemical behaviour of the gold coating on the tungsten tips by cyclic voltammetry in a 0.5 M H_2SO_4 solution using the same experimental set up. The voltammograms were recorded in a potential window from -0.01 to 1.5 V vs Ag/AgCl (1M KCl) in order to find the characteristic oxidation and reduction peaks of a polycrystalline gold surface.

5 RESULTS

5.1 Experiments at tungsten wires

The electrochemical response of tungsten wires was studied by CV in 0.5 M H_2SO_4 in order to find conditions where tungsten can be used as an electrode in acidic media. Figure 5.1 shows the cyclic voltammograms of the wire at two different scan rates. When scanning at 100 mV s^{-1} there are two main peaks in the voltammogram located at 0.47 V and 0.70 V indicating that two different tungsten oxides are formed during the scan. According to the literature, the first peak corresponds to the formation of WO_2 and the second one to the formation of WO_3, which are the most thermodynamically stable tungsten oxides [62]. The total anodic oxidation reaction of tungsten in acidic media is as follows [66]:

$$W + 3H_2O \rightarrow WO_3(s) + 6H^+ + 6e^- \quad (5)$$

In the reverse scan of the first cycle there is a remarkable decrease in the anodic current reaching almost 0 A for potential below 1.2 V vs Ag/AgCl (1 M KCl) indicating that the anodic polarization produces a passivation film. This is confirmed in the following cycles where almost no current is recorded below 1.2 V vs RE.

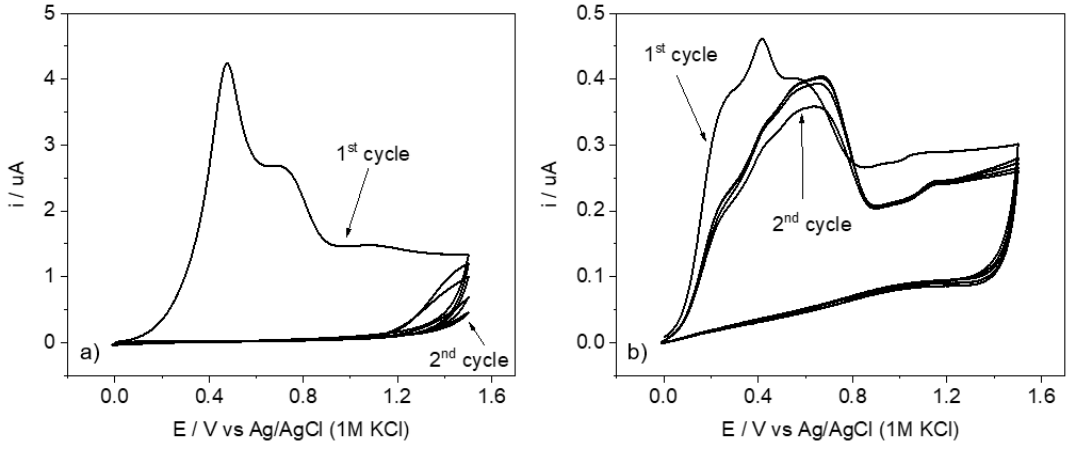

Figure 5.1 Cyclic voltammograms of tungsten wires in acid solution at different scan rates
The cyclic voltammograms were recorded in a 0.5 M H_2SO_4 solution at (a) 100 mVs^{-1} and (b) 10 mVs^{-1}.

The behavior between 1.2 and 1.55 V vs Ag/AgCl (1M KCl) is interesting because, the current in this region increases in the following cycles, pointing for a slow dissolution of the WO_3 layer that allows the surface to recover its conductivity. The dissolution of tungsten trioxide in acidic media has been demonstrated before [22] and follows the next reaction in acidic media:

$$WO_3 + H_2O \rightarrow WO_3.H_2O(s) = H_2WO_4(aq) \quad (6)$$

Figure 5.1b shows the voltammograms in the same potential window at 10 mV s^{-1}. In this case, there are three main signals: at 0.27 V, at 0.46 V and at 0.55 V. It has been suggested that the first shoulder corresponds to the formation of a suboxide WO_{2-x} that is not thermodynamically stable [23] and that cannot be sensed at high scan rates. The peak and the second shoulder correspond to the same electrochemical processes that are observed at 100 mVs^{-1}. In the reverse sweep a small increase in the current can be observed at 1.32 V which can be attributed to a reactivation of the surface after the anodic polarization.

In the following scan the oxidation signals can still be recognized despite of the decrease in the peak currents after the first cycle. The fact that the recovery of the surface conductivity becomes more important at low scan rates can be due to the chemical dissolution of the electroformed species during the positive scan in a similar way as it happens for alkaline solutions [23].

Additionally, the electrochemical response of tungsten was recorded in a narrower potential window (Figure 5.2) corresponding to the first peak (red line). It can be seen that the response in this potential window presents a very similar behavior to the one obtained in the full scan, meaning that either the first oxide is able to form a passivation layer on the surface of the electrode, or that after the first cycle the surface of the electrode is not reactive anymore due to a complete transformation of tungsten to WO_2. As expected, the signal at 10 mVs^{-1} presents a very low passivation effect and the peaks can be identified in the following cycles too.

To probe the conductivity of the WO_2 formed at the first peak for both scan rates we decided to perform cyclic voltammetry in the presence of the ferro-ferricyanide redox couple as a probe.

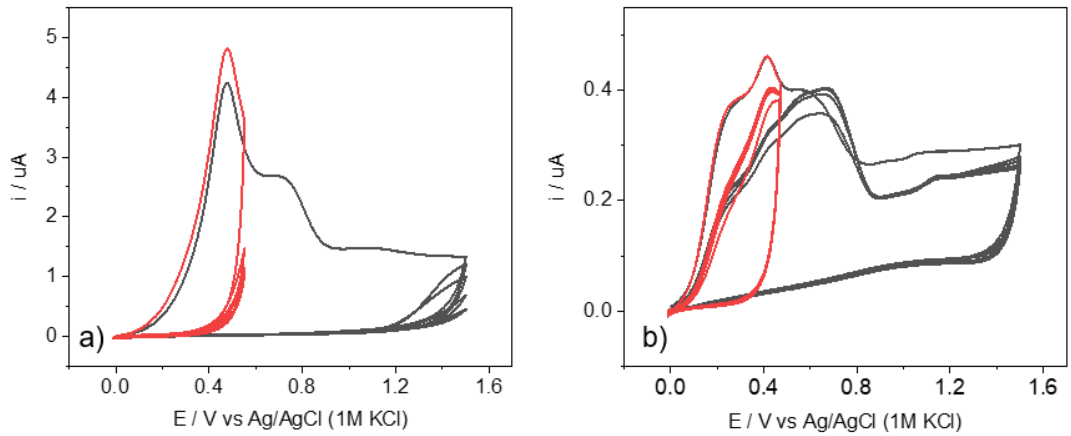

Figure 5.2 **Cyclic voltammograms of tungsten wires in acid solution at different scan rates and potential windows.**

The cyclic voltammograms were recorded in a 0.5 M H_2SO_4 solution at (a) 100 mVs^{-1} and (b) 10 mVs^{-1}. The red curves represent the scans corresponding to the formation of the conductive oxide, WO_2.

Before performing the voltammetries with the probe, blank tests were made in solutions containing only 0.5 M KCl, which is the electrolyte that is typically used with the ferro-ferricyanide solution. Those voltammograms were recorded at 10 and 100 mVs^{-1} at the same two potential windows than the ones recorded in acidic media. Figure 5.3 shows that the behaviour of the voltammograms at 100 mVs^{-1} is like the one recorded in acid solution. In both cases there are two main oxidation peaks in the full scan (black curve) and there is a clear passivation of the tungsten surface.

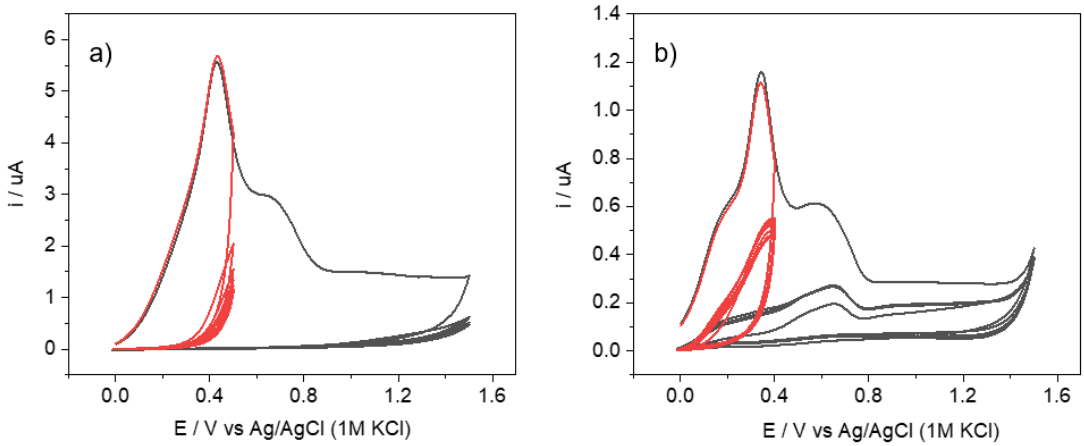

Figure 5.3 **Cyclic voltammograms of tungsten wires in a 0.5 M KCl solution at different scan rates and potential windows.**

The cyclic voltammograms were recorded at (a) 100 mVs^{-1} and (b) 10 mVs^{-1}. The red curves represent the scans corresponding to the formation of the conductive oxide, WO_2.

In the case of the CV's recorded at 10 mVs^{-1}, the peak current for the first cycle is higher than that recorded in acid, but the partial passivation of the surface can be still observed during the following cycles. In the full scan (black curve) it is also possible to see the start of the oxygen evolution reaction at 1.4 V vs Ag/AgCl (1M KCl).

In the case of the short scans (red curves) at both scan rates the behaviour is similar to that one presented in acidic media. This means that the conductivity of the WO_2 formed at the first peak can be evaluated in the proposed solution.

Figure 5.4 shows the voltammograms obtained from the scanning of the electrode in the probe solution in the same two different potential windows and at two different scan rates (10 and 100 mVs^{-1}). When the scans are performed at 100 mVs^{-1}, an additional peak appears at 0.28 V which corresponds to the oxidation of the iron reduced species.

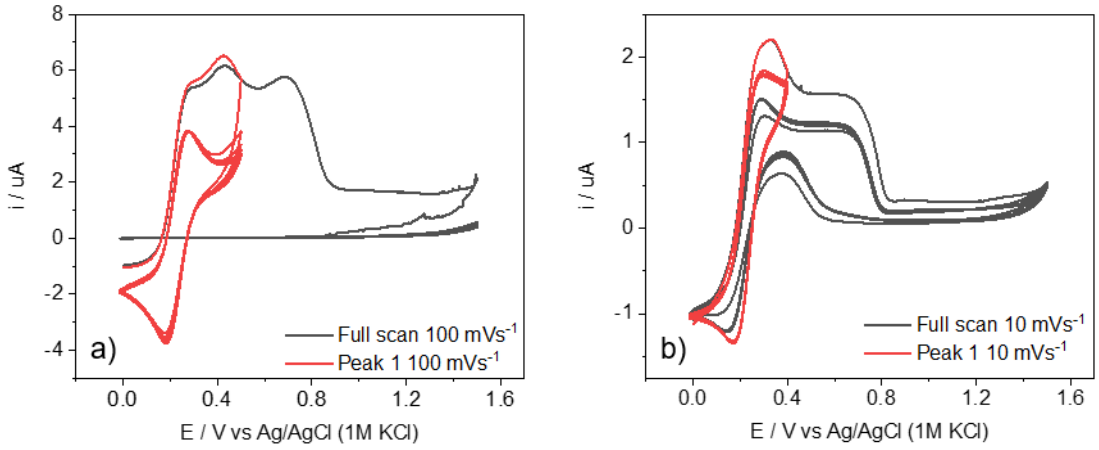

Figure 5.4 **Cyclic voltammograms of tungsten wires in 5 mM ferro-ferricyanide solution at different scan rates and in different potential windows**

When the scans are performed in the complete potential window (from -0.01 to 1.5 V) at 100 mVs^{-1}, the surface is completely passivated after the first cycle and no signal is recorded at all during the next cycles. This is consistent with the formation of an insulating oxide layer and therefore the material cannot be used as an electrode to study electrochemical reactions in solution.

At 10 mVs^{-1} in the same potential window the obtained response is like the one in acid solution: even though there is a decrease in the peak currents and potentials, after the first cycle it is still possible to see the corresponding oxidation signals. However, in this case due to the displacement of the peak potential to less positive values, the peak corresponding to the formation of WO_2 overlaps with the one of the iron species oxidation and therefore the current that is

observed in the first cycle at the first peak corresponds to the sum of the currents corresponding to the oxidation of both the metallic surface and the iron reduced species. In the reverse scan an additional oxidation peak appears at 0.38 V vs Ag/AgCl (1 M KCl) that is not present in the CV's at 100 mVs^{-1}. This peak could be due to the oxidation of "fresh" ferrocyanide ions ($Fe(CN_6)_6^{3-}$) that are allowed to move from the bulk to the diffusion layer zone due to the low scan rate and then be oxidised. At high scan rates, the diffusion is not fast enough to allow these fresh ions to move towards the interface to be oxidized in the reverse scan.

When performing cyclic voltammetry in a shorter potential window (red curves), it can be seen that the oxidation/reduction signal of the probe can still be observed even after the first cycle and eventually a stable voltammogram is obtained. In the first cycle we observe the oxidation of the surface plus the one of the probe, but once the layer of conductive tungsten oxide is formed on the electrode surface it impedes the pure tungsten to be oxidized in the further scans. This is why in the following scans we can see only the peaks corresponding to the oxidation/ reduction of the probe.

From these results, it was decided as part of the experimental protocol for the electrochemical characterization of the tips, that before starting any measurements, the electrodes would be intentionally oxidized in the ferro-ferricyanide solution to obtain tips made of WO_2 rather than elemental W. Each tip was cycled in the working solution (0.5 M KCl + 5 mM $Fe(CN)_6^{3-}$+ 5 mM $Fe(CN)_6^{4-}$) from -0.01 V to 0.45 V vs Ag/AgCl (1M KCl) at 100 mV s^{-1}. For these experiments the complete surface of the etched tips was submerged in solution along with approximately 5 mm of the tungsten wire in order to make sure that any portion of the wire in contact with the working solution has been oxidized.

Figure 5.5 shows the typical response during the intentional oxidation process of tungsten tips. In the first cycle the oxidation of both the surface and the probe are observed and in the further scans only the oxidation of the probe remains, putting in evidence the suitability of the material to be used as an electrode for the study of redox reactions from a probe in solution. The cycling was continued until a stable voltammogram was obtained (typically 10 cycles), and afterwards the obtained tips were directly used to perform the electrochemical characterization.

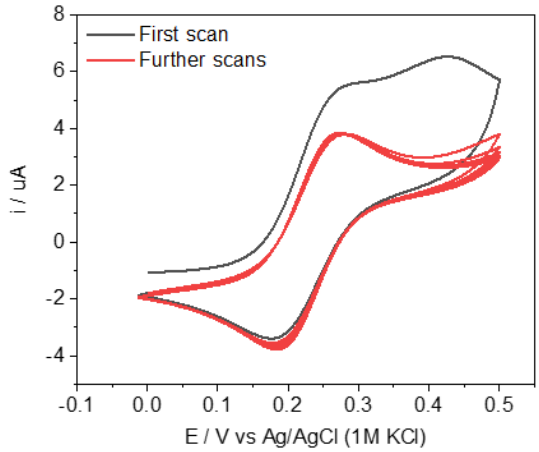

Figure 5.5 Typical response from the intentional oxidation of W tips to obtain WO_2 tips

CV's recorded in a 0.5 M KCl + 5 mM $Fe(CN)_6^{3-}$ + 5 mM $Fe(CN)_6^{4-}$ solution at 100 mVs^{-1}. The black curve corresponds to the first scan and the red ones are the following scans. It can be appreciated that a stable response is achieved.

5.2 Experiments performed at tungsten tips

5.2.1 Fabrication of the tungsten tips

Several electrochemical etching approaches were conducted in order to obtain tungsten tips with the desired features, i.e. high aspect ratio *H*, low roughness and small radius of curvature. The shape, roughness, size and diameter of the resulting tips depend noticeably on the conditions under which the electrochemical etching is performed. Accordingly, the first step was to monitor this process with an USB optical microscope. Figure 5.6a shows a scheme related to the necking effect produced during the etching process, as previously described in detail in section 4.2.1. Figure 5.6b displays the tungsten tip at two different times. It can be seen that few minutes after applying a voltage, there is a necking effect in the tungsten wire at the liquid-air interface.

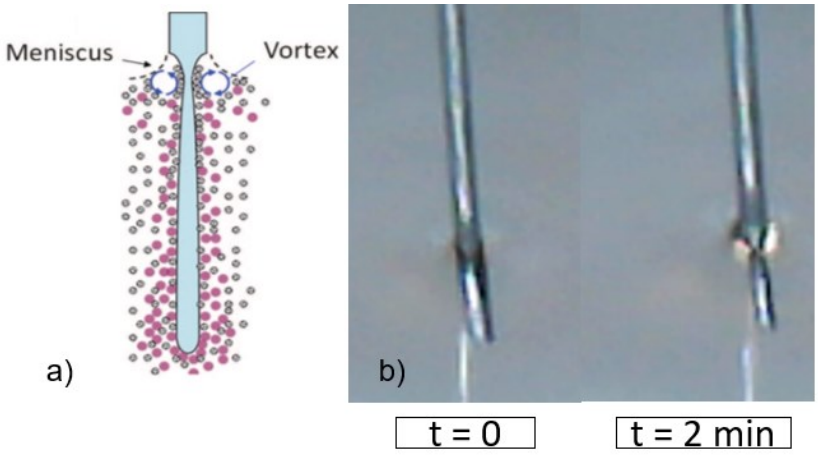

Figure 5.6 Monitoring the electrochemical etching process.

a) scheme showing the mechanism of the necking effect during the electrochemical etching. Reprinted from W. T. Chang, I. S. Hwang, M. T. Chang, C. Y. Lin, W. H. Hsu, and J. L. Hou, "Method of electrochemical etching of tungsten tips with controllable profiles," *Rev. Sci. Instrum.*, vol. 83, no. 8, pp. 1–7, 2012, with the permission of AIP publishing; and b) optical image showing the tungsten wire etching process at different times.

Among the factors that affect the final shape and size of the tips, we have the concentration of the electrolytic solution, the applied voltage, the depth of the tungsten wire in the solution and the capillary effects that produce the formation of a meniscus at the liquid-air interface.

As mentioned in section 4.2, one of the main concerns when etching tungsten tips is the behavior of the meniscus caused by the wettability of the tungsten surface by the working solution. It was attempted to prepare tips in a static meniscus regime to analyze the impact of other variables on the shape of the tips and to find a way to get the longest possible tips.

The effect of the applied voltage and the concentration of the KOH solution on the tip shape was investigated. Different tips were prepared in two different etching solutions (1M and 8M KOH) and it was found that when using the lowest concentration, the tip length tends to be larger for all the applied potentials (See Figure 5.7a). Also, it was observed that for both concentrations, the tip length does not vary with the applied voltage above 2 V.

Figure 5.7 b shows the relationship between the tip length and the tip diameter (as measured by SEM) and it can be seen that the diameter tends to decrease as the tip length increases. It also shows that low concentrated solutions must be used in order to get longer and therefore sharper tungsten tips.

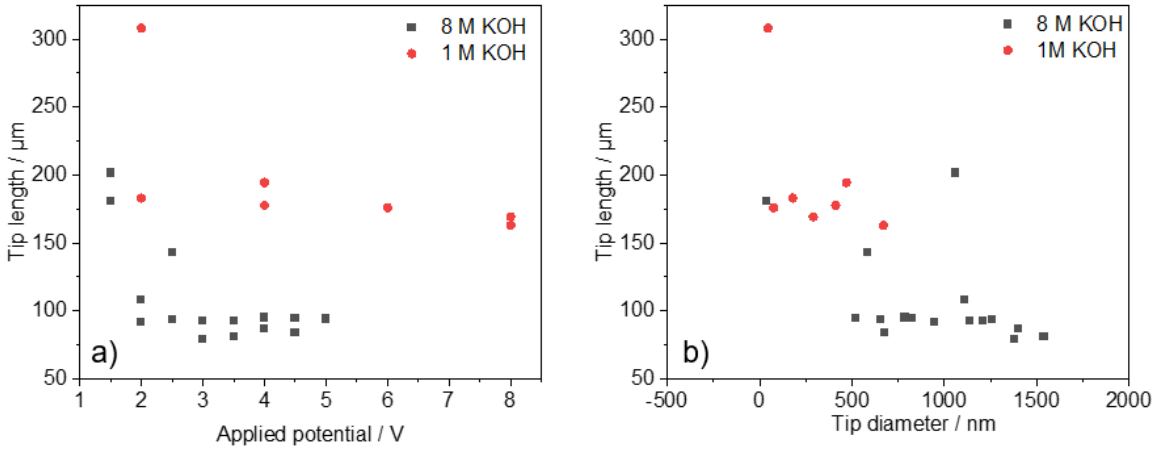

Figure 5.7 **a) Tip length as a function of the applied potential and b) tip diameter as a function of their length**

Figure 5.8 shows four tips obtained using different applied potential values and solution concentrations under a static meniscus regime. In general, long tips are more easily obtained with low concentrated solutions or by applying low voltages during the etching just as explained before. However, these tips are also very rough while the ones obtained with concentrated solutions or by applying high voltages, are very smooth. From these experiments it was decided to use middle concentrations and potential values to get tips that are both long and smooth to be used as electrodes in our further experiments.

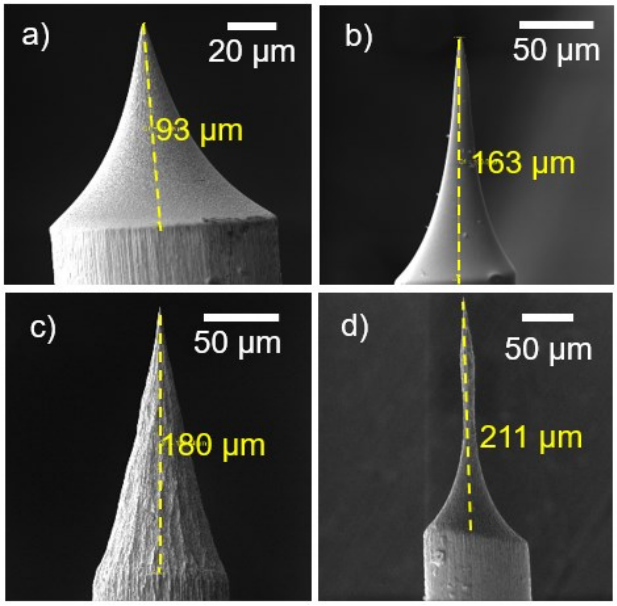

Figure 5.8 Tungsten tips obtained under different etching conditions.

Prepared in KOH a) 8 M solution at 3.5 V; b) 1 M solution at 8 V; c) 8 M at 1.5 V; and d) 3 M solution with two potential steps, one at 3 V and a second one at 1 V.

As mentioned in section 4.2 we then attempted to induce a dynamic meniscus regime in order to see the differences in the tips profile. Figure 5.9 a-d shows the progression of the etching process and it can be seen how the meniscus moves as the etching goes on, giving place to the formation of a very long and sharp tip that has a very smooth surface (see Figure 5.9e) in comparison to the ones that are obtained in the static meniscus regime.

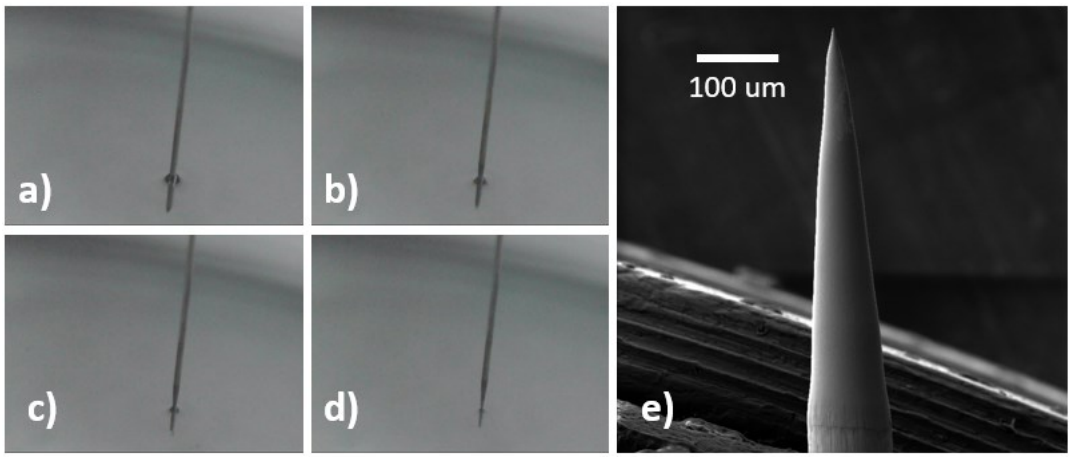

Figure 5.9 Induced dynamic meniscus regime to get sharp and smooth tips.

Optical photographs showing: a) the position of the wire at the beginning of the etching process, b) the position at 30 s, c) wire position at 1 min and) wire position after 1.5 min. e) SEM image of the tip obtained by this method. Tip prepared in a 5 M KOH solution with an applied voltage of 5 V vs W.

In order to further reduce the roughness of the tip surface, some of the produced tips with the dynamic meniscus regime method were subsequently etched by FIB. In this case, the ion beam was focused parallel to the tungsten tips and the etching was performed following a radial regime starting from the outer part of the wire and moving towards the rotation axis of the tip. Figure 5.10 shows how sharp a tip can get after FIB etching, and in the inset it is noticeable that the surface becomes smoother with a tip radius of curvature (*ROC*) was 12 nm.

Based on the obtained results, it was decided that the tips to be used for electrochemical measurements would be prepared by electrochemical etching in a 5 M KOH solution by applying 5 V and inducing a dynamic meniscus regime. Additionally, some of the tips would be FIB etched in order to minimize the roughness of the surface and therefore reduce the capillarity effects during the electrochemical experiments. Finally, the characterization of their electrochemical response as a function of the surface area exposed to the probe solution was performed as it will be explained in the following section.

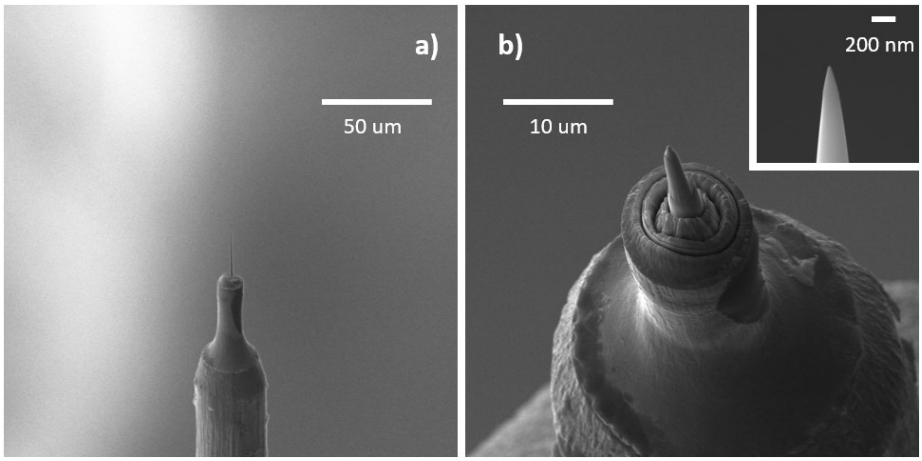

Figure 5.10 SEM images of FIB etched tip.

SEM images showing a) the tip after FIB etching at low magnification and b) same tip at high magnification; inset shows the frontal image of the tungsten tip at higher magnification.

5.2.2 Electrochemical characterization of tungsten tips

In the past, electrochemical techniques were used in order to determine the electrode shape because it was not possible at that time to get high resolution images of electrodes with radius of a few nanometers. However, in our case the aim of performing cyclic voltammetry as a function of the surface area exposed to the probe solution, is to find solid evidence of the effect of the electrode shape and size on the rate of electron transfer and therefore its potential applications for the study of single entities. In this work three different tips with different profiles were electrochemically characterized.

Cyclic voltammetry was performed using a tungsten tip named as tip 1 with a tip *ROC* of 100 nm in the ferro-ferricyanide solution. The voltammograms were recorded at different depths of the tip in solution by controlling its position with the micrometer of the positioning stage. The image of tip 1 and some of the recorded cyclic voltammograms as a function of the depth are shown in Figure 5.11.

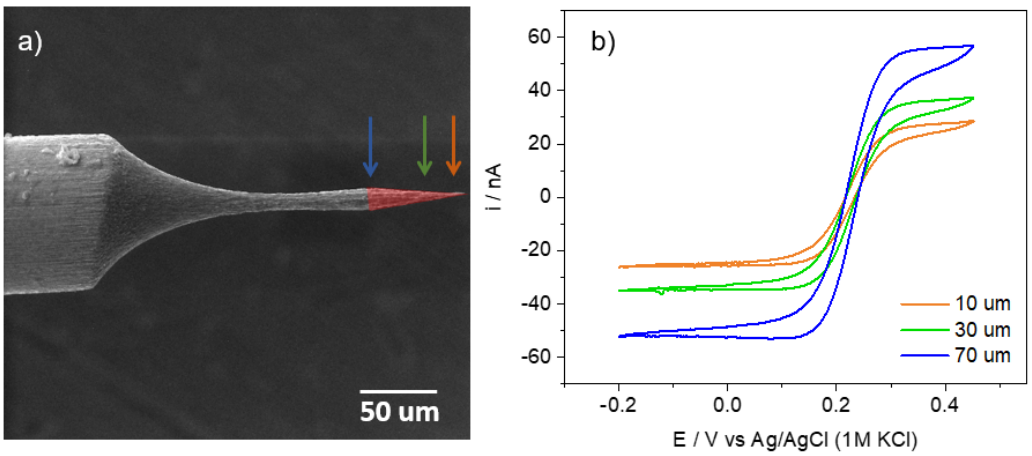

Figure 5.11 **a) SEM image of tip 1 showing the different depths in the working solution at which b) cyclic voltammograms were recorded.**

The CV's were recorded in a 0.5 M KCl + 5 mM $Fe(CN)_6^{3-}$ + 5 mM $Fe(CN)_6^{4-}$ solution at 10 mVs^{-1}.

As expected, cyclic voltammograms with a steady state behavior were obtained instead of the peak behavior that is usually observed for macro and micro electrodes. Additionally, the cyclic voltammograms recorded at different depth of the tip show an increase in the steady state current (i_{ss}) as the depth increases, which is expected due to an increase in the surface area that is exposed to the probe solution.

The electroactive surface area in contact with the probe solution was calculated from the oxidation steady state current from the cyclic voltammograms according to Equation 4. In the equation, *n* represents the number of electrons transferred during the process which in our specific case is one; *F* is the Faraday constant 96489 C mol^{-1}; *D* is the diffusion coefficient of the reduced species 0.667 x 10^{-5} cm^2 s^{-1}; *c* is the concentration of the reduced species in solution 5 x 10^{-6} mol cm^{-3}; *a* represents the radius of the base of the cone that is formed by the tip at the given depth in solution; *q* and *p* are statistical constants whose values are 0.30661 and 1.14466 respectively to get an accuracy to within 1 % [24]; and *H* represents the aspect ratio of the cone formed by the tip at the corresponding depth in solution. The aspect ratio, *H*, was calculated by dividing the depth of the tip in solution, *h* over the radius and, *a* was measured from the SEM images. For tip 1, *H* equals 10.

The steady state current i_{cone}^{ss} was measured at 0.4 V from the voltammograms obtained at each depth in solution. And the radius *a* was calculated using Equation 7, which is a different expression of Equation 4.

$$a = \frac{i_{cone}^{ss}}{4nFDc(1+qH^p)} \tag{7}$$

Since the tip is being treated as a perfect cone, after obtaining the radius, it is possible to calculate the surface area by using some simple geometrical factors of the cone (see Figure 4.5). In our case the area exposed to the solution corresponds to the lateral surface area of the cone (*LSA*) which can be calculated from Equation 8, where *a* represents the calculated cone radius and *l* is the slant height that can be calculated from *h* and using the Pythagorean theorem.

$$LSA = \pi a l \tag{8}$$

A comparison was made between the calculated electroactive surface area and the theoretical or geometric surface area. This last one was calculated directly from the SEM image shown in Figure 5.11 and was processed using the software *Image J*.

The electroactive surface area (ESA) and the geometric area (GA) plotted as a function of the depth of the tip in solution in Figure 5.12a, show that the obtained values are of the same order of magnitude. However, the electroactive surface area is higher, which is expected due to the roughness of the tip surface, which is noticeable Figure 5.12a. However, the trends followed by the increases in area with the depth are not the same in both cases. Because of this, we suspect that there are other effects affecting our calculation: i) the surface roughness of the tip electrode; ii) the contribution of the meniscus formed at the liquid-air interface between the solution and the tungsten tip; and iii) an effect of the electrical properties of the tip due to the shape and dimensions.

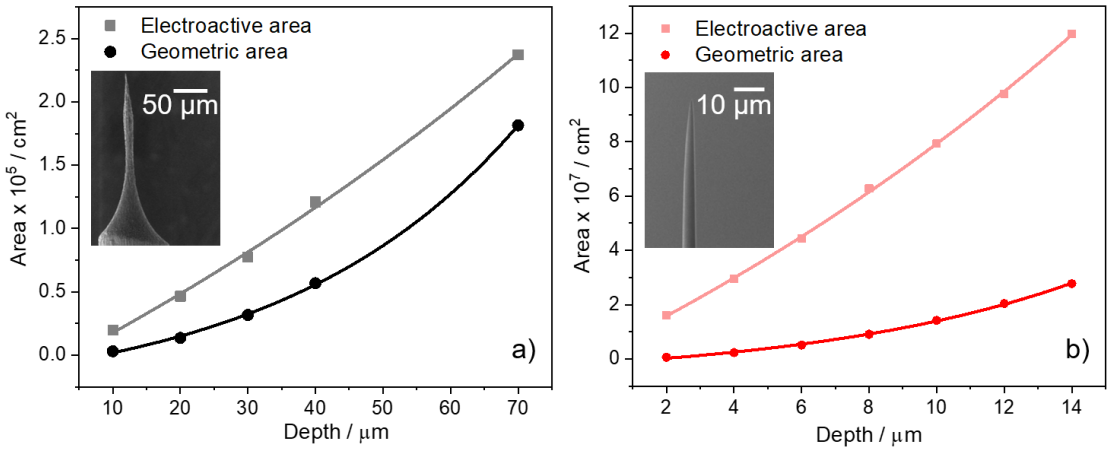

Figure 5.12 **Geometric parameters of the cone related to the lateral surface area for a) tip 1 and b) tip 2.**

A second electrode, named tip 2 was etched by FIB after the electrochemical fabrication in order to make it sharper and smoother (Figure 5.13b). For this electrode the surface area resulted to be significantly smaller compared to that of tip 1. As shown in Figure 5.12b the values of the electroactive surface area are comparable to the geometric one calculated by SEM. These studies were carried out with three different tips (Figure 5.13) but only two of them are shown in Figure 5.12, where a rough and a smooth tip are compared.

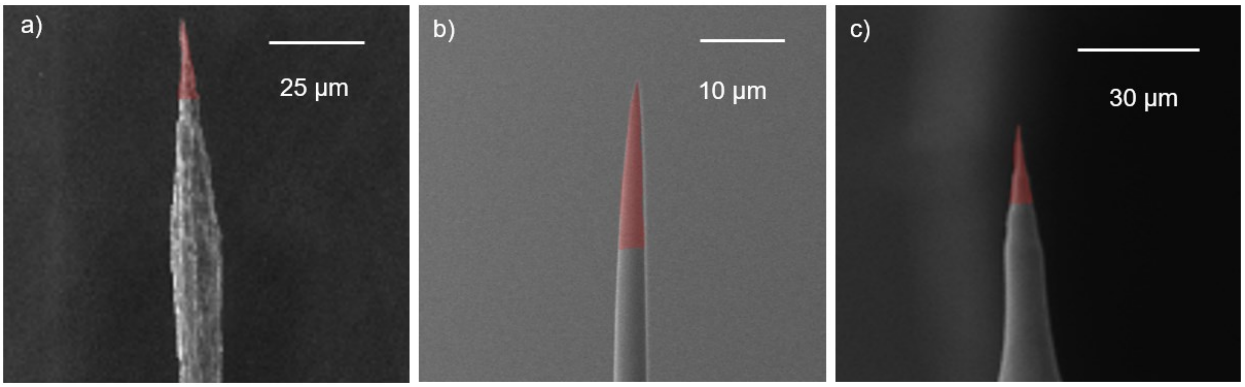

Figure 5.13 Electrochemically characterized tips.

(a) Tip 1obtained by electrochemical etching. *ROC*=100 nm, *H*=10. (b) Tip 2 obtained by electrochemical etching and FIB etching. *ROC*=65.6 nm, *H*=8. (c) Tip 3 obtained by electrochemical etching. *ROC*=65.6 nm, *H*=8. The red highlighted areas show the maximum depths at which the cyclic voltammograms were recorded for each tip.

Figure 5.14 shows the ratio of the electroactive surface area to the geometric one ESA/GA as a function of the depth of the tip in solution for the three different tips. The plot shows an interesting behavior in which the ratio ESA/GA rapidly increases when the depth of the tip in solution is lower than 20 µm. This behaviour suggests that at the apex of the conical structure there is an enhancement of the electron transfer due to the shape and the dimensions of the electrode. It results interesting that even though the tip shape, ROC, and aspect ratio *H,* are very different for the three tips showed, the behavior of the ratio ESA/GA is similar for all of them. However, there is no apparent relationship between the ratio ESA/GA and *ROC* or *H,* which is put in evidence by the fact that the ratio seems to decrease faster with the tip depth for tip 3 (blue curve), while for tips 1 and 2, the values seem to be closer.

In Figure 5.14 it is also noticeable that the values of the ratio ESA/GA are constant (between 1 and 2) when the tip depth is between 40 to 70 µm. We can conclude that the roughness factor of these tips is between 1 and 2. Therefore, the sudden increase in the ratio values with depths smaller than 20 µm is due to an enhancement of the electron transfer at the tip apex due to an electric field concentration effect, to the meniscus contribution, or to the combination of both.

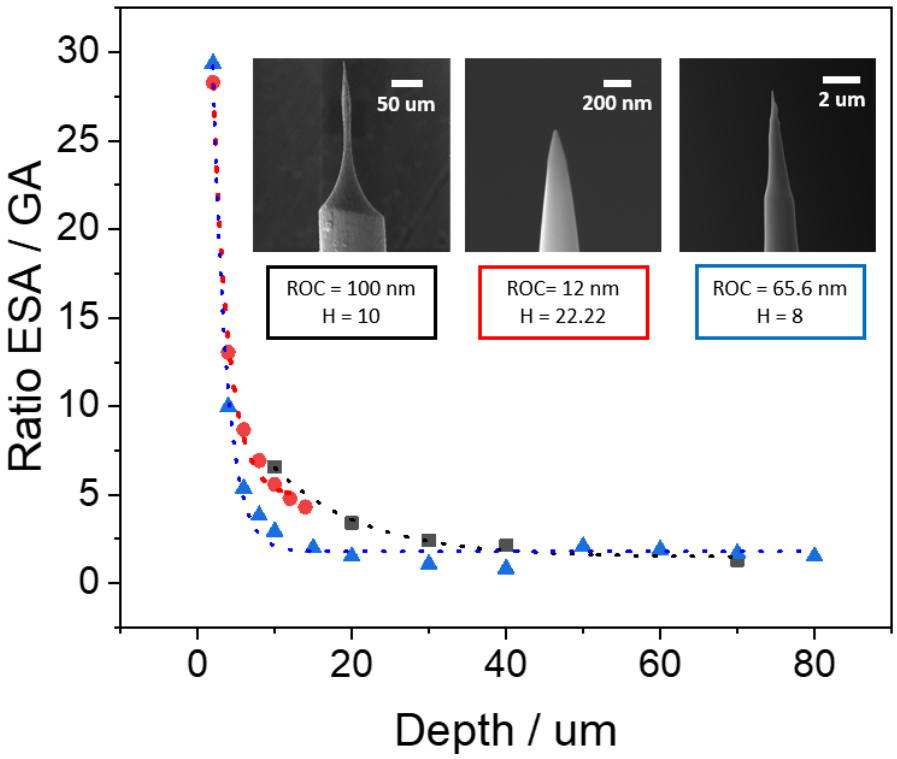

Figure 5.14 **Ratio ESA / GA as a function of the depth of the tip in solution, for three different tips.**

It has been previously reported [15], [17], [18] that electrode materials formed by needle-shaped structures are able to produce at low applied overpotentials, local high electric fields that concentrate electrolyte cations, leading to an enhancement of the CO_2 reduction due to an increased concentration. According to simulations performed by Liu et al. [17], this is due to a tenfold higher electric field associated with metallic nanometre-sized tips compared to quasi-planar electron regions. This fact results interesting because it was shown that the performance of a nanoneedle surpasses by an order of magnitude the performance of virtually any nanorod, nanoparticle and oxide derived noble metal catalyst [17].

Other studies based on simulations, propose the concentration of the electric fields at the apex of nanocone arrays made of Au [17], Cu@Sn [18] and Cu_1^0–Cu_1^{x+} pair structures [15]. This concentration of the electric field is thought to have enhanced the concentration of electrolytic cations because of a sharp conical feature that in turn leaded to a high local concentration of CO_2 enhancing its electrochemical reduction.

Unlike those studies, in our case the experiments were performed directly in solution and instead of nanoarrays, we used individual electrodes to perform our studies. Our results point to the possible existence of an electric field enhancement, and numerical simulations using COMSOL will be carried out in future works to complement our results.

After performing the electrochemical measurements, it was noticed that for tips whose ROC is smaller than 20 nm there is an oxide layer that forms on the tungsten surface (Figure 5.15a). This oxidation of the surface resulted to be a limitation because once the layer is formed, the surface is not conductive anymore and therefore the tip cannot be used for extra electrochemical measurements.

Figure 5.15 shows two different sharp tips (ROC=12 and 8 nm respectively) and in both cases it is observed that the thickness of the oxide layer increases (From 15 nm to 27 nm for a and from 10 to 16 nm for b) as it approaches the tip apex. For these tips it was not possible to perform the electrochemical characterization due to the fast formation of the oxide layer that impeded to record CV's after two depths in solution.

Despite the disadvantage that the oxide layer represents for the performance of electrochemical measurements, this can be taken as a direct evidence of the enhancement of the electric field at the tip apex due to a concentration of electrons that facilitate the reduction of oxygen molecules at this specific zone of the tips than in the rest of the surface.

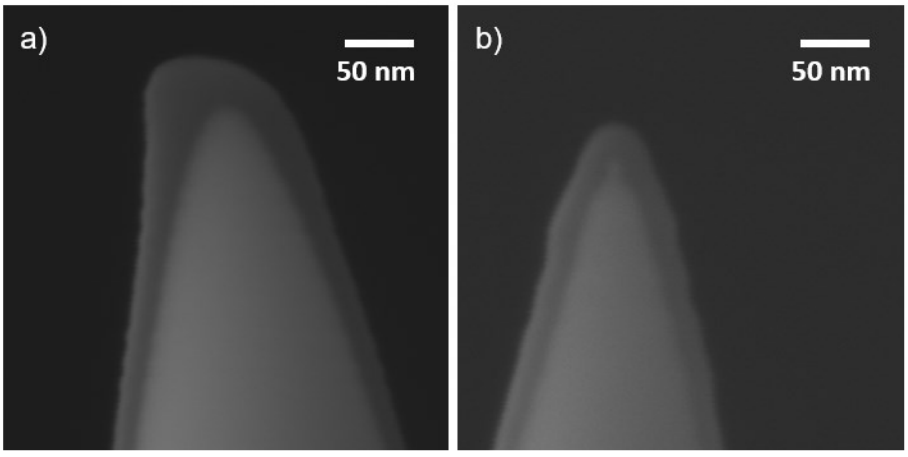

Figure 5.15 Oxide layer formed on tips after electrochemical characterization

5.3 Electrochemical deposition of gold on tungsten wires and tips

As mentioned in the last sections, one of the factors that affect the shape of the resulting tungsten tips is the meniscus that is formed at the air-solution interface when etching wires. However, this meniscus is also present when performing electrochemical measurements at tungsten tips. Therefore, it is important to quantify its contribution to the electrochemical signal recorded in the cyclic voltammograms. In the present work the meniscus height was measured as a function of the wire diameter, to quantify the surface area of the electrode covered by the meniscus.

The firs step consisted in the fabrication of tungsten wires of different diameters. This was achieved by performing electrochemical etching of tungsten wires under a static meniscus regime during short periods of time (15 to 30 seconds). As an example, Figure 5.16a shows a wire after four etching steps at different heights, where it can be appreciated that different diameters of the wire (from 10 to 100 µm) were achieved depending on the number of etching steps.

Then, the electrochemical deposition of gold was performed on the resulting tungsten wires in a 1 % wt solution of chloroauric acid ($HAuCl_4$) at the meniscus height as described in section 4.4. To achieve this, the tungsten wires were approached to the solution surface helped by the micro positioning stage, using a similar technique to the one described in section 4.3.2, that consisted in the monitoring of the OCP. Once in contact with the solution, a potential of -0.2 V vs AgAgCl (1M KCl) was applied to the wires for 15 seconds to carry on the cathodic deposition of gold.

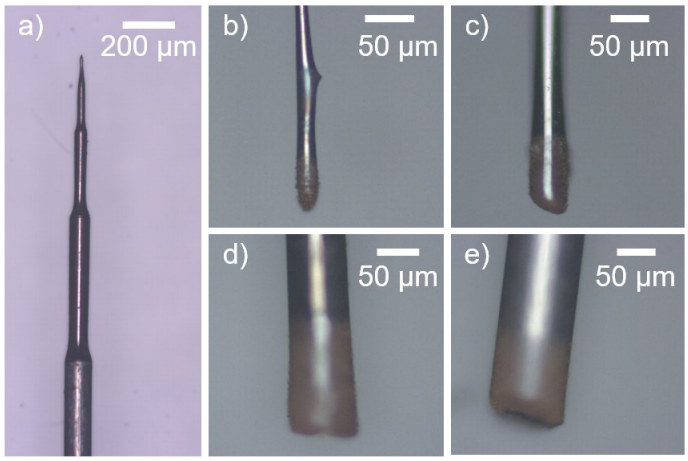

Figure 5.16 Tungsten wires of different diameters after the cathodic deposition of gold.

a) Tungsten wire after multiple etching steps in a 5 M KOH solution to get different diameters b-e) Tungsten wires with diameters of 30.1, 51.2, 76.8 and 100 µm respectively, after the cathodic deposition of gold in a 1 % wt solution of $HAuCl_4$.

Figure 5.16b-e shows the images of four wires of different diameters after the deposition of gold, obtained with an optical microscope. Using the software *image J*, the height of the gold layer (corresponding to the meniscus height) deposited on the tungsten wires was measured. The values of the height were plotted as a function of the tungsten wire diameter as shown in Figure 5.17. The behaviour of the meniscus height (*h*) presents a linear variation with the wire diameter (*d*). The equation describing this fit indicates that the meniscus height approximately doubles the wire diameter, and following this trend, the meniscus height for the fabricated tungsten tips would go from approximately 25 to 635 nm if we take the apex diameters as *d*. However, the variation of the diameter due to the conical structure of the tips is not considered in these results and it was necessary to perform similar studies using conical tips rather than wires.

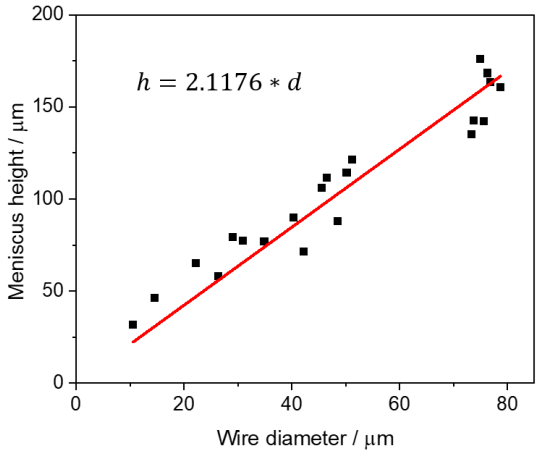

Figure 5.17 **Meniscus height as a function of the tungsten wire diameter.**

The cathodic deposition of gold was performed on different tungsten tips in a 0.1 % wt $HAuCl_4$ solution, varying the deposition time from 5 to 15 seconds. After the deposition, the tips were analyzed in the SEM. Figure 5.18 shows four different tungsten tips after the deposition of gold. The corresponding tip diameters are as follows: a) 264 nm; b) 300 nm; c) 300 nm; and d) 200 nm. According to the relationship stablished from Figure 5.17, the meniscus heights should be of less than 1 µm for all of them. However, it is not the case, as shown in Figure 5.18, where it is evident that the gold coatings cover more than 5 µm height for all the tips. This means that the previously established relationship is not valid at this scale, probably due to the geometry of the electrodes.

Figure 5.18 a, c and d, points for a capillarity effect during the deposition process. This effect is put in evidence by the presence of an area covered by a high density of gold near to the tip apex (probably corresponding to the meniscus height), followed by a gradually less dense coating along the tip length (due to the rise of the solution). This effect can be attributed to the surface roughness of the tips and therefore its extent is different for each one of them.

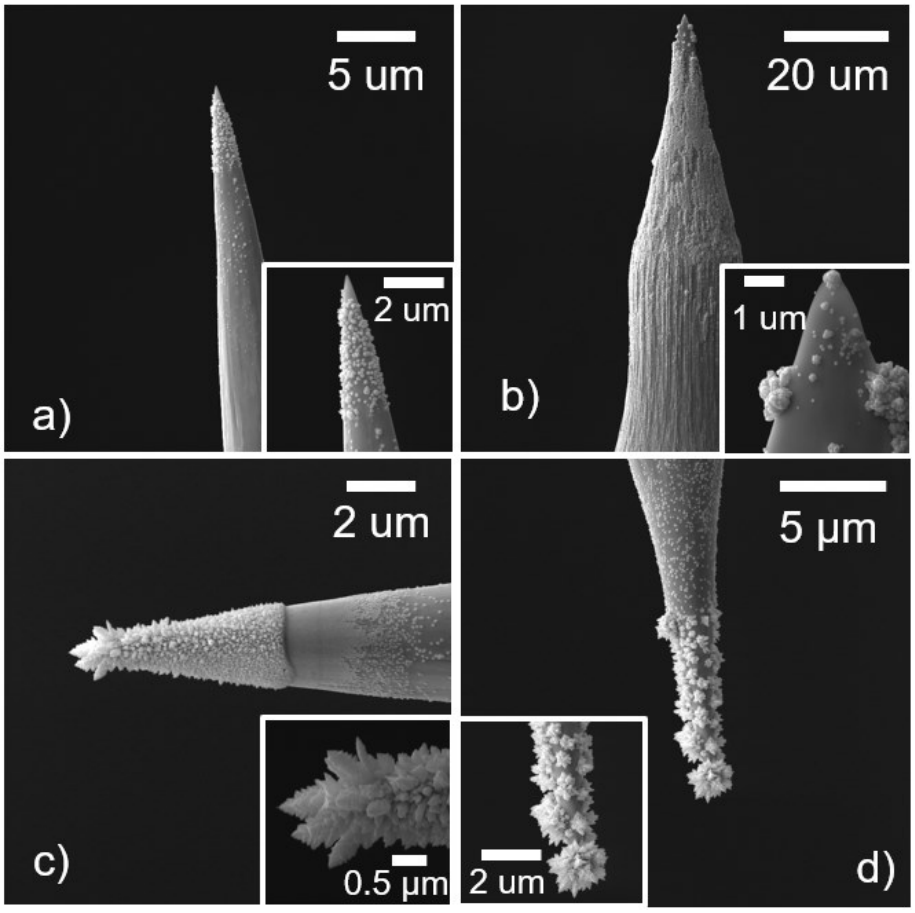

Figure 5.18 Tungsten tips after gold deposition.

The deposition of gold was performed in a 0.1 % wt $HAuCl_4$ aqueous solution at -0.2 V vs Ag/AgCl (1M KCl), for a-b) 5 s; c) 10 s; and d) 15 s.

In Figure 5.18 it can be observed that the morphology of the gold growth is different depending on the deposition time. For a and b, small clusters of gold cauliflower-like particles and agglomerates of 200-500 nm grew near to the tip apex, leaving the apex of the tungsten tip surface exposed. For c and d, the tungsten surface near the tip apex is fully covered by the gold coating. In this case the growth consists in dendrites whose length is higher (600-800 nm) when growing nearer to the tip apex. These results are not surprising since it is well known that electrochemical

deposition of metals allows to control the size, mass, thickness and morphology of the nanostructured materials by adjusting the operating conditions and bath chemistry [78].

The different morphologies obtained, could be an indication of changes in the growth direction of gold crystal faces on the tungsten tips, depending on the deposition conditions. This has been previously studied by El-Deab and coworkers, who used potential step electrolysis to grow Au nanoparticles on a glassy carbon electrode from an electrolytic bath comprising $NaAuCl_4$ and H_2SO_4. The characterization revealed that the deposited particles exhibited Au (111) plane as the predominant crystal orientation with a particle size higher than 100 nm [25], [26].

The electrochemical behaviour of different surface states of gold, from single crystals to polycrystalline structures and at different index faces has been previously studied and characterized in sulfuric acid (H_2SO_4) [27], [79]–[82]. These studies show that different index faces of gold present a different voltammetric response, regarding the position of the oxidation peaks. Figure 5.19 shows the typical voltammograms of a polycrystalline gold electrode in 0.1 M H_2SO_4 after activation in 0.37 M HCl. Three main oxidation peaks can be identified, and it was proposed that each one of them corresponds to a different crystal plane of the gold surface [27]. Jeyabharathi and co-workers demonstrated that the crystal planes of Au can be reliably distinguished based on the peak potentials of oxide formation [27]. Table 5.1 shows the corresponding potential peak values for the three low-index crystal planes of gold, measured versus the standard hydrogen reference electrode (SHE) at 100 mVs^{-1}. For these reasons, we decided to use voltammetric experiments to characterize the different structures grown on the tungsten tips.

Table 5.1 Peak potentials for different gold crystal planes [27]

Crystal plane	Peak potential / V vs SHE
(100)	0.93
(110)	0.99
(111)	1.14

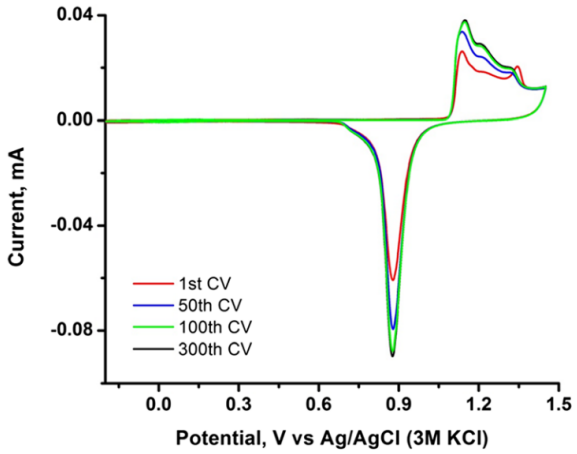

Figure 5.19 Typical cyclic voltammetry of polycrystalline gold electrode.

HCl_{aq}-activated gold surface in 0.1M H_2SO_4 solutions at the scan rate of 0.1 V s^{-1} for 300 cycles. The peaks at a (1.14 V), b (1.2 V) and c (1.35 V) are attributed to the oxidation of Au(100), Au(110) and Au(111) faces, respectively. Reprinted by permission from Springer Nature: Springer Journal of Solid State Electrochemistry [27], COPYRIGHT 2020.

Figure 5.20 shows three different tips after the electrochemical deposition of gold under different conditions of concentration, deposition time and number of deposition cycles. These tips were selected for the electrochemical measurements due to the notably different morphology of the gold deposits.

When the $HAuCl_4$ solution was concentrated (1% wt), and the potential was applied for longer times, large agglomerates were obtained as shown in Figure 5.20 a. Despite the agglomeration, the growth is ordered and shows a dendritic behaviour. In contrast, when the solution is diluted (0.1 % wt) the agglomeration effect is appeased, the deposition is homogeneous but the growth at the tip apex presents a different behaviour compared to the rest of the tip and wire as shown in Figure 5.20 b and c. In these two last figures it can be seen that even though the concentration of the solution was the same, the time had also a great effect on the gold growth behaviour (as demonstrated by El-Deab and co-workers [25]), being dendritic in both cases but sharp when doing the deposition for 5 s (Figure 5.20b) and more of an accumulation of cauliflower-like structures when doing it for 10 s (Figure 5.20c). In both cases the length of the dendrites is higher (200-400 nm) when they are nearer to the tip apex.

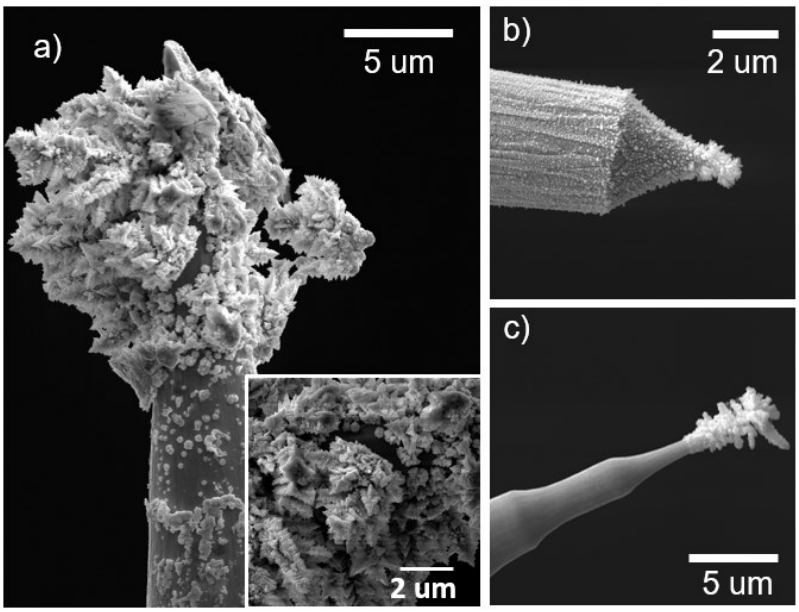

Figure 5.20 Gold deposited on tungsten tips under different experimental conditions.

a) Tips obtained in 1 % wt $HAuCl_4$ aqueous solution at -0.2 V vs Ag/AgCl (1 M KCl) for 15s, two times. *H=6.58*; b) Tip obtained in 0.1 % $HAuCl_4$ aqueous solution at -0.2 V vs Ag/AgCl (1 M KCl) for 5 s. *H=3.4*; and c) Tip obtained in 0.1 % $HAuCl_4$ aqueous solution at -0.2 V vs Ag/AgCl (1 M KCl) for 10 s. *H=7.6*.

Cyclic voltammetry of the tips shown in Figure 5.20 was performed in a 0.5 M H_2SO_4, using them as working electrodes. Figure 5.21 b-d shows the corresponding cyclic voltammograms. The expected voltammogram would show an oxidation peak at 1.37 V and a reduction one at 0.88 V vs Ag/AgCl (1M KCl). These peaks correspond to the oxidation of the gold surface to form Au_2O_3 and the reduction of such oxide, respectively. Figure 5.21a shows the voltammogram of a gold wire recorded under the same conditions that those for the tips.

The oxidation and reduction peaks were observed for the three tested tips, and even though the working potential window is the same in which tungsten gets oxidized, no signal corresponding to the formation of the tungsten oxides is observed. For each electrode, the peak current for both oxidation and the reduction peaks decreases with continuously cycling, which is indicative of dissolution of gold; behaviour that is also commonly observed in macroelectrodes [19].

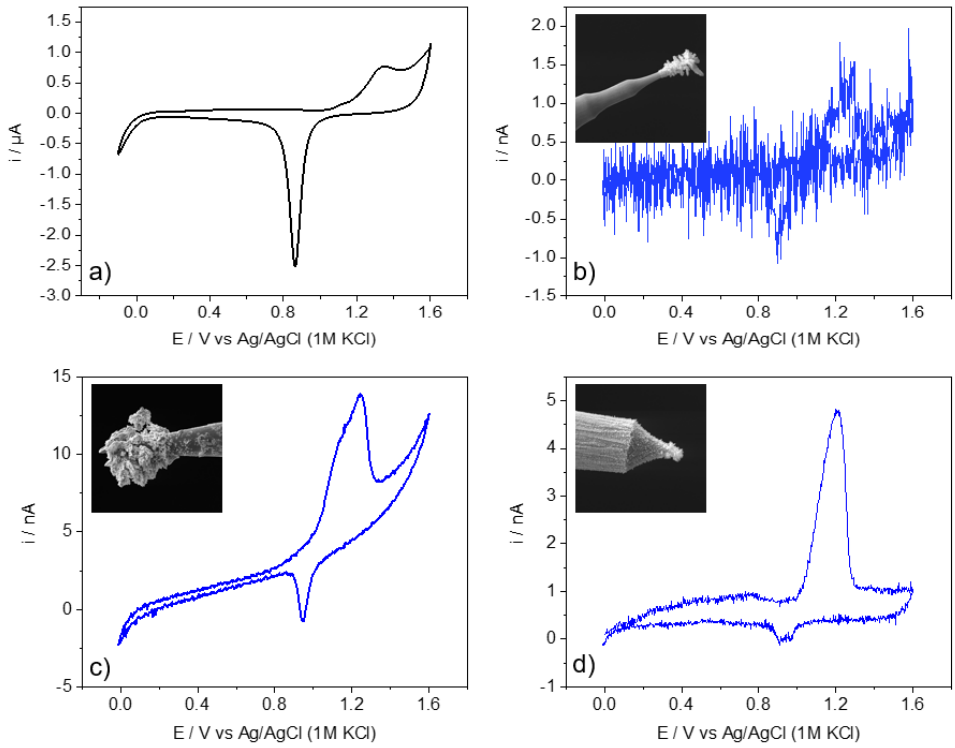

Figure 5.21 Cyclic voltammograms of tips deposited with gold in sulfuric acid 0.5 M.

Voltammograms recorded in a 0.5 M H_2SO_4 solution at 50 mVs^{-1} of: (a) gold wire (b-d) gold-deposited tungsten tips. Only the first cycles are shown.

As seen in Figure 5.21 b-d, the CV's show peak potential values for the oxidation of gold as follows: 0.99, 0.93 and 0.98 V vs SHE respectively. According to this information, the predominant planes in each of the tips are (110) for b, (100) for c and (110) for d. However, these experiments need further validation because the scan rates from the literature and the experimental ones are different. Besides it is expected that Au (111) dominates because it is the most thermodynamically stable plane [27]. However, from the voltammograms in Figure 5.21 it can be concluded that there are different planes growing on our tips based on the different position of the oxidation peaks. The SAED patterns are to be gotten in order to confirm this information.

The differences in the preferential orientation of the Au crystal planes electrochemically growth on the tungsten tips are of importance. Au nanoparticles and nanostructures are known to have electrocatalytic activity for the oxidation of different molecules like alcohols, CO, for the oxygen reduction reaction and for the CO_2 reduction. These molecules adsorb directly on the metallic surface undergoing electron transfer reactions, and therefore the kinetic of these reactions depend directly on the electrode properties such as the exposed crystal planes and the defects. The shape of the conical electrodes is particularly suitable for this kind of studies. In one hand, it

allows for enhanced mass transfer to the active sites. On the other hand, the conical shape of the electrodes [83], [84] should avoid the accumulation of gas bubbles that block the active surface.

Thus, electrochemical characterization of few well-defined Au nanoparticles would allow to correlate activity and stability with structure. It will overcome a limitation of traditional approaches where the current is originated from large macroscopic areas and thus it averages-out different structures and morphologies.

6 CONCLUSION AND PERSPECTIVES

We achieved the construction and calibration of an experimental set-up suitable for the preparation of sharp tungsten tips and we carried out their electrochemical characterization, after controlling the surface area that is exposed to the working solutions during the measurements. Due to the high resolution of the translation stage, our set up has a great potential to be used in further experiments with increasingly small surface areas until we achieve the study of a single entity.

A method based on the intentional induction of perturbations to the system by slowly retracting the tungsten wires from the solution during the etching process was developed, resulting in a dynamic meniscus regime giving place to long and sharp tips. A general relationship between the tip length and diameter was established and evaluated as a function of the working solution concentration and the applied voltage during the etching process.

The main limitations of the use of conical-shaped ultra micro electrodes were identified to be the tip diameter, the roughness of the surface, and the possible non-homogeneous contribution of the meniscus to the electrochemical signal at the air-solution interface. The tip diameter can be partially controlled during the electrochemcal etching and further modified by focused ion beam etching. This last technique was successfully used to address the problem of the surface roughness. However the non-homogenous contribution of the meniscus to the electrochemical signal is still to be studied. Numerical simulations of similar experiments will be carried out in order to find out the accordance with the experimental results as an approach to dismiss the contribution of the meniscus to the electrochemical signal.

We found direct experimental evidence sugesting a concentration of the electric field at the tip apex due to its shape and size. The first evidence was found by electrochemistry, where it was observed that the ratio of the electroactive surface area to the geometric one presents a huge exponential increase when performing the measurements at zones nearby to the apex and coming almost constant when the tip is deeper in solution. The second direct evidence is the growth of the tungsten oxide layer with a gradually increasing thickness as it aproaches the tip apex which means that there is an increased number of free electrons at this area that can be transferred to the oxygen molecules in air or the ones that are dissolved in the working solutions. Oxygen ions are thus generated and enter the metal surface leading to the corrosion of the material, forming an oxide layer.

Moreover, small clusters of gold cauliflower-like particles where successfully grown on tungsten tips. However when a low gold content is deposited it is challenging to record the characteristic electrochemical signal of gold. This was related to the the high surface area of tungsten that is left exposed after the depostion, consequently presenting a stronger signal due to its oxidation. On the other hand, when increasing the amount of gold deposited on the surface not only it was possible to record the oxidation and reduction characteristic signals of gold surfaces but also it was found that depending on the tip shape and size, and the conditions used during the deposition, different crystallographic orientations can be selectively grown.

All the obtained results show that the approach we used has a huge potential to study single entity electrochemistry on single-crystal gold surfaces, which would contribute to the overall understanding of the underlying physical principles, reaction mechanisms and dynamics of electrochemical processes that are well known to occur on many length and timescales. Besides, thanks to the size and shape of the obtained electrodes, they have also potential biological applications for the study of metabolic redox reactions occuring inside individual living cells, or even single organelles such as mitochondrion whose reactions have been widely studied by biochemist and that not only have a huge importance for the general function of living organisms, but also play a very important role in the development of certain chronic diseases such as cancer.

7 BIBLIOGRAPHY

[1] R. J. Young, J. R. A. Cleaver, and H. Ahmed, “Gas-assisted focused ion beam etching for microfabrication and inspection,” *Microelectron. Eng.*, vol. 11, no. 1–4, pp. 409–412, 1990.

[2] J. Zhao, F. Meng, X. Zhu, K. Han, S. Liu, and G. Li, “Electrochemistry of mitochondria: A new way to understand their structure and function,” *Electroanalysis*, vol. 20, no. 14, pp. 1593–1598, 2008.

[3] T. Wang and S. D. Minteer, “Effect of riboflavin metabolites on mitochondrial electrochemistry,” *J. Electrochem. Soc.*, vol. 163, no. 13, pp. H1047–H1052, 2016.

[4] V. A. Hernández, U. Lendeckel, and F. Scholz, *Electrochemistry of Adhesion and Spreading of Lipid Vesicles on Electrodes*. 2013.

[5] F. Meng, J. Yang, T. Liu, X. Zhu, and G. Li, “Electric communication between the inner part of a cell and an electrode: The way to look inside a cell,” *Anal. Chem.*, vol. 81, no. 21, pp. 9168–9171, 2009.

[6] A. Auerbach and F. Sachs, “Patch Clamp Studies of,” pp. 269–302, 1984.

[7] L. Santos *et al.*, “Synthesis of WO3 nanoparticles for biosensing applications,” *Sensors Actuators, B Chem.*, vol. 223, pp. 186–194, 2016.

[8] G. Li and P. Miao, “Electrochemical analysis of Proteins and Cells,” *SpringerBriefs Mol. Sci.*, pp. 5–7, 2013.

[9] N. Zouaoui *et al.*, “Electroreduction of CO2 to formate on amine modified Pb electrodes,” *J. Mater. Chem. A*, vol. 7, pp. 11272–11281, 2019.

[10] R. Elshafey, M. Siaj, and A. C. Tavares, “Au nanoparticles decorated graphene nanosheets for electrochemical immunosensing of p53 antibodies for cancer prognostics,” *Analyst*, vol. 141, no. 9, pp. 2733–2740, 2016.

[11] A. C. T. F. Capitanio, S. Siracusano. A. Stassi, V. Baglio, A.S. Arico, “AC Impedance Spectroscopy Investigation of Carbon Supported Pt3Co and Pt Cathode Catalysts in Direct Methanol Fuel Cell,” *Int. J. Hydrog. Energy2*, vol. 39, pp. 8026–8033, 2014.

[12] X. Shan *et al.*, “Imaging the electrocatalytic activity of single nanoparticles,” *Nat. Nanotechnol.*, vol. 7, no. 10, pp. 668–672, 2012.

[13] L. A. Baker, “Perspective and Prospectus on Single-Entity Electrochemistry,” *J. Am. Chem. Soc.*, vol. 140, pp. 15549–15559, 2018.

[14] E. N. Saw, V. Grasmik, C. Rurainsky, M. Epple, and K. Tschulik, “Electrochemistry at single bimetallic nanoparticles - using nano impacts for sizing and compositional analysis of individual AgAu alloy nanoparticles,” *Faraday Discuss.*, vol. 193, pp. 327–338, 2016.

[15] J. Jiao *et al.*, “Copper atom-pair catalyst anchored on alloy nanowires for selective and efficient electrochemical reduction of CO 2,” *Nat. Chem.*, vol. 11, no. 3, pp. 222–228, 2019.

[16] C. Chen, Y. Pang, F. Zhang, J. Zhong, B. Zhang, and Z. Cheng, “Sharp Cu@Sn nanocones on Cu foam for highly selective and efficient electrochemical reduction of CO2 to formate,” *J. Mater. Chem. A*, vol. 6, no. 40, pp. 19621–19630, 2018.

[17] M. Liu *et al.*, “Enhanced electrocatalytic CO2 reduction via field-induced reagent concentration,” *Nature*, vol. 537, no. 7620, pp. 382–386, 2016.

[18] C. Chen, Y. Pang, F. Zhang, J. Zhong, B. Zhang, and Z. Cheng, “Sharp Cu@Sn nanocones on Cu foam for highly selective and efficient electrochemical reduction of CO2 to formate,” *J. Mater. Chem. A*, vol. 6, no. 40, pp. 19621–19630, 2018.

[19] Y. Li, J. T. Cox, and B. Zhang, “Electrochemical responses and electrocatalysis at single Au nanoparticles,” *J. Am. Chem. Soc.*, vol. 132, no. 9, pp. 3047–3054, 2010.

[20] H. Hua, Y. Liu, D. Wang, and Y. Li, “Size-Dependent Voltammetry at Single Silver Nanoelectrodes,” *Anal. Chem.*, vol. 90, no. 16, pp. 9677–9681, 2018.

[21] S. J. Konopka and B. McDuffie, “Diffusion Coefficients of Ferri- and Ferrocyanide Ions in Aqueous Media, Using Twin-Electrode Thin-Layer Electrochemistry,” *Anal. Chem.*, vol. 42, no. 14, pp. 1741–1746, 1970.

[22] M. S. El-Basiouny, S. A. Hassan, and M. M. Hefny, “On the electrochemical behaviour of tungsten: the formation and dissolution of tungsten oxide in sulphuric acid solutions,” *Corros. Sci.*, vol. 20, no. 7, pp. 909–917, 1980.

[23] P. I. Ortiz, M. L. Teijelo, and M. C. Giordano, “Electrochemical behaviour of tungsten in alkaline media. Part I. NaOH solutions,” *J. Electroanal. Chem.*, vol. 243, no. 2, pp. 379–391, 1988.

[24] C. G. Zoski and M. V. Mirkin, “Steady-state limiting currents at finite conical microelectrodes,” *Anal. Chem.*, vol. 74, no. 9, pp. 1986–1992, 2002.

[25] M. S. El-Deab, “On the preferential crystallographic orientation of Au nanoparticles: Effect of electrodeposition time,” *Electrochim. Acta*, vol. 54, no. 14, pp. 3720–3725, 2009.

[26] M. S. El-Deab, T. Okajima, and T. Ohsaka, “Electrochemical Reduction of Oxygen on Gold Nanoparticle-Electrodeposited Glassy Carbon Electrodes,” *J. Electrochem. Soc.*, vol. 150, no. 7, p. A851, 2003.

[27] C. Jeyabharathi, P. Ahrens, U. Hasse, and F. Scholz, “Identification of low-index crystal planes of polycrystalline gold on the basis of electrochemical oxide layer formation,” *J. Solid State Electrochem.*, vol. 20, no. 11, pp. 3025–3031, 2016.

[28] C. H. Chen, E. R. Ravenhill, D. Momotenko, Y. R. Kim, S. C. S. Lai, and P. R. Unwin, “Impact of Surface Chemistry on Nanoparticle-Electrode Interactions in the Electrochemical Detection of Nanoparticle Collisions,” *Langmuir*, vol. 31, no. 43, pp. 11932–11942, 2015.

[29] M. V. Mirkin, T. Sun, Y. Yu, and M. Zhou, “Electrochemistry at One Nanoparticle,” *Acc. Chem. Res.*, vol. 49, no. 10, pp. 2328–2335, 2016.

[30] Y. Yu *et al.*, “Electrochemistry and Electrocatalysis at Single Gold Nanoparticles Attached to Carbon Nanoelectrodes,” *ChemElectroChem*, vol. 2, no. 1, pp. 58–63, 2015.

[31] A. J. Melmed, “The art and science and other aspects of making sharp tips,” *J. Vac. Sci. Technol. B Microelectron. Nanom. Struct.*, vol. 9, no. 2, p. 601, 1991.

[32] W. T. Chang, I. S. Hwang, M. T. Chang, C. Y. Lin, W. H. Hsu, and J. L. Hou, “Method of electrochemical etching of tungsten tips with controllable profiles,” *Rev. Sci. Instrum.*, vol. 83, no. 8, pp. 1–7, 2012.

[33] M. V. Mirkin, F. R. F. Fan, and A. J. Bard, “Scanning electrochemical microscopy part 13. Evaluation of the tip shapes of nanometer size microelectrodes,” *J. Electroanal. Chem.*, vol. 328, no. 1–2, pp. 47–62, 1992.

[34] J. T. Cox and B. Zhang, “Nanoelectrodes: Recent Advances and New Directions,” *Annu. Rev. Anal. Chem.*, vol. 5, no. 1, pp. 253–272, 2012.

[35] National Science & Technology Council, “National Nanotechnology Initiative: Leading To the Next Industrial Revolution. A Report by the Interagency Working Group on Nanoscience, Engineering and Technology, Committee on Technology, National Science and Technology Council,” no. February, pp. 205–212, 2000.

[36] R. Chang and K. Goldsby, “Electrochemistry,” in *Chemistry*, 11th ed., R. Alvarez-Manzo and S. Ponce-Lopez, Eds. Mexico: Mc Graw Hill, 2013, p. 815.

[37] D. Skoog, D. West, J. Holler, and S. Crouch, “Electrochemical Methods,” in *Fundamentals of Analytical Chemistry*, 9th ed., Brooks/Cole, Cengage Learning, 2013, pp. 442–648.

[38] A. Bard and L. Faulkner, *Electrochemical Methods*, 2nd ed., vol. 1. John Wileyand Sons, Inc., 2001.

[39] D. Harvey, “CHAPTER 2. Electrochemical Methods,” in *Analytical chemistry 2.0*, 2015, pp. 12–25.

[40] L. R. Faulkner, “Understanding electrochemistry: Some distinctive concepts,” *J. Chem. Educ.*, vol. 60, no. 4, pp. 262–264, 1983.

[41] J. T. Maloy, “Factors affecting the shape of current-potential curves,” *J. Chem. Educ.*, vol. 60, no. 4, pp. 285–289, 1983.

[42] N. Elgrishi, K. J. Rountree, B. D. McCarthy, E. S. Rountree, T. T. Eisenhart, and J. L. Dempsey, “A Practical Beginner’s Guide to Cyclic Voltammetry,” *J. Chem. Educ.*, vol. 95, no. 2, pp. 197–206, 2018.

[43] N. M. Nanoparticles, R. W. Murray, and R. W. Murray, “Nanoelectrochemistry : Metal Nanoparticles , Nanoelectrodes , and Nanopores,” *Chem. Rev.*, vol. 108, no. 7, pp. 2688–2720, 2008.

[44] S. M. Oja, M. Wood, and B. Zhang, “Nanoscale electrochemistry,” *Anal. Chem.*, vol. 85, no. 2, pp. 473–486, 2013.

[45] T. Albrecht, S. Horswell, L. K. Allerston, N. V. Rees, and P. Rodriguez, “Electrochemical processes at the nanoscale,” *Curr. Opin. Electrochem.*, vol. 7, pp. 138–145, 2018.

[46] S. M. Oja, Y. Fan, C. M. Armstrong, P. Defnet, and B. Zhang, “Nanoscale Electrochemistry Revisited,” *Anal. Chem.*, vol. 88, no. 1, pp. 414–430, 2016.

[47] H. Zhang and J. F. Banfield, “Size Dependence of the Kinetic Rate Constant for Phase Transformation in TiO 2 Nanoparticles,” vol. 17, pp. 3421–3425, 2005.

[48] R. M. Wightman, “Microvoltammetric Electrodes,” *Anal. Chem.*, vol. 53, no. 9, pp. 1125A-1134A, 1981.

[49] A. J. Bard, F. R. F. Fan, J. Kwak, and O. Lev, “Scanning Electrochemical Microscopy. Introduction and Principles,” *Anal. Chem.*, vol. 61, no. 2, pp. 132–138, 1989.

[50] D. W. M. Arrigan, “Nanoelectrodes, nanoelectrode arrays and their applications,” *Analyst*, vol. 129, no. 12, pp. 1157–1165, 2004.

[51] N. Ebejer, A. G. Güell, S. C. S. Lai, K. McKelvey, M. E. Snowden, and P. R. Unwin, “Scanning Electrochemical Cell Microscopy: A Versatile Technique for Nanoscale Electrochemistry and Functional Imaging,” *Annu. Rev. Anal. Chem.*, vol. 6, no. 1, pp. 329–351, 2013.

[52] J. Kwak and A. J. Bard, “Scanning electrochemical microscopy. Theory of the feedback mode,” *Anal. Chem.*, vol. 61, no. 11, pp. 1221–1227, 1989.

[53] P. Actis *et al.*, “Electrochemical nanoprobes for single-cell analysis,” *ACS Nano*, vol. 8, no. 1, pp. 875–884, 2014.

[54] M. Kulakov, I. Luzinov, and K. G. Kornev, “Capillary and surface effects in the formation of nanosharp tungsten tips by electropolishing,” *Langmuir*, vol. 25, no. 8, pp. 4462–4468, 2009.

[55] A. Bani Milhim and R. Ben Mrad, “Electrochemical etching technique: Conical-long-sharp tungsten tips for nanoapplications,” *J. Vac. Sci. Technol. B, Nanotechnol. Microelectron. Mater. Process. Meas. Phenom.*, vol. 32, no. 3, p. 031806, 2014.

[56] A. Hermans and R. M. Wightman, “Conical tungsten tips as substrates for the preparation of ultramicroelectrodes,” *Langmuir*, vol. 22, no. 25, pp. 10348–10353, 2006.

[57] C. J. Slevin, N. J. Gray, J. V. MacPherson, M. A. Webb, and P. R. Unwin, “Fabrication and characterisation of nanometre-sized platinum electrodes for voltammetric analysis and imaging,” *Electrochem. commun.*, vol. 1, no. 7, pp. 282–288, 1999.

[58] S. Chen and A. Kucernak, “The voltammetric response of nanometer-sized carbon electrodes,” *J. Phys. Chem. B*, vol. 106, no. 36, pp. 9396–9404, 2002.

[59] D. H. Woo, H. Kang, and S. M. Park, “Fabrication of Nanoscale Gold Disk Electrodes Using Ultrashort Pulse Etching,” *Anal. Chem.*, vol. 75, no. 23, pp. 6732–6736, 2003.

[60] D. K. Y. Wong and L. Y. F. Xu, “Voltammetric Studies of Carbon Disk Electrodes with Submicrometer-Sized Structural Diameters,” *Anal. Chem.*, vol. 67, no. 22, pp. 4086–4090, 1995.

[61] Y. Gonzalez, R. Sany, and A. Ruediger, “A facile fabrication procedure for platinum nanoprobes with high-aspect-ratio and low tip radii via electrochemical etching A facile fabrication procedure for platinum nanoprobes with high-aspect-ratio and low tip radii via electrochemical etching,” vol. 033702, no. December 2019, 2020.

[62] M. Anik and K. Osseo-Asare, “Effect of pH on the anodic behavior of tungsten,” *J. Electrochem. Soc.*, vol. 149, no. 6, 2002.

[63] A. M. Baticle, J. L. Sculfort, P. Vennerau, and J. Vernieres, “Comportement Electrochimique d’Electrodes Monocristallines de Tungstene (Plan 110),” *Electrochim. Acta*, vol. 21, pp. 839–847, 1976.

[64] M. Anik, “Anodic reaction characteristics of tungsten in basic phosphate solutions,” *Corros. Sci.*, vol. 52, no. 9, pp. 3109–3117, 2010.

[65] M. Anik and T. Cansizoglu, “Dissolution kinetics of WO_3 in acidic solutions,” *J. Appl. Electrochem.*, vol. 36, pp. 603–608, 2006.

[66] M. Anik, T. Cansizoğlu, and S. Çevik, “Diffusion effect on the anodic reactions of tungsten,” *Turkish J. Chem.*, vol. 28, no. 4, pp. 425–439, 2004.

[67] M. Anik, “pH-dependent anodic reaction behavior of tungsten in acidic phosphate solutions,” *Electrochim. Acta*, vol. 54, no. 15, pp. 3943–3951, 2009.

[68] T. Hagedorn, M. El Ouali, W. Paul, D. Oliver, Y. Miyahara, and P. Grütter, “Refined tip preparation by electrochemical etching and ultrahigh vacuum treatment to obtain atomically sharp tips for scanning tunneling microscope and atomic force microscope,” *Rev. Sci. Instrum.*, vol. 82, no. 11, pp. 1–5, 2011.

[69] Y. Nakamura, Y. Mera, and K. Maeda, “A reproducible method to fabricate atomically sharp tips for scanning tunneling microscopy,” *Rev. Sci. Instrum.*, vol. 70, no. 8, pp. 3373–3376, 1999.

[70] J. B. Lalanne, W. Paul, D. Oliver, and P. H. Grtter, “Note: Electrochemical etching of sharp iridium tips,” *Rev. Sci. Instrum.*, vol. 82, no. 11, pp. 1–2, 2011.

[71] J. P. Ibe *et al.*, “On the electrochemical etching of tips for scanning tunneling microscopy,” *J. Vac. Sci. Technol. A Vacuum, Surfaces, Film.*, vol. 8, no. 4, pp. 3570–3575, 1990.

[72] A. S. Lucier, H. Mortensen, Y. Sun, and P. Grütter, “Determination of the atomic structure of scanning probe microscopy tungsten tips by field ion microscopy,” *Phys. Rev. B - Condens. Matter Mater. Phys.*, vol. 72, no. 23, pp. 1–9, 2005.

[73] M. Maria and S. Neves, “Advanced Nanoscale Approaches to Single- (Bio) entity Sensing and Imaging,” 2018.

[74] S. Zhang, M. Li, B. Su, and Y. Shao, “Fabrication and Use of Nanopipettes in Chemical Analysis,” *Annu. Rev. Anal. Chem.*, vol. 11, no. 1, pp. 265–286, 2018.

[75] J. Clausmeyer and W. Schuhmann, “Nanoelectrodes: Applications in electrocatalysis, single-cell analysis and high-resolution electrochemical imaging,” *TrAC - Trends Anal. Chem.*, vol. 79, pp. 46–59, 2016.

[76] M. Zhou, J. E. Dick, and A. J. Bard, “Electrodeposition of Isolated Platinum Atoms and Clusters on Bismuth - Characterization and Electrocatalysis,” *J. Am. Chem. Soc.*, vol. 139, no. 48, pp. 17677–17682, 2017.

[77] M. Zhou, S. Bao, and A. J. Bard, “Probing Size and Substrate Effects on the Hydrogen Evolution Reaction by Single Isolated Pt Atoms, Atomic Clusters, and Nanoparticles,” *J. Am. Chem. Soc.*, vol. 141, no. 18, pp. 7327–7332, 2019.

[78] U. S. Mohanty, “Electrodeposition: A versatile and inexpensive tool for the synthesis of nanoparticles, nanorods, nanowires, and nanoclusters of metals,” *J. Appl. Electrochem.*, vol. 41, no. 3, pp. 257–270, 2011.

[79] L. D. Burke and A. P. O’Mullane, “Generation of active surface states of gold and the role of such states in electrocatalysis,” *J. Solid State Electrochem.*, vol. 4, no. 5, pp. 285–297, 2000.

[80] L. D. Burke and P. F. Nugent, “The electrochemistry of gold: I. The redox behaviour of the metal in aqueous media,” *Gold Bull.*, vol. 30, no. 2, pp. 43–53, 1997.

[81] A. Hamelin, “Cyclic voltammetry at gold single-crystal surfaces. Part 1. Behaviour at low-index faces,” *J. Electroanal. Chem.*, vol. 407, no. 1–2, pp. 1–11, 1996.

[82] A. Hamelin and A. M. Martins, “Cyclic voltammetry at gold single-crystal surfaces. Part 2. Behaviour of high-index faces,” *J. Electroanal. Chem.*, vol. 407, no. 1–2, pp. 13–21, 1996.

[83] A. V. Sokirko and K. B. Oldham, “The voltammetric response of a conical electrode,” *J. Electroanal. Chem.*, vol. 430, no. 1–2, pp. 15–24, 1997.

[84] L. J. J. Janssen, “Mass transfer at rotating ring-cone electrodes,” *J. Appl. Electrochem.*, vol. 22, no. 11, pp. 1091–1094, 1992.

8 Appendix I. Calibration of the piezoelectric translation stage

Piezoelectricity is the effect that certain crystals present in which when squeezed, electricity can flow through them. Usually the opposite is true as well: when passing electricity through the crystal, it squeezes itself by vibrating back and forth. Usually the expansion is very small, but it can be finely controlled by varying the strength of the electric field. And it is because of this and the fact that the resolution is limited only by the noise and stability of the drive electronics that piezoelectric materials form the basis of very high precision actuators.

Even though they have a very high resolution there is an inherent problem of piezoelectric actuators: hysteresis. This effect is the tendency of the actuator to reach a final position that lags the demand position. Therefore, if a cyclic voltage is applied, the positions reached on the upward sweep are smaller than those on the downward sweep showing a behavior like the one plotted in Figure 8.1.

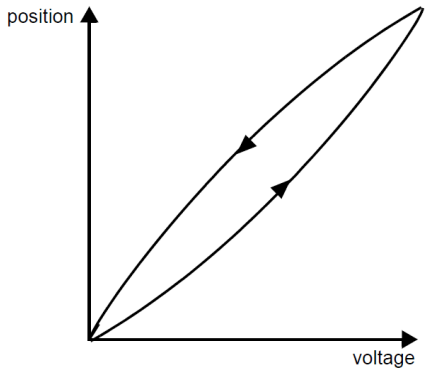

Figure 8.1 Hysteresis effect of the position as a function of the voltage in piezoelectric actuators.

In order to compensate for this effect, the calibration of our piezoelectric actuator was performed using a Michelson interferometer. This device consists of two mirrors that are usually denominated M1 and M2 and a beam splitter inclined at 45º to the mirrors. The collimated beam of a laser is incident on the beam splitter, and it divides in two different beams when striking the partially reflecting surface. A part of the light goes to M1 and gets reflected back to the beam splitter. Some of this light goes through the semitransparent beam splitter. Originally, another light ray passes through the beam splitter going towards M2 where it gets reflected and goes back to the beam splitter where is superimposed on the first ray.

The two rays contain only a part of the original light because the rest has been lost due to the reflection and transmission at the beam splitter and have returned towards the laser. These two

rays reach each other at the beam splitter generating what is called an interference between them generating an interference pattern incident at a detector.

Precise distance measurements can be made with the Michelson interferometer by fixing one of the mirrors to an actuator, moving the mirror and counting the interference fringes which move by a reference point. The distance *d* associated with *m* fringes is described by the following equation:

$$d = \frac{m\lambda}{2}$$

For our purposes, we constructed a Michelson interferometer and fixed one of the mirrors to the translation stage in order to find out the relationship between the voltage applied to the piezoelectric actuator and the distance that it moves. In order to do so, voltage steps of 0.1 V were applied from 0 to 75 volts in order to cover the complete movement range of the piezoelectric actuator. The measurements were made both upwards by slowly increasing the voltage, and downwards by slowly decreasing it in order to get two different calibration curves that will allow us to correct the hysteresis effect when performing electrochemical measurements on tungsten tips and to better control their position in solution. The experimental set up is shown in Figure 8.2.

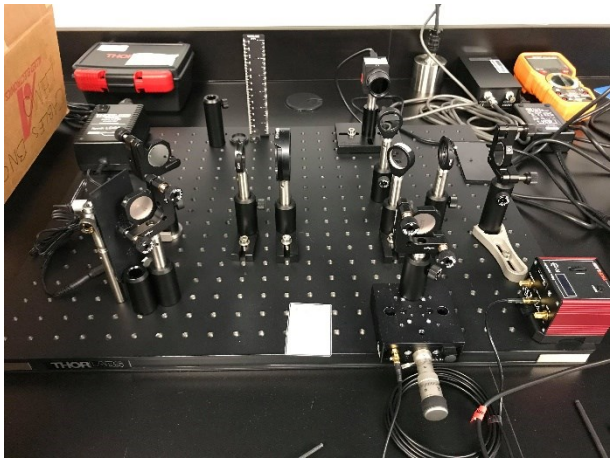

Figure 8.2 **Michelson interferometer used for the calibration of the piezoelectric stage.**

In Figure 8.3 the results from the calibration of the piezoelectric stage are shown. In order to perform a fine calibration and avid the hysteresis effect mentioned before a potential range of two out of 75 V was used. It was found that under these conditions the minimum displacement achievable can be done with 36 nm precision.

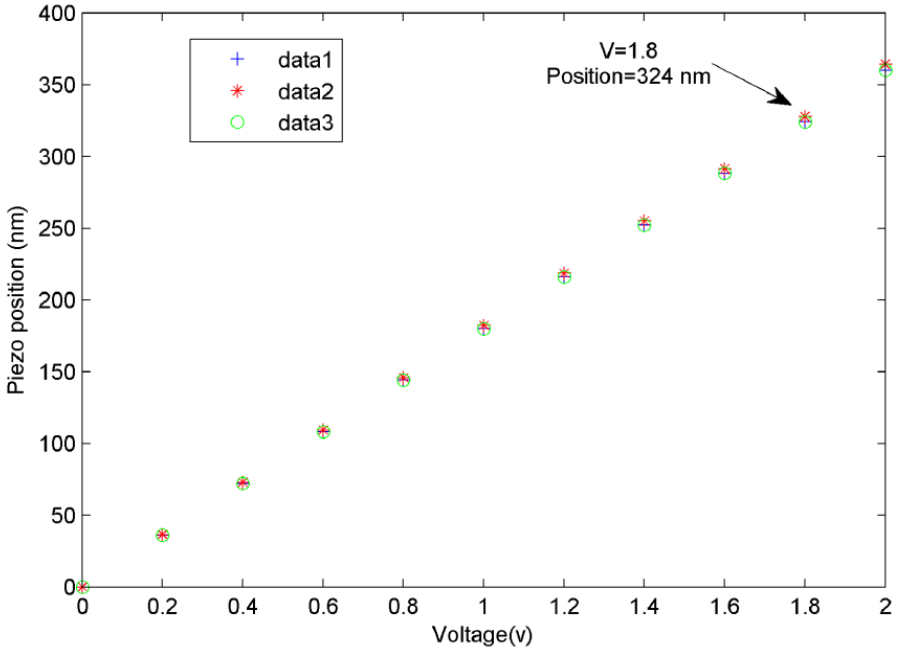

Figure 8.3 **Results from the calibration of the piezoelectric actuator of the stage.**